View metadata, citation and similar papers at core.ac.uk

brought to you by CORE

provided by D-Scholarship@Pitt

FUNCTIONAL TISSUE ENGINEERING OF THE HEALING ANTERIOR CRUCIATE LIGAMENT: A COMBINED EXPERIMENTAL AND COMPUTATIONAL APPROACH

by

Matthew Bruce Fisher

Bachelor of Science, Columbia University, 2005

Submitted to the Graduate Faculty of

Swanson School of Engineering in partial fulfillment

of the requirements for the degree of

Doctor of Philosophy

University of Pittsburgh

2010

UNIVERSITY OF PITTSBURGH

SWANSON SCHOOL OF ENGINEERING

This dissertation was presented

by

Matthew Bruce Fisher

It was defended on

July 21, 2010

and approved by

Alejandro J. Almarza, Assistant Professor, Department of Oral Biology

Stephen F. Badylak, Professor, Department of Surgery

Patrick J. McMahon, Adjunct Associate Professor, Department of Bioengineering

Michael S. Sacks, Professor, Department of Bioengineering

Yongjie Zhang, Assistant Professor, Department of Mechanical Engineering, Carnegie Mellon University

Dissertation Director: Savio L-Y. Woo, Distinguished University Professor, Department of Bioengineering

Copyright © by Matthew Bruce Fisher

2010

FUNCTIONAL TISSUE ENGINEERING OF THE HEALING ANTERIOR CRUCIATE LIGAMENT: A COMBINED EXPERIMENTAL AND COMPUTATIONAL APPROACH

Matthew Bruce Fisher, PhD

University of Pittsburgh, 2010

The anterior cruciate ligament (ACL) is the most important knee stabilizer and is frequently injured during sports and work related activities. Unfortunately, midsubstance ACL ruptures have a limited healing capacity. As such, surgical reconstruction using soft tissue autografts is often performed. However, long-term follow-up studies have revealed that 20-25% of patients had a less than satisfactory outcome. These negative results have renewed clinical interests in healing of a torn ACL by means of biological stimulation. Thus, there is a need for basic science studies in order to better understand such an approach and also to logically develop an effective functional tissue engineering (FTE) treatment for an injured ACL.

The overall objective of this dissertation was to evaluate the positive impact of biological and mechanical augmentation on the healing of the ACL using a combined experimental and computational approach. The ability of an extracellular matrix (ECM) bioscaffold in combination with an ECM hydrogel to enhance ACL healing following suture repair was first demonstrated in the goat model. At 12 weeks of healing, ECM-treatment led to an increase in neo-tissue formation as well as improved biomechanical properties of the healing ACL compared to suture repair alone. Second, as the healing process of the ACL was relatively slow even with ECM treatment, mechanical augmentation to better restore initial joint stability was required. Therefore, a suture augmentation procedure was developed, and improved joint function was achieved versus suture repair alone at the time of surgery. Further, there was increased tissue

formation and improved biomechanical properties of the healing ACL at 12 weeks of healing. Finally, as a step toward predicting long-term outcomes following these biological and mechanical augmentation procedures, a preliminary mathematical model was developed to describe the remodeling process of healing ligaments. The results of this work can now be used to guide future experiments using FTE treatments to enhance ACL healing. With a sound scientific basis, it is hoped that such exciting new technologies could then be translated into the clinical arena to improve patient outcome following ACL injuries.

TABLE OF CONTENTS

LIST OF TABLES

LIST OF FIGURES

PREFACE

When I entered graduate school, my goal was to obtain a Ph.D. What I didn't realize is that the journey toward that degree would be many times more fruitful and rewarding than obtaining the degree itself, which is simply a material representation of these experiences, for me anyway. The events in graduate school have shaped the rest of my life, but as always, the most important factor is the people in my life, who are really responsible for getting me here and are owed significant thanks.

To my mentor, Professor Savio L-Y. Woo: You are truly an educator, first and foremost. Only a small percentage of what I've learned from you was science and research, and only a percentage of that resulted in this dissertation. The vast majority of the knowledge, advice, and teaching given to me went above and beyond the typical training received by graduate students. I am deeply grateful for the time, effort, and concern you gave to my education as a person. It has been an honor to be your student! I can never re-pay you for such experiences, but I can do my best to follow your example in the future and care deeply about the education of future generations of students.

To my committee members, Drs. Almarza, Badylak, McMahon, Sacks, and Zhang: Your expertise and advice has been invaluable and has allowed great improvements in this dissertation. I'd also like to thank Dr. Borovetz and the Department of Bioengineering for their unending support as well as the National Institutes of Health, National Science Foundation, Commonwealth of Pennsylvania, McGowan Institute for Regenerative Medicine, and Asian♦American Institute for Research and Education for financial support.

To my friends at the Musculoskeletal Research Center: One of the best things about the MSRC is that you establish life-long relationships. I was lucky enough to meet many amazing people over the past five years, some of whom have become my closest friends. No one can get through graduate school on their own, and the daily support from the MSRC family never fails.

To my parents: You always made your children your first priority. You've allowed all of us to pursue our interests, and because of your support, I've been able to achieve my goals. Thank you!

To my family and friends: I've been very fortunate to have a wonderful extended family, and many friends whom I consider family. You've helped me to develop into the person I am today.

Finally, to my wife, Lisa: Your support has been essential to my success. I couldn't have done it without you. Marrying you was the easiest decision I ever made, I couldn't be happier to spend the rest of my life with you. I dedicate this dissertation to you.

1.0 MOTIVATION

The anterior cruciate ligament (ACL) is an important knee stabilizer and is subjected to high loads during sports and work related activities [87, 258]. As such, it tears frequently and the numbers are approximately 100,000 cases per year in the U.S. alone [27]. The loss of knee stability after ACL injury results in increased loading of the remaining tissues, such as the medial collateral ligament (MCL), medial meniscus, and articular cartilage, that could predispose them to damage [6, 113, 189, 208, 225]. It is also well known that midsubstance ACL ruptures have a limited healing capacity [13, 164, 169, 281]. Initially, surgeons tried suture repair of a torn ACL and had unsatisfactory outcome, with up to 80% failure [13, 61, 119, 120, 185, 237, 281]. For the last thirty years, surgical reconstruction using soft tissue autografts to replace a torn ACL has been used because these procedures could improve knee stability and allow patient to return to preinjury activities [9, 117, 130, 276]. Nevertheless, long-term (10+ years) follow-up studies revealed that 20-25% of patients with such surgeries had less than satisfactory outcome, including complications associated with the graft donor site and premature osteoarthritis of the knee [54, 209, 246].

With the advent of new technologies, surgeons have revisited the possibility of healing a torn ACL by means of biological augmentation [29, 141, 167, 168, 231, 257]. A successfully healed ACL would have many advantages over ACL reconstruction including avoiding donor site morbidity and preserving the complex anatomy of the ACL (e.g. its original insertion sites,

proprioceptive nerve endings, and so on) that could improve patient outcome in the long-term [216]. At the same time, laboratory studies using functional tissue engineering (FTE) approaches, such as the use of scaffolds, growth factors, and cells, have shown positive effects on restoring the structure and function of an injured ACL [29, 143, 144, 231, 257, 275]. In light of these growing interests, there is an increasing need of basic science studies in order to properly evaluate as well as to logically develop an effective FTE approach for healing of the ACL.

In our research center, we have used extracellular matrix (ECM) bioscaffolds, namely the porcine-derived small intestinal submucosa (SIS), to enhance patellar tendon (PT) and MCL healing. The ECM-SIS was found to encourage tissue formation, improving the overall quality and function of the healing tissue while limiting its hypertrophy [121, 142, 143, 267]. In the case of the ACL, the healing following FTE treatments has been relatively slow [29, 143, 144, 231, 257, 275]. As the ACL plays a vital role maintaining joint stability, additional mechanical augmentation with suture techniques have been added to restore initial joint stability while the ACL heals [73, 120, 218]. Nevertheless, there still remains a need for experimental data to asses both FTE treatments, such as ECM bioscaffolds, as well as associate suture techniques in terms of their ability to enhance ACL healing and maintain joint function.

While in-vivo experiments are vital to the understanding of the complex biological and mechanical stimulus during ligament healing, they are time and resource consuming, particularly for longer time points. An alternative would be to develop a mathematical model to describe the biomechanical properties of the ACL throughout the healing process. An experimentally validated model could then be used to predict the effects of FTE treatments in the long-term in a time- and cost-efficient manner. Ultimately, such a model could be implemented within other

models, such as a finite element model of the ACL, to design proper rehabilitation protocols. ***Thus, the overall objective was to use a combined experimental and computational approach to evaluate the positive impact of biological and mechanical augmentation on the healing of the ACL.***

2.0 BACKGROUND

2.1 ACL ANATOMY AND FUNCTION

The ACL is an important knee stabilizer in preventing excessive anterior tibial translation, varus-valgus rotation, and internal-external rotation of the knee (Figure 1) [259]. Grossly, the ACL can be represented by two bundles: the anteromedial (AM) and the posterolateral (PL) bundle. The AM bundle is tauter in flexion and the PL bundle tauter in extension. With these two bundles, the ACL is well designed to stabilize the knee throughout knee flexion by resisting tensile loads under various loading conditions.

Its biochemical composition consists mostly of water (65-70%) along with fibroblasts and their extracellular matrix (30-35%), which is primarily composed of type I collagen, with small amounts of other collagens, elastin, proteoglycans, and glycolipids [33, 145, 146, 178, 255]. The collagen matrix of the ACL is primarily aligned along the axis of loading, so as to effectively bear tensile loads and prevent excessive translation of the tibia with respect to the femur. Although anatomically intra-articular, the ACL is protected from the synovial fluid by the synovium, a thin connective tissue which lines the ACL [57, 97]. The synovium supports a dense network of nerves as well as small blood vessels, which are the primary sources of nutrition for the ACL [12, 15, 16, 18, 36, 39, 43, 55, 97, 129, 161, 211]. Indeed, if the synovium is removed, collagen necrosis and a gradual deterioration of mechanical properties have been

observed even when there was no direct injury to the ACL substance [59]. Thus, the synovium clearly plays a vital role in maintaining homeostasis of the ACL.

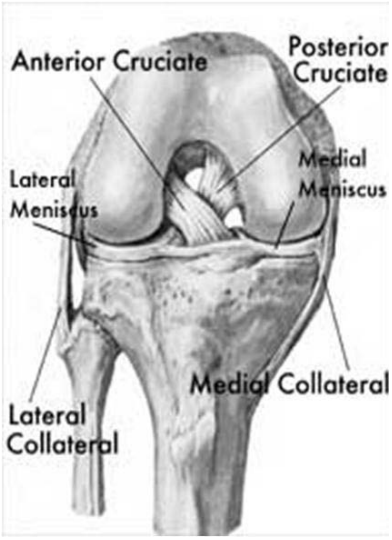

Figure 1. Depiction of the knee joint, showing the important structures for stabilization.

2.2 ANTERIOR CRUCIATE LIGAMENT INJURIES

The ACL is the most frequently injured knee ligament during sports and work related activities, with tears occurring in over 100,000 people in the United States each year— resulting in an annual cost to society on the order of 1 billion dollars [27, 44]. Unfortunately, midsubstance ACL ruptures have a limited capacity for healing [13, 98, 119, 164, 252, 281]. If left untreated, the injured ACL will often resorb over time [164]. Since the ACL is a primary knee stabilizer, joint stability is compromised after its injury.

As such, a major concern is the potential negative impact on the other tissues in the knee. For example, following ACL-deficiency, the other tissue structures of the knee, e.g. the MCL and medial meniscus, experience altered loading [6, 113, 189, 208, 225]. In the goat model, the

degenerative changes to the medial meniscus as well as the articular cartilage were found as early as 8 months following ACL-deficiency [113]. Thus, restoring knee stability and preventing damage to surrounding soft tissues are primary goals for treatment after ACL injury [63, 91, 117].

2.3 CLINICAL TREATMENT

2.3.1 Conservative treatment

Non-surgical treatment of ACL injuries includes bracing of the knee and rehabilitation protocols which aim to increase muscular activity [13, 26, 40, 61, 64, 119, 120, 180, 183, 185, 220, 237, 238, 281]. These are designed to address the lack of stabilization of the knee, and are still a common choice for less active patients or those over 40 years of age. In some studies, after conservative treatment for ACL injuries with appropriate bracing and rehabilitation, as many as 16% of patients showed evidence of continuity between the femoral and tibial attachment via MRI, with others healing to the PCL or lateral femoral condyle [233]. However, most studies show unfavorable results in terms of knee stability and return to normal activity levels in about 50-70% of patients after conservative treatment of an ACL rupture, particularly in those with high levels of activity [26, 64, 65, 149, 180, 212, 238, 253]. Another major concern is that upwards of 70% of patients with conservative treatment eventually develop osteoarthritis of the knee [13, 40, 61, 119, 120, 183, 185, 220, 237, 281].

2.3.2 Suture repair

In light of the poor results following conservative treatment, clinicians have investigated surgical alternatives to treat ACL injuries. A number of suture repair techniques have been developed in an attempt to reapproximate the torn ends of the ACL to permit healing as well as to restore initial knee stability [13, 61, 120, 156, 167, 218, 220, 237, 248, 281]. In some techniques, the ACL tissue stumps were directly sutured to each other. In other techniques, each tissue stump was sutured separately. These sutures were then passed through bone tunnels created in the tibia and femur and fixed to the outer bony cortex.

Clinical results of these techniques had approximately a 50% success rate at 2 years post-operatively [182], but by 5 years the results had worsened [13, 61, 120, 156, 169]. It should be noted that some successes were noted in these studies; however, the percentage of acceptable outcomes were highly variable. For most studies, the levels of knee instability and lower activity levels were similar to those for conservative treatment, and the percentage of osteoarthritis has not been improved. A significant number (20-25%) needed a second surgical procedure in which the ACL was replaced entirely. These poor initial findings have been corroborated in follow-up studies carried out to the long-term (30 years) [237, 241]. These results led to the popularization of ACL reconstruction as a means to improve clinical treatment.

2.3.3 ACL reconstruction

For the majority of younger and active patients, surgeons perform reconstruction procedures using tissue autografts with the primary goal being the restoration of knee stability such that patients can return to sports or work. The most popular grafts include the bone-PT-bone (BPTB)

and hamstrings tendon autografts. Although these procedures have proved effective at restoring initial knee stability [9, 30, 62, 117, 230, 272, 276], 20-25% of patients experience post-operative complications, such as anterior knee pain, arthrofibrosis, and flexion/extension deficits, many of which are associated with the graft donor site [7, 37, 107, 115, 122, 157, 158, 191, 201, 205, 209, 219, 273]. More importantly, long-term (7-24 years) outcome studies demonstrated that the incidence of osteoarthritis (OA) in patients with ACL reconstruction remain significantly high [11, 52, 54, 72, 116, 155, 170, 201, 204, 209, 227, 245]. In fact, some follow-up studies which have directly compared reconstruction to conservative treatment have found similar levels of osteoarthritis [19, 52, 72, 155, 245].

Animal studies of ACL reconstruction have been performed in the dog, pig, sheep and goat models to shed light on the ongoing graft remodeling response [5, 167, 168, 174, 175, 190, 249, 274]. Almost all studies document a large increase in anterior-posterior tibial translation of the joint (2-6x normal) within a few weeks after surgery. At the same time, the biomechanical properties of the healing graft rapidly decrease. For example, by 6 weeks, the stiffness of the healing graft was only 13-30% of the normal ACL in the goat model [5, 175]. The biomechanical properties slowly recover, but over a period of years. By 3 years of healing, the stiffness of the healing graft was only 50% of the normal ACL [175]. In the same study, the anterior-posterior joint stability had been restored by 3 years, despite large increases at early timepoints. These data suggest that the ACL is still not functioning normally even in the long-term. However, remodeling in other tissues of the joint may occur due to altered loading, so that the joint stability is slowly restored.

2.4 MOTIVATION FOR ALTERNATIVE TREATMENTS

As opposed to ACL reconstruction, a successfully healed ACL would have many advantages including avoiding graft donor site morbidity and preservation of the complex anatomy of the ACL (e.g. its original insertion sites, proprioceptive nerve endings, and other anatomical features). The latter is essential to recruit muscles, maintain knee stability, and avoid reinjury [216]. Additionally, the bone tunnels created in these procedures would be greatly reduced compared to ACL reconstruction procedures, which could help to limit the potential for associated neurological and vascular problems. Finally, it could also reduce the reliance on expensive hardware needed for ACL reconstruction procedures, e.g. fixation devices; thereby, reducing the costs of treating ACL injuries. Overall, healing of the ACL has potential to allow for both a faster return to normal activities and improved patient outcome in the long-term. Thus, we wish to explore suture repair of the ACL in combination with FTE treatment as a potential alternative to ACL reconstruction.

2.5 LIGAMENT HEALING

2.5.1 Phases of ligament healing

For studying ligament healing, the MCL of the knee has been an excellent model. In general, its continuous healing process following injury can be roughly divided into three overlapping phases [74, 186, 250]. The inflammatory phase is marked by hematoma formation which starts immediately after injury and lasts for 1-2 weeks. It is followed by the reparative phase (often

called the proliferative phase) where fibroblasts proliferate and produce a matrix of proteoglycan and collagen, especially type III collagen, to bridge the gap between the torn ends. Over the next 6 weeks or so, an increasingly organized matrix, predominantly type I collagen, develops and cellular proliferation occurs. Finally, the remodeling phase, which is marked by gradual alignment of collagen fibers and increased collagen matrix maturation, can continue for years [74, 76].

Nevertheless, the biochemical constituents of the healing ligament are abnormal even after one year [77, 78]. It contains increased amounts of proteoglycans, a higher ratio of type V to type I collagen, a decrease in the number of mature collagen crosslinks, and fibrils with homogenously small diameters (70 nm) [177, 194, 221]. Although there is an increase in the number of collagen fibrils of the healed ligament, the diameters of these fibrils are smaller than those of a normal ligament [75].

These biochemical changes are reflected in altered biomechanical properties of the healing ligament. For example, the structural properties of the healing femur-MCL-tibia complex (FMTC) are inferior to controls at 6, 12, and 26 weeks after injury [186, 250, 262]. By 52 weeks post-injury the stiffness of the injured FMTC at low loads can be recovered, suggesting at least a partial return to normal function; however, the varus–valgus rotation of the joint remained elevated and the ultimate load of the FMTC remained lower than normal [112, 151, 186]. Concomitantly, the cross-sectional area (CSA) of the healing ligament increases rapidly by 6 weeks and remains high, measuring as much as 2 1/2 times its normal size at 52 weeks [186, 187]. On the other hand, the mechanical properties of the healing MCL midsubstance (indicative of tissue quality) are inferior to those of the normal ligament at early timepoints following injury

and remain consistently low up to one year [186, 187, 250]. Thus, the recovery of the stiffness of the FMTC is largely the result of an increase in tissue quantity, not a restoration of tissue quality.

2.5.2 Effects of altered loading on normal and healing ligaments

Based on many years of experimental analyses, it is commonly believed that normal and healing ligaments alter their size and biomechanical properties over time via the mechanism of stress- and strain-dependent homeostasis [260-262, 268, 269]. For example, immobilization of the normal joint for even a few weeks could elicit marked decreases in the structural properties of the FMTC and the mechanical properties of the MCL substance in the rabbit model [173, 262], with only small decreases in the tissue CSA. If the joint is remobilized, the properties of the ligament could return to normal levels; however, up to one year of remobilization was required following 9 weeks of immobilization [262]. Similar results have been noted for the femur–ACL–tibia complex (FATC) in the primate and rabbit models [173, 179]. Long periods of exercise training, on the other hand, only showed marginal increases in the structural properties of ligaments with a 14% increase in linear stiffness of the porcine FMTC and only a slight change in the mechanical properties of the ligament substance [133, 256, 263].

Based on the results of these and other related studies, a highly non-linear representation of the relationship between different levels of stress and ligament properties is depicted in Figure 2. The normal range of physiological activities is represented by the middle of the curve. Immobilization results in a rapid reduction in tissue properties and mass. In contrast, long term exercise resulted in a slight increase in mechanical properties and mass as compared with those observed in normal physiological activities.

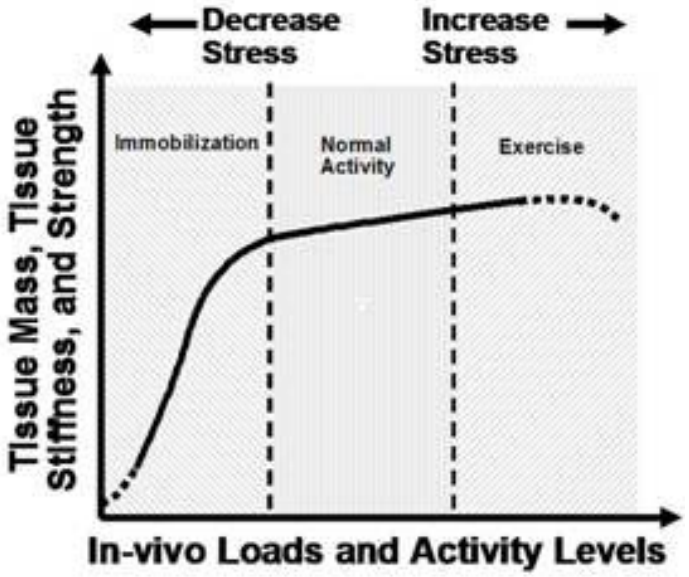

Figure 2. A schematic diagram describing the homeostatic responses of ligaments and tendons in response to different levels of stress and motion (reprinted with permission from [262]).

After injury, the healing tissue has also been found to be sensitive to loading. For example, conservative treatment (with no immobilization) of an isolated MCL injury produced better results than those with immobilization [34, 250, 264]. Immobilization after ligament injury was shown to lead to decreased structural properties of the FMTC and mechanical properties of the ligament substance, with concomitant changes to the tissue microstructure [264]. However, the CSA of the healing tissue was similar at both 6 and 12 weeks with or without immobilization. These experimental findings mirror clinical studies which have reported that patients with a complete tear of the MCL respond well to conservative treatment without immobilization [110, 199].

2.5.2.1 Response of Ligament and Tendon Fibroblasts to Loading

Although ligaments and tendons generally undergo tensile loading at the macroscopic scale, a number of different mechanisms have been proposed for how these macroscopic deformations are transmitted to the cells, i.e. fibroblasts, within the tissue [25, 47, 134, 135]. No matter the mechanism for how cells transmit the applied loads, there is a vast body of experimental results showing that cyclically applied tissue-level tensile loads lead to gene expression of anabolic proteins, e.g. collagen type I, and eventually tissue production [24, 25, 136, 176].

At the same time, macroscopic unloading of ligaments and tendons, leads to increased gene expression of catabolic proteins, e.g. matrix metalloproteases, eventually resulting in tissue degradation [17, 58, 89]. Thus, although macroscopic strains, or even microscopic, fiber-level strains, may be insufficient to describe the complex loading processes at the cellular level, they could serve as a simple, generalized measure of how the cells respond in terms of matrix production and degradation.

2.5.3 Rationale for ACL healing

Unlike extra-articular ligaments, there exist several key biological and mechanical factors that prevent the ACL from undergoing the normal phases of healing after injury [98, 127, 164, 168, 252]. First, a number of studies have documented the lower intrinsic healing capacities of the ACL compared to the MCL [74, 110, 250], including reduced cellular proliferation [172], ECM production [172], gene expression [137, 251] and migration [128], as well as less vascularity [35, 36]. Second, the thin synovium surrounding the ACL, which plays an important role and

contains vasculature and nerves, is disrupted and not regenerated until 3-6 weeks following ACL injury [16, 84, 164]. Experimental studies showed that migrating cells and newly-formed collagen fibers were most prominent in the explants with the preserved synovium, suggesting that it could play a critical role in enhancing the healing capacity of the ACL [53]. Without the synovium, the synovial fluid can enter the injury site. Since the joint is constantly moving, this creates a "washing effect" which effectively prevents hematoma formation, which is the crucial initial step in normal ligament healing. Third, histological examination of the human ACL reveals that it retracts following rupture, creating a large gap between the torn ends. Thus, even if the synovium was preserved, restoration of a continuous tissue would be difficult [164]. Finally, since the ACL is a primary stabilizer of the knee, the lack of mechanical stabilization following its injury also increases the distance between the torn ends and would cause altered loading and kinematics even if the ACL were to heal.

Combined, these factors lead to a large injury site, for an already intrinsically poor healing tissue, which is exposed to the synovial fluid. Thus, creating an appropriate environment in which the ACL could heal is a complex problem, which requires addressing these multiple biological and mechanical factors simultaneously. As such, these requirements have inspired the FTE treatments with proper surgical techniques suggested in this dissertation.

2.6 FUNCTIONAL TISSUE ENGINEERING OF THE ACL

2.6.1 Recent clinical attempts

Surgeons have pursued new interventions that could increase healing ACL tissue formation and improve knee stability [95, 234-236]. One such treatment is biological augmentation of the injured ACL by creating small holes in the bone (microfractures) near the femoral insertion of the ACL to introduce bone marrow and blood to the injury site. This allows formation of a blood clots in order to elicit a healing response more similar to the healing of extra-articular ligaments. These procedures have proved to be mostly successful to treat ACL tears near the femoral insertion site. Over 95% of patients over 40 years of age had restoration of knee function with little pain in the short-term [235]. Positive results were also obtained for younger, skeletally immature patients. However, 23% of these patients were had reinjuries that required additional intervention [94, 234]. Nevertheless, the clinical evidence for the potential of ACL healing is indeed encouraging, and suggests that additional laboratory studies should be done to improve on these early results.

2.6.2 Basic science studies

Laboratory research has also shown that ACL cells can be stimulated through the use of scaffolds and growth factors [127, 144, 163, 165-168, 214, 279]. These positive findings have motivated in-vivo treatment of partial ACL injuries in animal models with a variety of different approaches, including the application of bFGF, hyaluronic acid, and cell therapy using bone marrow-derived mesenchymal stem cells [10, 127, 252]. Based on histomorphological

assessments in the short-term, these approaches generally revealed more tissue growth, vascularity at the injury site, and better matrix organization compared to the non-treated injury. However, all treated ACLs remained considerably abnormal in terms of their morphology and biomechanical properties when compared to the normal ACL.

More recently, Murray and coworkers have developed the use of a platelet-rich plasma (PRP) hydrogel to treat ACL injuries, which is intended to simulate a healing clot. Interestingly, a completely transected ACL with PRP treatment in combination with suture repair only minimally improved over suture repair alone even at 14 weeks post surgery [165]. The authors have suggested the need for additional scaffolding and have developed a collagen-platelet rich plasma (C-PRP) scaffold to treat a partial ACL tear in a canine model [168] as well as a complete ACL transection in a porcine model following suture repair [118, 162, 165, 167]. In the canine partial ACL tear model, histological evidence of more healing tissue filling the injury site as well as improved biomechanical properties were found compared to non-treatment at 6 weeks [168]. The C-PRP hydrogel was then extended to a full ACL transection model in pigs, which revealed that ACL healing took place at 4 weeks but with hypertrophic neo-tissue formation as measured by MRI [167]. Tensile testing of the healing femur-ACL-tibia complexes (FATCs) also showed significant improvements in its tensile stiffness and ultimate load. By 3 months, treatment with a collagen-platelet composite (CPC) and suture repair led to a 3 fold increase in the stiffness of the healing FATCs compared to suture repair alone. Thus, these findings on ACL healing are extremely encouraging.

However, it should also be noted that the biomechanical properties of the healing ACL were still well below those of a normal ACL. In addition, excessive hypertrophy of the healing ACL was observed at all time points, which raises the issue regarding the lack of quality of the

healing tissue and its level of contribution to joint function, which was not tested. Thus, there is still a need for novel FTE solutions to induce appropriate tissue growth while limiting its hypertrophy to bring about a much improved healing ACL and joint stability.

2.6.3 Suture techniques in combination with FTE

In order to achieve the needed joint stability during the early healing process, these new biological approaches are often coupled with suture repair and/or augmentation of the torn ends of the ACL [61, 120, 167, 184, 218, 248]. As previously mentioned, the goals of suture repair are to reapproximate the torn ends of the ACL to permit healing as well as to restore initial joint stability. Most techniques involve suturing of each tissue stump and passing these sutures through bone tunnels created in the tibia and femur and fixed to the outer bony cortex.

A recent study by Fleming and coworkers has shown that suture repair of the ACL tissue alone is insufficient to restore anterior-posterior knee [73]. The authors hypothesize that this is likely due to sliding of the sutures relative to the soft tissue as well as the difficulty in applying tension to the sutures. Alternatively, augmentation of the injured ACL, by passing sutures directly from bone to bone, has been suggested in combination with suture repair to better restore knee stability while also reapproximating the ACL tissue stumps. In this approach, the augmentation sutures would provide bone to bone fixation, and thus, would greatly reduce the possibility of sliding and allow proper tensioning. In fact, Fleming and coworkers found that this technique could better restore anterior-posterior knee stability compared to suture repair [73].

However, there are a number of limitations in this study, including 1) only 1 degree-of-freedom motion [111], 2) assessment of knee stability at only one flexion angle (60 degrees), 3) applied loads were below the levels of physiological loading, and 4) the study did not consider

the outcome of these suture techniques after healing. All of these concerns can be addressed by combining in-vivo animal studies with a robotic testing system to assess joint function.

2.7 EXTRACELLULAR MATRIX BIOSCAFFOLDS

2.7.1 Advantages of ECMs

ECM bioscaffolds are particularly attractive because they are readily available and consist of a naturally organized matrix [100, 247]. Examples include small intestine submucosa (SIS), urinary bladder matrix, acellular dermis, amniotic membrane tissue, and fascia [100]. Generally, these bioscaffolds are extracted from an animal or human source and processed to remove the native cells before being used. ECM bioscaffolds have been utilized in numerous clinical settings involving general surgery [14, 41, 56, 79, 80, 148, 215], neurosurgery [28], urology [126, 181, 224], and orthopaedics [160, 217, 242], and have been implanted in over a million patients to date.

One bioscaffold, namely porcine ECM-SIS, has been widely utilized because it has many desirable biological and ultrastructural advantages. ECM-SIS is mostly comprised mainly of type I collagen that has a well arranged ultrastructural hierarchy. It has been found that 40% of the ECM-SIS can be degraded in-vivo within one month [198] and its by-products are chemoattractants for cells [22, 139, 277] and contain bioactive agents, e.g. growth factors, fibronectin, angiogenic factors, and so on [101, 159, 247]. Further, its ultrastructural characteristics can provide contact guidance for cells in-vivo (Figure 3) [176]. It is our hypothesis that the ECM-SIS bioscaffold could accelerate healing by allowing for more rapid

cell migration and proliferation in the scaffold as well as new matrix production [23, 38]. Additionally, the ECM-SIS bioscaffold could serve as a temporary substitute for the synovium during the first few weeks to contain the healing response and limit tissue hypertrophy until the early healing phase is complete and a new synovium could be formed.

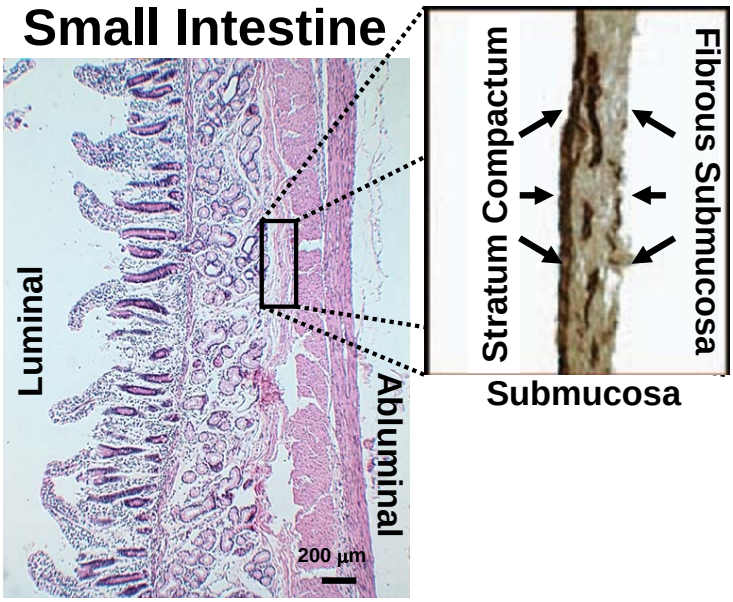

Figure 3. A longitudinal section of the small intestine demonstrating the location of the submucosa and its ultrastructural differences between the luminal and abluminal sides (Modified from [38]).

2.7.2 Use of ECMs to improve extra-articular ligament healing

The potential of porcine ECM-SIS bioscaffolds to guide and support soft tissue regeneration, promote extracellular matrix organization, and eventually improve the quality of the healing tissue has been demonstrated in a rabbit MCL model of extra-articular ligament healing [143, 171, 257]. A single layer of ECM-SIS was applied to a 6 mm gap injury of the MCL. At 12 and

26 weeks, the morphology of collagen fibers in the ECM-treated group showed denser and more aligned along the longitudinal axis of the ligament at both time points, and there were more spindle–shaped cells in the ECM-treated neo-MCL [142, 143, 267]. The ECM bioscaffold also helped to limit the hypertrophy of the healing tissue as the CSA in the ECM-treated group decreased by 28% compared to non-treatment and was closer to sham control at 26 weeks (Figure 4).

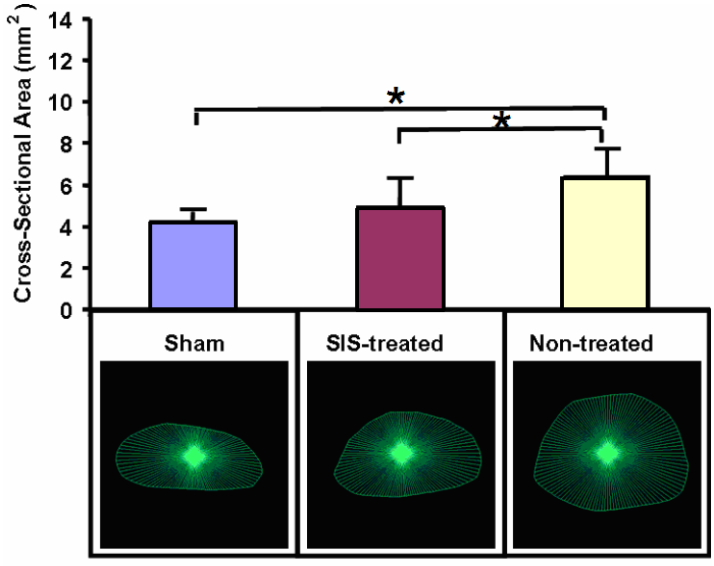

Figure 4. Cross-sectional area and shape of the MCL following ECM treatment compared to non-treated and sham at 26 weeks (*p<0.05) (reprinted with permission from [143]).

At 6 weeks, the gene expressions of other small leucine-rich proteoglycans (SLRP) molecules, such as decorin, biglycan and lumican, which are thought to control the formation of small collagen fibrils, were down-regulated [142]. By 26 weeks, the collagen content in the neo-ligament increased by 36% with ECM-treatment, while the collagen type V/I ratio became 33% lower than the non-treated group ($p < 0.05$). Lowering the type V/I ratio is important because excessive collagen type V has been known to limit the formation of larger collagen fibrils [31, 32]. Correspondingly, the diameter of collagen fibrils increased by 22% at 26 weeks [257].

Functionally, the mechanical properties of the healing ECM-treated MCL were also significantly improved, as the tangent modulus was 50% higher at 12 weeks and 33% higher at 26 weeks when compared to those of non-treated ($p<0.05$) (Figure 5). The ultimate tensile strength at 26 weeks was also 49% higher ($p<0.05$) [143]. In other words, a single layer ECM-SIS bioscaffold, could provide contact guidance to the neo-ligament to have a more organized matrix while limiting tissue hypertrophy; thereby increasing the mechanical stresses in the healing tissue so that it could remodel into a ligament with better quality.

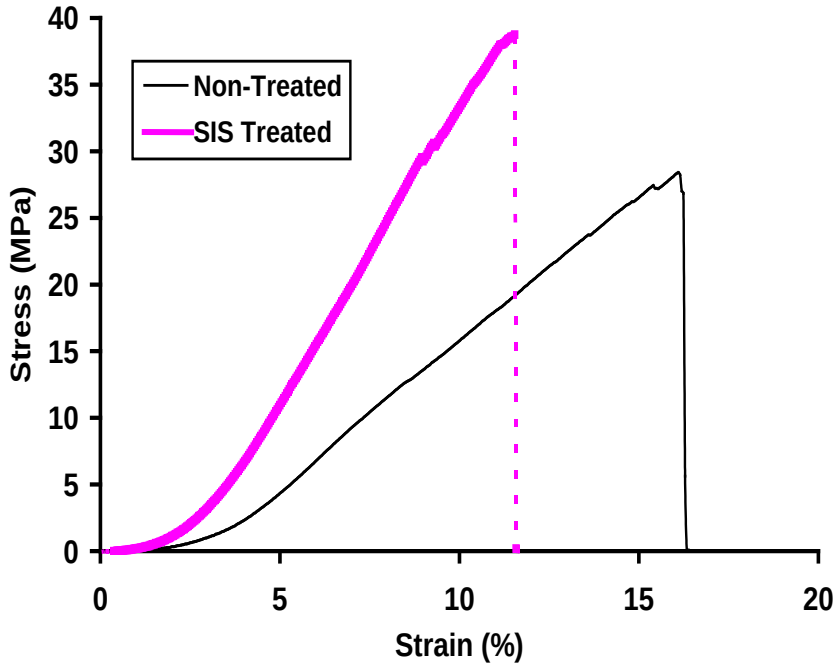

Figure 5. Typical stress-strain curves for ECM-treated and non-treated groups at 26 weeks (reprinted with permission from [143]).

2.7.3 Use of ECMs to improve extra-articular tendon healing

In another study, the feasibility of ECM to regenerate the PT after removal of its central third for use as an autograft for ACL reconstruction was tested [121]. Using the rabbit model, a 3 mm wide defect (about 1/3 of the width of the PT) was created and one strip of ECM-SIS was sutured anterior and one posterior to the PT defect. The defect was left open for the non-treated group.

Gross examination revealed that abundant neo-PT tissue formed in and around the defect area in the ECM-treated group at both 3 and 12 weeks. Conversely, those for the non-treated group had concavities. Also, it was abundantly clear that there was little or no noticeable adhesion formation between the neo-PT and infrapatellar fat pad in the ECM-treated group. In contrast, significantly more diffuse adhesive formations between the neo-PT and the underlying fat pad were created in the non-treated group.

Morphological examination of the ECM-treated group showed that the neo-PT had areas of high cellularity at 3 weeks while those for the non-treated group showed loose, disorganized fibrous tissue with low cellularity. The former had a large number of spindle shaped cells with organized collagen matrix at 12 weeks while the latter still had a sparse distribution of cells with patches of disorganized collagen.

After careful dissection [1, 66], the CSA of the neo-PT tissue was measured and the ECM-treated group had 68% higher CSA than the non-treated group ($p<0.05$). Tensile testing showed that the biomechanical properties of the neo-PT tissue from the ECM-treated group had a 98% higher stiffness and a 113% higher ultimate load than those from the non-treated group ($p<0.05$). Thus, the results showed that ECM bioscaffold can improve tissue growth, matrix organization, and biomechanical properties of the neo-PT, while containing the neo-PT tissue within the injury site and preventing its ability to form detrimental adhesions to the surrounding

tissues. In summary, this study showed that ECM-treatment could allow the production of abundant tissue in an injury model which has limited ability to heal, and show promise to heal other ligaments and tendons with poor healing potential, such as the ACL.

2.7.4 Use of genetically-modified ECM bioscaffolds

In orthopaedic surgery, the use of porcine ECM-SIS bioscaffolds has become less enthusiastic among clinicians because of the negative impression of inflammatory reactions after the application of multilayer ECM-SIS bioscaffolds to treat massive rotator cuff repairs [20, 88, 109, 154, 217]. In one study, an overt inflammatory reaction was noted in 4 of 25 patients at two weeks post-implantation, which required open irrigation and debridement [154].

One possible contributor to the hyperacute inflammatory response observed in applications of ECM-SIS bioscaffolds may be the presence of galactosyl-α(1,3)galactose (αGal) [20, 109, 154, 217]. Although almost all mammals contain αGal in their cellular membranes and extracellular matrix proteins, humans as well as New World primates possess a genetic mutation which prevents the formation of αGal. As such, humans express antibodies to αGal, which could lead to hyperacute inflammation and rejection of ECMs from porcine sources. To alleviate this concern, we have collaborated with Revivicor Inc. and have recently obtained a novel ECM-SIS bioscaffold derived from genetically-modified pigs (GalSafe^{TM}), in which the galactosyltransferase alpha 1, 3 gene (GGTA1) is knocked out [50, 192, 196]. Such αGal(-) ECM-SIS bioscaffolds could offer significantly greater potential for future translation in the clinical arena once it is proven to successfully heal injured ligaments.

2.7.4.1 Comparison of genetically-modified and wild-type ECM bioscaffolds

In a preliminary study, we wished to examine whether the intrinsic biological properties and biomechanical properties of the αGal(-) ECM bioscaffolds remained unchanged; and also, when used in hydrogel form, whether they could stimulate ACL fibroblasts. We examined the morphological, bioactive and biomechanical properties of SIS and UBM bioscaffolds (n=5) and compared them with those from wild type (n=5) pigs. Morphologically, the αGal(-) ECMs were found to be similar to the wild type ECMs via both gross observation and H&E staining. With ELISA, western blot and immunohistochemistry, growth factors, including FGF-2, TGF-β, VEGF, IGF-1 and PDGF-BB, showed no significant differences in terms of quantity ($p>0.05$) and their distribution within the tissue. Further, a BrdU cell proliferation assay confirmed the bioactivity of the extracts from the αGal(-) bioscaffolds to be similar as the wild type bioscaffolds. Under uniaxial tensile testing, no significant difference were found for their viscoelastic and mechanical properties ($p>0.05$). The results suggested that genetic modification had not altered the properties of the ECM bioscaffolds, and as such, they could be used in tissue engineering for human application with the advantage of reduced immunogenicity.

2.8 MATHEMATICAL MODELING OF LIGAMENTS

Numerous mathematical models have been developed in order to capture the biomechanical nature of soft tissues [85, 104, 107, 131, 132, 195, 206]. For ligaments, this is most often represented by the stress-strain behavior under uniaxial tension. Due the parallel orientation of the collagen fibers (Section 2.1), ligaments are often assumed to be transversely isotropic, and a number of constitutive models for ligaments have been developed based on this assumption.

One such model is presented in Section 2.8.1. On the other hand, for healing ligaments, the assumption of transverse isotropy may not be valid, so a more general model to describe the biomechanical behavior of these tissues may be required, and an example is presented in Section 2.8.2.

2.8.1 A constitutive relationship for transversely isotropic tissues

To describe the 3-D mechanical behavior of ligaments, investigators have developed a quasi-static, hyperelastic strain energy model based on the assumption of transverse isotropy [195]. The total strain energy, W, in response to a stretch along the collagen fiber direction, λ, is defined to be equal to the sum of the strain energy resulting from the ground substance (F1) and collagen fibers (F2):

$$W = F_1(I_1) + F_2(\lambda) + \frac{K}{2}\ln(J)^2 \qquad 2\text{-}1$$

with uncoupled deviatoric and volumetric components. I_1 is the first deviatoric invariant of the deformation tensor, while λ represents the deviatoric stretch along the collagen fiber direction. K is the bulk modulus, and J is the determinant of the deformation tensor. The ground substance is described as an isotropic and nearly incompressible matrix (neo-Hookean material), and the strain energy function is described as:

$$F_1 = \frac{1}{2}C_1(I_1 - 3) \qquad 2\text{-}2$$

where C_1 is a constant. The collagen fiber matrix is assumed to not support compressive load, and the tensile stress-stretch relationship for the collagen matrix is approximated by an exponential toe region followed by a linear region:

$$\lambda \frac{\partial F_2}{\partial \lambda} = \begin{cases} 0 & \lambda < 1 \\ C_3(e^{C_4(\lambda-1)} - 1) & 1 < \lambda < \lambda^* \\ C_5\lambda + C_6 & \lambda > \lambda^* \end{cases}$$

$$C_6 = C_3(e^{C_4(\lambda^*-1)} - 1) - C_5\lambda^* \qquad 2\text{-}3$$

where C_3 scales the exponential stress, C_4 specifies the rate of collagen uncrimping, C_5 is the modulus of straightened collagen fibers, λ^* is the stretch at which the collagen is straightened, and C_6 ensures continuity at λ^*. The Cauchy stress is then determined from the strain energy function. It was found that this model could fit both the data obtained from both longitudinal and transverse dumbbell shaped specimens cut from the human MCL to show its transversely isotropic behavior [195]. This constitutive relation has also been applied to a subject-specific finite element model of the human ACL and used to predict the stress and strain distribution in the ACL under applied loads [228, 278].

2.8.2 A general constitutive relationship for soft tissues

The constitutive model described in Section 2.8.1 is specific for highly aligned tissues. Another approach is a more general formulation for collagenous soft tissues which can account for varying degrees of fiber alignment [108, 125, 131, 206, 207, 280]. One such model has been developed by Sacks et al. for the pericardium [206] based on the work of Lanir [131, 132] and is presented in some detail below.

One primary assumption of the model is that the total strain energy of the tissue, W, can be related to the strain energy of the collagen fibers within the tissue, w(), by accounting for their angular distribution within the tissue, $R(\theta)$, and the strain of the fibers, ε:

$$W = \int_{-\pi/2}^{\pi/2} R(\theta) w(\varepsilon) d\theta \qquad 2\text{-}4$$

Thus, W is simply the sum of the strain energies of the tissue fibers. Since the tissue is mostly comprised of collagen, the contribution of other matrix components (i.e. elastin, ground substance) and the hydrostatic forces were assumed to be negligible.

For R(θ), Sacks et al. collected data on fiber orientation using the small angle light scattering (SALS) technique [207]. To determine the stress-strain relationship, the tissue was assumed to be a hyperelastic solid. As such:

$$S = \frac{\partial W}{\partial E} + pC^{-1} \qquad 2\text{-}5$$

where S is the 2nd Piola-Kirchoff stress, E is the Green-Lagrange strain tensor, p is the Lagrange multiplier which accounts for the incompressible nature of the matrix, and C is the Right Cauchy Green tensor.

The model also assumes that the tissue could be represented in terms of fiber ensembles, i.e. the collection of fibers with the same orientation. Another key assumption was that the strain of the fiber ensemble, E^{ens}, could be computed as a transformation of the tissue strain with respect of the fiber ensemble coordinates (affine transformation). Thus:

$$E^{ens} = N^T E N \qquad N = \cos(\theta)\hat{i} + \sin(\theta)\hat{j} \qquad 2\text{-}6$$

where N is a unit vector parallel to the long axis of the fiber. Then, formulations for the 2nd Piola-Kirchoff stress of an individual collagen fiber, S^f, were developed. It was assumed that the fibers cannot support compressive loading, and that each fiber can only carry tensile loads along its long axis. Thus:

$$S^f(E^{ens}) = S_{11}^f(E^{ens}) \qquad 2\text{-}7$$

Two models to describe the nonlinear fiber stress-strain law were provided. The first was a simple exponential function. The second model accounted for the gradual recruitment of linear elastic collagen fibers within each fiber ensemble by means of a statistical distribution. In the latter representation, it was assumed that the collagen fibers are crimped and transmit loads only after they are straightened. After that, the stress in the fiber was assumed to be linearly related to the strain in the fiber. However, due to the slack region, the true strain of each fiber is represented by $E^t = \frac{E^{ens} - E^s}{1 + 2E^s}$, where E^t is the true fiber strain, E^{ens} is the fiber ensemble strain, and E^s is the fiber slack strain. Thus, the fiber stress-strain relation can be written as

$$S_f = \frac{\partial W_f}{\partial E_f} = \frac{\partial W_f}{\partial E^t}\frac{\partial E^t}{\partial E_f} = k\frac{E^{ens} - E^s}{(1 + 2E^s)^2} \qquad 2\text{-}8$$

The total stress-strain relation of the fiber ensemble is then represented as the sum of the fiber strain energies weighted by the percentage of fibers at each slack strain as

$$S^{ens} = \int_0^{E^{ens}} D(x)S_f(x)dx = k\int_0^{E^{ens}} D(x)\frac{E^{ens} - x}{(1 + 2x)^2}dx \qquad 2\text{-}9$$

where D(x) is a function which represents the fraction of fibers which are straightened at a given strain. The form of D(x) will be discussed in more detail in Section 7.1. Also, it should be noted that k incorporates the relative mass fraction of the collagen fibers.

The components of S can then be calculated to determine the tissue stress-strain relationship. For example the tensile stress along the axis of loading was:

$$S_{11} = \int_{-\pi/2}^{\pi/2} R(\theta)S^{ens}(E^{ens})\cos^2(\theta)d\theta \qquad 2\text{-}10$$

Using experimental data on the fiber distribution and mechanical properties, these models were able to predict the biaxial behavior of the pericardium and urinary bladder wall [206, 254].

2.8.3 Growth and remodeling

The healing of biological tissues, in particular the idea of stress- and strain-induced homeostasis, has been studied extensively throughout the literature, especially in the areas of vascular and bone remodeling [45, 86, 200, 202, 222, 223]. This concept dates back to the development of Wolff's law, which suggested that the structure of trabecular bone coincides with the principal stresses due to external loads [202]. The hypothesis was that stress (or strain) could alter the growth and remodeling of bone. Since then, important contributions to tissue remodeling have been made by Skalak, Fung, and many others [86, 200, 202, 222, 223]. Skalak et al. focused on defining relationships which could describe finite growth of tissues [222]. These ideas led to the concept of residual stresses within tissues, in the absence of external loading [223]. Rodriquez et al. built on the work of Skalak and developed a stress-dependent relationship for growth [200]. In these studies, the deformation gradient was separated into parts describing its elastic deformation as well as deformation due to growth. Later, Fung would describe growth in terms of a mass-stress relationship, based on general observations in that an increase or decrease in stress would lead to a corresponding change in tissue mass [86]. Most of these early attempts described these biological processes using phenomenologic models to capture their general behavior.

More recently, there has been an emphasis by Humphrey, Gleason, and others, on characterizing growth and remodeling based on a tissue's microstructural components (e.g. collagen, elastin, etc.) [93, 96, 106, 197, 243, 244]. These models, based on mixture theory, assume that the mechanical response of the tissue is the sum of the mechanical responses of its components, multiplied by their mass fractions. These models attempt to provide enhanced predictive capability with knowledge of the tissue biochemistry and their metabolic turnover

rates. As the tissue is subjected to stresses and strains over time, the matrix is allowed to turnover. In other words, the matrix components are allowed to be deposited and degraded at different configurations. The end result is that the stress-strain relationship varies with time and depends on the stretch at which the new matrix is deposited. In the vast majority of these models, the stimulus, e.g. stress or strain, is chosen based on empirical evidence. Additionally, the specific form of the "stimulus function" which determines how a given parameter will change based on the current and homeostatic values of the stimulus is generally phenomenologic, and not typically based on a biological mechanism.

3.0 OBJECTIVES

3.1 BROAD GOALS

The broad goal of this dissertation was to develop a methodology to quantitatively assess the effects of FTE approaches on the healing process of an injured ACL. The overall objective was to evaluate the positive impact of biological and mechanical augmentation on the healing of the ACL using a combined experimental and computational approach. To accomplish this objective, three Specific Aims are proposed.

3.2 SPECIFIC AIMS AND HYPOTHESES

Specific Aim 1: *To determine the advantages of biological augmentation using an ECM bioscaffold, in combination with ECM hydrogel on the healing of a transected ACL following suture repair in the goat model.* The stifle joint stability as well as the biomechanical properties and histological appearance of the healing ACL were evaluated at 12 weeks. As ECM-SIS bioscaffolds have been shown to enhance ligament and tendon healing by encouraging neo-tissue formation with improved overall tissue quality [121, 142, 143, 267], we wished to address the research question of whether an ECM bioscaffold used in combination with ECM hydrogel could accelerate healing of a transected ACL following suture repair.

Hypothesis 1: As ECM bioscaffolds contain a number of bioactive agents that could attract healing cells, stimulate matrix production, and accelerate the healing process [42, 188, 210], we hypothesized that an ECM hydrogel that fills the ACL injury site could encourage more rapid healing tissue formation. Further, we hypothesized an ECM bioscaffold wrapped around the transected ACL could help to contain the healing response at the injury site while limiting hypertrophy of the healing ACL to further enhance healing. A healed ACL with appropriate cross-sectional area would increase its mechanical demand under loading and thus produce neo-tissue with better biomechanical properties [121, 142, 143, 267]. As a result, it could help to better maintain stability of the stifle joint.

Specific Aim 2: *To evaluate the advantages of mechanical augmentation using sutures to restore joint stability in the goat model.* As biological augmentation for healing a transected ACL is relatively slow, mechanical augmentation would be needed to replace the role of the ACL during early healing. Thus, appropriate suture techniques are needed to restore initial joint stability while the healing process of the ACL takes place [73, 120, 218]. In suture repair, the torn ends of the ACL are either sutured together or tensioned by passing the sutures through bone tunnels drilled in the tibia and femur and fixing them against the bone. In suture augmentation procedures, the sutures are passed directly from bone to bone and tied under tension. Thus, we wished to address two research questions: 1) Does suture augmentation of the transected ACL restore initial joint stability closer to that of the normal joint at time-zero compared to suture repair?, and 2) Does additional suture augmentation positively affect the healing process of the ACL and the function of the stifle joint compared to suture repair alone?

Specific Aim 2.1: *To quantify the joint stability and the in-situ forces in the ACL in response to externally applied loads following suture repair and suture augmentation at time-zero and compare the data with those for the intact and ACL-deficient stifle joint.*

Hypothesis 2.1: We hypothesized that suture augmentation will better restore joint stability, i.e. anterior tibial translation, compared to suture repair of the ACL substance alone, since the former provides fixation of the sutures from bone to bone, while the sutures in the latter case would have the potential to slip along the ligament tissue.

Specific Aim 2.2: *To evaluate the advantage of suture augmentation plus simple suture repair over suture repair alone in terms of maintaining joint stability as well as the gross morphological, histological, and biomechanical properties of the healing ACL at 12 weeks post-surgery in a goat model.*

Hypothesis 2.2: We hypothesized that if suture augmentation could restore initial joint stability closer to normal at time-zero and prevent excessive loading of the ACL (See **Specific Aim 2.1**) while simple suture repair could reapproximate the torn ends of the ACL, then the distance between the injured ACL tissue created following its transection would be minimized and would allow tissue formation to heal the ACL. Over time, loading of the healing ACL would allow both the biomechanical properties of the healing ACL as well as the joint stability to be closer to normal at 12 weeks of healing compared to suture repair alone.

Specific Aim 3: *To develop a mathematical model to describe the healing process of the ACL during its remodeling phase.* As the healing process evolves from inflammation and

proliferation to tissue remodeling, both the size and biomechanical properties of ligaments change correspondingly over time [260-262, 268, 269]. Based on a large amount of previous experimental data obtained [260-262, 268, 269], it is commonly believed that normal and healing ligaments alter their size and biomechanical properties over time in response to stress- and strain-dependent homeostasis. Thus, we wished to address the research question of whether a mathematical model based on strain-based homeostasis could describe the size and biomechanical properties of the healing ACL throughout the remodeling process.

Specific Aim 3.1: *To formulate a mathematical model to describe the healing ligament over time in terms of its tissue growth and biomechanical properties during its remodeling phase.*

Specific Aim 3.2: *Validate the model using experimental data collected for the rabbit MCL at 12 and 26 weeks of healing.*

Specific Aim 3.3: *Use the model to provide preliminary insights on the mechanisms for the results obtained in Specific Aims 1 and 2.*

Hypothesis 3: We hypothesize that a mathematical model based on strain-dependent remodeling could capture the alterations in size and biomechanical properties in the healing ligament which occur in order to restore a homeostatic level of strain.

4.0 EXPERIMENTAL METHODS

4.1 STUDY DESIGN

The three Specific Aims and the accompanying hypotheses were tested by the experiments as outlined in the following sections. In Specific Aim 1, the effects of ECM treatment on joint function as well as the gross morphology, histological appearance, and biomechanical properties of the healing ACL were assessed at 12 weeks of healing. In Specific Aim 2, the ability of suture techniques to restore joint function were examined both at time-zero and 12 weeks of healing, and the gross morphology, histological appearance, and biomechanical properties of the healing ACL will be assessed at 12 weeks. In Specific Aim 3, a mathematical model to describe the remodeling of a healing ligament was developed. For Specific Aims 1-2, a power analysis, based on preliminary data on the healing ACL as well as published works related to the effects of ECM treatment [143, 167, 168, 171, 267], was performed to determine the number of animals needed for biomechanical testing using G*Power [60].

For Specific Aim 1, two experimental groups were needed: 1) suture repair alone and 2) suture repair with ECM treatment. Goats underwent surgery according to Section 4.3 and were euthanized at 12 weeks. Histomorphological evaluation was done according to Section 4.4.1. Joint function was assessed according to Section 4.4.2.1. The CSA of the ACL was measured (Section 4.4.2.2), and its biomechanical properties were evaluated (See Section 4.4.2.3).

Since treatment was done only in one hindlimb of each animal, an unpaired t-test was performed to compare the treatment groups. In order to detect a mean difference of 3 mm in terms of anterior-posterior tibial translation, 20 N in terms of in-situ force, and 25 N/mm in terms of stiffness between groups with an overall α=0.05 and a power of 0.8, five (5) animals per treatment group were needed. Two additional animals were used for histomorphological assessment. Further, for increased statistical power, an additional four (4) goats were added to the ECM-treated group, with two (2) used for biomechanical testing and two (2) used for histological evaluation. Additional animals were not done for the suture repair group due to the large variability noted in the initial animals. Thus, a total of **eighteen (18) animals** were utilized for Specific Aim 1.

For the first part of Specific Aim 2.1, four separate suture augmentation groups were compared to each other as well as the intact and ACL-deficient joint in an in-vitro study using a robotic/UFS testing system, according to the protocol described in Section 4.4.2.1(a). Since all conditions were done on the same set of joints, a paired statistical analysis was done. As such, eight (8) joints were needed to detect a mean difference of 2 mm in anterior tibial translation (ATT) and 10 N of in-situ force between groups with an overall α=0.05 and a power of 0.8. The value for the mean difference in ATT was chosen based on the clinical literature in which a successful reconstruction procedure following ACL injury could restore translation to within 2-3 mm at the time of surgery [9, 81, 230]. The value for the mean difference in in-situ force was chosen based on the repeatability of our testing system (6-9 N).

For the second part of Specific Aim 2.1, the goal was to compare suture repair and suture augmentation in terms of their ability to restore initial joint function. Both were also compared to the intact and ACL-deficient conditions. To accomplish this, goat joints were tested in-vitro

on our robotic/UFS testing system, according to the protocol described in Section 4.4.2.1(a). Using this system, all experimental conditions were tested in the same set of stifle joints. As such, a paired statistical analysis was done. In order to detect a mean difference of 2 mm in terms of anterior-posterior tibial translation and 10 N of in-situ force between groups with an overall α=0.05 and a power of 0.8, eight (8) goat joints were needed.

For Specific Aim 2.2, two experimental groups were required: 1) suture repair and 2) suture augmentation with simple suture repair. Goats underwent surgical procedures according to Section 4.3. At 12 weeks, all animals were euthanized, and specimens were assessed in terms of gross observation of the ACL, histomorphology of the ACL (See Section 4.4.1), joint function (See Section 4.4.2.1(b)), CSA (Section 4.4.2.2), and the biomechanical properties of the ACL (See Section 4.4.2.3).

Like Specific Aim 1, these treatments were done in separate animals. Thus an unpaired t-test was performed, and five (5) animals per treatment group were needed for biomechanics. Histological evaluation was done in two (2) goats per group. The suture repair only group was already completed in Specific Aim 1, and no additional animals were needed for this group. Seven (7) animals were needed for the suture augmentation group for Specific Aim 2.2.

For Specific Aim 3.1, a mathematical model for ligament healing was developed. A detailed description can be found in Section 7.1. The model was implemented within the computer programming package MATLAB (MathWorks, Inc, 7.9.0 (R2009b). In Specific Aim 3.2, the model was initially tested using data collected in our research center for the rabbit MCL [74, 143, 171, 186, 250], because there is a wealth of data for the healing rabbit MCL (relative to the goat ACL) collected throughout the healing process (See Section 7.3). This multiple time-point data is essential for development of the model and assessing its predictive capabilities. In

Specific Aim 3.3, some initial simulations for the healing ACL were run using the model based on the experimental data in Specific Aims 1 & 2.

4.2 PREPARATION OF ECM BIOSCAFFOLDS

To produce the αGal(-) ECM bioscaffolds, a small intestine from a genetically modified (α1,3-galactosyltransferase -/-) pig (GalSafe^{TM}, 13 mos., 180 kg.) was harvested immediately after euthanasia by Revivicor, Inc. and shipped overnight on dry ice. Once thawed, the small intestine was prepared as previously described [90]. In brief, the small intestine was rinsed, and the tunica muscularis externa and the majority of the tunica mucosa were mechanically removed. The remaining αGal(-) ECM (tunica submucosa and basilar portion of the tunica mucosa) was then disinfected and decellularized in a 0.1% peracetic acid/4% ethanol solution, rinsed twice each in phosphate-buffered saline and de-ionized water, and lyophilized. The αGal(-) ECM used to make sheets was then terminally sterilized with ethylene oxide. To make the αGal(-) ECM hydrogels, lyophilized αGal(-) ECM sheets were comminuted to a powder, as previously described [82, 90]. One gram of αGal(-) ECM powder and 100 mg of pepsin were added to 100 ml of 0.01 M HCl and kept at a constant stir for ~48 to 72 hrs at room temperature (25 °C). The resultant solution of digested αGal(-) ECM (pre-gel solution, 10mg/ml) was kept frozen at -20°C until needed.

4.3 IN-VIVO ANIMAL MODELS

All surgical procedures were done using well-established protocols developed in our research center and approved by the University of Pittsburgh Institutional Animal Care and Use Committee. The goat model was chosen due to its success as a model for ACL reconstruction [2, 190]. All surgical procedures were performed using sterile techniques under general endotracheal anesthesia using isoflurane (1-3%). The ACL in the right stifle joint was injured and repaired, while the contralateral leg served as a sham-operated control. A longitudinal midline anterior skin incision was made over the PT. A medial arthrotomy was performed to open the joint capsule, and the patella was retracted laterally to expose the ACL.

During the sham-operation, the ECM sheet and hydrogel were prepared. The ECM sheet was trimmed (~20 mm in length x ~5 mm in width) and sutured to a similarly-sized fibrin sponge (Surgifoam, Johnson & Johnson) via 4-0 non-absorbable sutures such that the luminal side of the ECM faced away from the fibrin sponge. Meanwhile, the ECM hydrogel was formed by mixing 0.1 N NaOH (1.0 ml), 10x PBS pH 7.4 (0.9 ml), 1x PBS pH 7.4 (4.1 ml), and the pre-gel solution (9.0 ml) at 4 °C to reach a final ECM concentration of 6 mg/ml. After, the solution was placed at 37 °C for ~45 min for gelation to occur.

For the suture repair groups, repair of the ACL was performed in the right hindlimb using a #1 Ethibond suture (Ethicon, Inc.) placed at variable depths in the proximal third of the ACL. The same was done in the distal third of the ACL, which resulted in two free suture strands in both the proximal and distal thirds of the ACL (Figure 6A). Next, two bone tunnels were made through both the femur and tibia using a 1.5 mm guide wire. The two femoral tunnels were created by aiming the guide wire at different angles immediately anterior to the insertion of the

ACL. The tibial tunnels were created using a using a drill guide system (Acufex, Smith & Nephew, Andover, MA) placed immediately medial and lateral to the tibial insertion of the ACL. This technique created bone bridges to tie the sutures later in the procedure. The free ends of the sutures were passed through the opposite bone tunnels and were loosened to avoid interference with the rest of the surgical procedure.

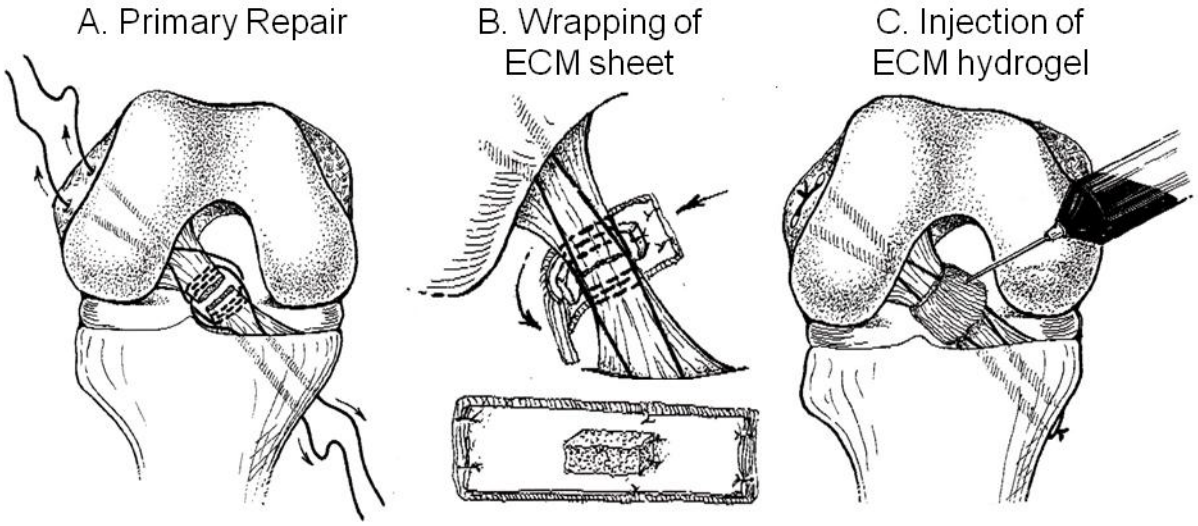

Figure 6. Details on suture repair (A), application of ECM bioscaffold (B), and injection of ECM hydrogel (C).

For all ECM-treated animals, the ECM sheet and fibrin sponge were placed posterior to the ACL stumps, with the fibrin sponge facing the anterior direction (Figure 6B). A small amount of the ECM hydrogel (1-2 ml) was injected into the sponge and allowed to soak for 2-3 minutes. Then, the free ends of the repair sutures were tied under manual tension to reapproximate the ACL tissue stumps and complete the repair. The ECM sheet and fibrin sponge were then wrapped around the ACL stumps and sutured so as to completely enclose the injury site. After, the ECM hydrogel (1-2 ml) was again injected into the injury site (Figure 6C).

The defect site in the suture repair only group will undergo the same suture procedures, only without ECM-treatment.

For the suture augmentation groups, each augmentation was created by passing two sutures (#2 Fiberwire, Arthrex, Inc., Memphis, TN) directly from the bone tunnels in the femur and tibia. For fixation, a large knot was created in the sutures, which was pulled snugly against the outer femoral cortex, while button fixation (Arthrex, Inc., Memphis, TN) was used on the tibial side at 60° of knee flexion under maximum manual tension.

For the first part of Specific Aim 2.1, two femoral tunnels were created and compared: 1) a tunnel anterior to the ACL footprint at the femoral origin (F_A), and 2) a tunnel through the ACL footprint at the femoral origin (F_T) (Figure 7A). For the tibial tunnel location, two groups were compared: 1) a single tunnel medial to the ACL footprint at the tibial insertion (T_M), and 2) tunnels medial and lateral to the ACL footprint at the tibial insertion (T_{LM}) (Figure 7B).

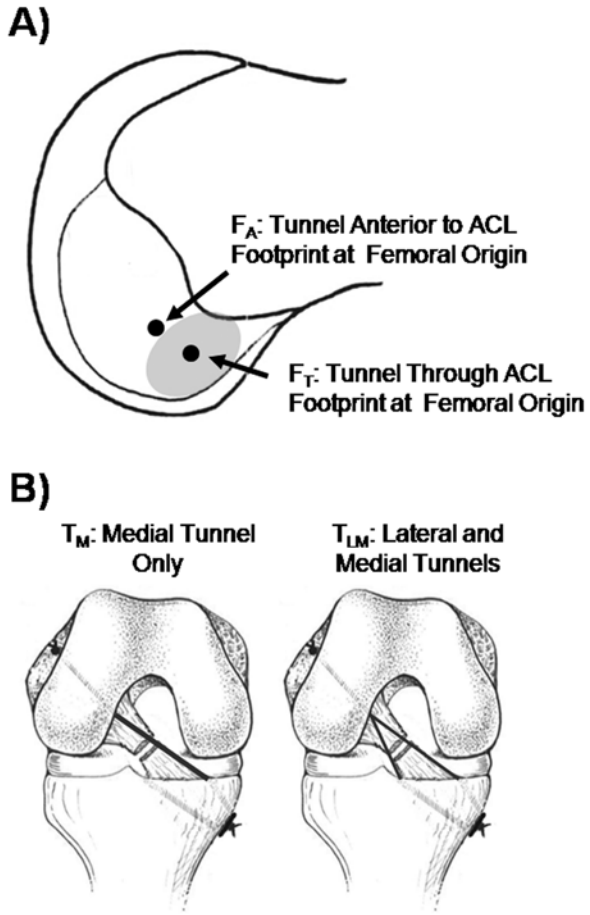

Figure 7. Schematic diagram depicting the tunnel locations for suture augmentation. For F_A, a tunnel was located anterior to the ACL footprint at the femoral origin, while for F_T, the tunnel was located through the ACL footprint at the femoral origin (A). In the T_M and T_{LM} augmentations, tunnels located medial and medial + lateral to the ACL footprint at the tibial insertion were utilized, respectively (B) (reprinted with permission from [69]).

Based on the results of the first portion of Specific Aim 2.1 (Section 6.1.1), a single femoral tunnel was created anterior to the femoral insertion of the ACL (Figure 7A), and a tibial tunnel was created medial to the ACL insertion (Figure 7B) for the second portion of Specific Aim 2.2. For Specific Aim 2.2, a simple suture repair using a modified Kessler technique and #2-0 Vicryl sutures (Ethicon, Inc.) was done in addition to suture augmentation (Figure 8). All

sutures were loosened to avoid interference with the rest of the surgical procedure. For both suture groups, the ACL was fully transected after placement of the sutures.

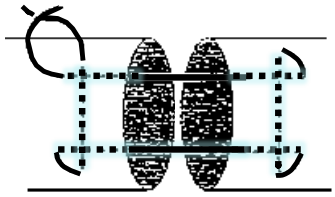

Figure 8. Illustration of Kessler technique for suture repair.

In all animals, the wounds were closed using standard suture technique. The capsule and skin were then closed. In the sham-operated control joint, the skin and capsule were incised and closed in the same manner as the treatment groups, without injuring the ACL.

Post-operatively, all animals were allowed free cage activity (cage area: 3 m^2). The status of weight bearing and general health condition of all animals were monitored during recovery. Banamine (1.1 mg/kg) was administered twice a day for five days post-operatively as an analgesic. To humanely euthanize the animals, ketamine was injected intramuscularly (30 mg/kg) for sedation, followed by a lethal injection of sodium pentobarbital (1 ml (390 mg)/ 10 lbs).

4.4 METHODS OF EVALUATION

For all specimens, digital photographs of the ACL were taken for gross observations. Histological analyses (Section 4.4.1) including hemotoxylin and eosin (H&E), were used to determine collagen fiber alignment and organization. Biomechanical testing included using a

robotic/UFS testing system to assess measure knee function (Section 4.4.2.1), a laser micrometer system to accurately measure of the cross-sectional shape and area (Section 4.4.2.2), followed by using an Instron testing machine (model 5565) to measure the structural properties of the FATCs (Section 4.4.2.3) [3, 190, 213].

4.4.1 Histomorphology

Portions (distal, middle, or proximal) of the healing ACL were sectioned for histological evaluation which was used to visualize the distribution and arrangement of matrix within the ACL as well as the relative number and morphology of the cells within the tissue. For histological examination, the ACLs were examined grossly, carefully removed at the insertion sites at the femur and tibia, embedded in O.C.T. compound, and frozen immediately in liquid nitrogen following euthanasia. Serial cryosections of 8 μm thickness were cut through the healing tissue (both sagittal and transverse sections). Slides were stained with hematoxylin and eosin and observed under a light microscope.

4.4.2 Biomechanical testing

For Specific Aims 1 and 2.2, after the animals were euthanized, their hindlimbs were disarticulated at the hip joint, wrapped in saline-soaked gauze, placed in double plastic bags, and immediately stored at –20°C [265]. Prior to testing, specimens were thawed overnight at room temperature. Surrounding tissues beyond 10 cm proximal and distal to the joint line were removed. Specimens were kept moist with a 0.9% saline solution during dissection and biomechanical testing.

4.4.2.1 Joint Kinematics and In-Situ Forces in Ligaments

The robotic/UFS testing system is an innovation developed in our research center over the past two decades and was used to determine the kinematics of the goat stifle joint, as well as non-contact measurements of in-situ forces in the ACL and other tissues of the joint under the application of externally applied loads [4, 5, 190, 203, 271]. The system consists of a 6-degree of freedom (DOF) robotic manipulator (Puma Model 762, Unimate, Inc.), which is capable of achieving position control of the joint, and a UFS (Model 4015, JR3, Inc., Woodland, California), which can measure three orthogonal forces and moments (Figure 9). The robotic manipulator has a specified repeatability of 0.2 mm and 0.2˚ for position and orientation, respectively, and the UFS is capable of measuring forces and moments with repeatability of 3.5 N and 0.35 N-m, respectively. The UFS enables the system to operate in a force-controlled mode via force feedback from the UFS to the robot to allow the application of specific loads to the knee [4, 5, 152, 190, 271].

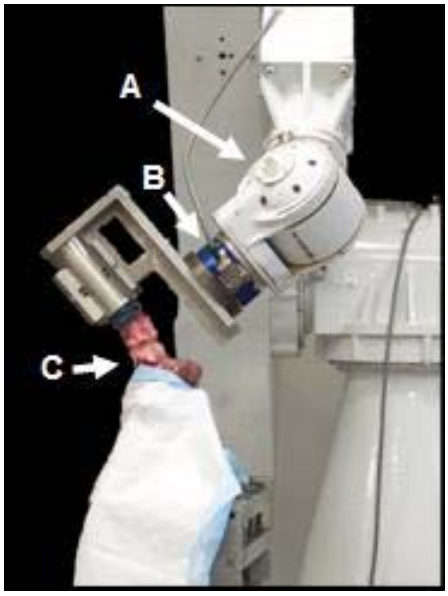

Figure 9. A photograph of a specimen tested on the robotic/ UFS testing system. (A) 6 DOF robotic manipulator; (B) UFS; (C) Goat stifle joint (reprinted with permission from [69]).

The joints were mounted on the robotic/UFS testing system, and the path of passive flexion-extension of the joint was measured at 1º increments throughout a range of joint flexion (from full extension to 90º) by maintaining a net force/moment of zero in all DOF except flexion-extension [203]. The positions that make up this path served as the starting positions for the application of external loads. External loading conditions were then applied at fixed joint flexion angles of 30º, 60º, and 90º degrees. Different experimental protocols were used for the data at time-zero (Specific Aim 2.1) [69] and data at 12 weeks of healing (Specific Aims 1 and 2.2), and the remainder of these protocols will be presented separately.

(a) Protocol for Specific Aim 2.1

Effect of Bone Tunnel Location

The summary of the testing protocol is shown in Table 1. The robotic/UFS testing system was operated in force-control mode to apply external loads to the joint at pre-selected angles of joint flexion (30°, 60°, 90°), while the resulting 5 DOF joint motions (medial-lateral, proximal-distal, anterior-posterior (A-P) translations, and internal-external and varus-valgus (V-V) rotations) were measured [5, 258]. Two loading conditions were used: 1) a 67 N A-P tibial load, and 2) a 5 N-m V-V torque. For the V-V torque, internal-external rotation was constrained using the robotic/UFS testing system. This was done due to the large amount of natural laxity of the goat stifle joint in the internal-external direction, which impacts the ability to apply the V-V torque to the joint. Further, a preliminary study was done to assess the repeatability of the force measurements.

A 67 N A-P tibial load was applied to a set of eight intact joints, and the resulting kinematics were measured. For each joint, the same kinematics were repeated without altering the joint in any way, while measuring new forces. It was found that the robotic testing system could repeat the applied load to within 6-9 N.

Table 1. Outline of experimental protocol and data acquired to assess the effect of the tunnel locations for suture augmentation.

Protocol	Data acquired
I. Intact joint	Intact joint kinematics
Path of passive flexion-extension	
External loading conditions	
A. 67 N anterior tibial load	
B. 5 N-m varus-valgus moment	
Transect ACL	
Repeat kinematics (I.A, I.B)	In-situ forces in ACL
II. ACL-deficient joint	
Apply loads A and B	ACL-deficient joint kinematics
III. Augmented joint	
Perform suture augmentation (Random selection)	
Apply loads A and B	Augmented joint kinematics
Release sutures	
Repeat kinematics (III.A, III.B)	In-situ forces in sutures
Repeat III for each augmentation	

At each joint flexion angle of interest, each loading condition was applied five times to the intact joint. The amount of anterior tibial translation was closely monitored during testing to ensure that there were no significant increases between loading cycles (<0.5 mm). Following application of these loading conditions to obtain the kinematics of the intact joint, the bone tunnels were created, before transecting the ACL. To determine the

influence of the bone tunnels on the joint, the kinematics recorded for the intact joint were repeated by the robotic manipulator while the UFS recorded a new set of forces and moments. These were then compared to the values before the tunnels were made. The difference in forces due to drilling the tunnels (<5 N) were found to be similar to the repeatability of our robotic testing system (6-9 N).

Then, the ACL was completely transected. By the principle of superposition, the difference in the forces measured before and after cutting the ACL was the in-situ force carried by the ACL under the applied loads [83, 258]. Then, the loading conditions were again applied to determine the kinematics of the ACL-deficient joint.

To determine the effect of tunnel locations for suture augmentation, a two-way factorial design was used, as described in Section 4.3. As such, four augmentation groups were utilized and compared (Table 2). For example, the augmentation using the anterior femoral tunnel and a single tibial tunnel was designated as Group 1 (F_A/T_M).

Table 2. Summary matrix of augmentation procedures.

		Femoral Tunnel Location (Relative to ACL origin)	
		Anterior (F_A)	Through Substance (F_T)
Tibial Tunnel Location (Relative to ACL insertion)	Medial Tunnel Only (T_M)	Group 1 (F_A/T_M)	Group 2 (F_T/T_M)
	Medial & Lateral Tunnels (T_{LM})	Group 3 (F_A/T_{LM})	Group 4 (F_T/T_{LM})

The surgical procedure for all augmentation groups was done according to Section 4.3; however, no additional simple suture repair was performed. After, the two external loading conditions were applied and the kinematics of the augmented joint were recorded. The in-situ force carried by the augmentation sutures was obtained by removing the sutures and replaying the kinematics of the augmented joint [83, 258]. This procedure was then repeated for each augmentation. The order of the augmentations was randomized for each specimen.

In-vitro Comparison of Suture Techniques

For the in-vitro comparison of suture techniques, two loading conditions were used: 1) a 67 N A-P tibial load, and 2) a 67 N A-P tibial load with 100 N of axial joint compression. These loads were largely based on those in the literature, and

were meant to approximate the average A-P and axial joint loading during normal gait in the goat [103]. The summary of the testing protocol is shown in Table 3.

Following application of these loading conditions to obtain the kinematics of the intact joint, the ACL was completely transected through a medial arthrotomy, created prior to the start of testing. The kinematics recorded for the intact joint under the loading conditions were repeated by the robotic manipulator while the UFS recorded a new set of forces and moments. By the principle of superposition, the difference in the forces measured before and after cutting the ACL was the in-situ force carried by the ACL under the applied loads [258]. Then, the loading conditions were again applied to determine the kinematics of the ACL-deficient knee.

After, suture repair of the ACL was performed according to Section 4.3. Following fixation, the two external loading conditions were applied and the kinematics of the suture repaired joint were recorded. The in-situ force carried by the repair sutures was obtained using the principle of superposition by removing the sutures and replaying the kinematics of the repaired joint to obtain a new set of forces and moments [258]. Then, suture augmentation was done according to Section 4.3. Like for suture repair, the kinematics of the suture augmented joint and the in-situ force carried by the augmentation sutures were determined [258].

To determine the relative contribution of the other tissues of the joint, each tissue of interest was sequentially removed. Then, the kinematics for the intact, ACL-deficient, suture repaired, and suture augmented conditions were repeated while recording new forces in order to determine the in-situ force in each tissue.

This procedure was done for the MCL, lateral collateral ligament (LCL), medial meniscus, and lateral meniscus. After removal of all soft tissue, only the bony contact connected the femur and tibia, and thus, the remaining forces during replay of the kinematics represented those due to bony contact.

Table 3. Outline of experimental protocol and data acquired to compare suture repair and suture augmentation.

Protocol	Data acquired
I. Intact joint	Intact kinematics
Path of passive flexion-extension	
External loading conditions	
A. 67 N anterior tibial load (ATL)	
B. 67 N ATL + 100 N joint compression	
Transect ACL	
Repeat kinematics (I.A, I.B)	In-situ forces in ACL
II. ACL-deficient joint	
Apply loads I.A and I.B	ACL-deficient kinematics
III. Suture repair	
Perform suture repair	
Apply loads I.A and I.B	Suture repair kinematics (III.A, III.B)
Release sutures	
Repeat kinematics (III.A, III.B)	In-situ forces in repair sutures
IV. Suture augmentation	
Perform suture augmentation	
Apply loads I.A and I.B	Augmentation kinematics (IV.A, IV.B)
Release sutures	
Repeat kinematics (IV.A, IV.B)	In-situ forces in augmentation sutures
V. Remove soft tissue (e.g. MCL)	
Repeat kinematics (I, II, III, IV)	In-situ forces in soft tissue
(repeat for each soft tissue of interest)	

(b) Protocol for Specific Aims 1 and 2.2

For Specific Aims 1 and 2.2, a single loading condition was used: a 67 N A-P tibial load. Afterward, the MCL, LCL, capsule, medial meniscus, lateral meniscus, and bony contact were removed sequentially. Following each step, the kinematics found for each loading condition were repeated while recording new sets of forces. The difference in forces represented the in-situ force in each tissue, via the principle of superposition. After removal of the bony contact, only the ACL connected the femur to the tibia. Thus, at this step, any forces recorded during replay of the kinematics represented the in-situ forces of the ACL under the external loading condition. Afterward, the CSA and biomechanical properties of the ACL were determined.

4.4.2.2 Cross-Sectional Area and Shape Measurements

A laser micrometer system was used to determine the CSA of the ACL [138]. The accuracy of the CSA has been determined to be within 5.0% for known shapes and the measurements can be done in approximately 1 minute, limiting dehydration of soft tissues. The FATCs were removed from the robotic/UFS testing system and mounted on the laser micrometer system. The CSA and shape measurements were made at the longitudinal center of the ligament [213].

4.4.2.3 Uniaxial Tensile Testing

All FATCs were secured in customized clamps, which were mounted onto a materials testing machine (Instron^{TM} 5565) (Figure 10) [4, 171, 213]. A crosshead speed of 10 mm/min was used for all tests. The specimens were preloaded to 2 N and preconditioned between limits of elongation that equate to loading within the toe region of the load-elongation curve (0-1 mm).

Following these steps, the ACL was left unloaded for 15 minutes. After, the 2N preload was reapplied, and specimens were loaded to failure. The structural properties (i.e., stiffness, ultimate load to failure, elongation to failure, and energy absorbed) of the FATCS were determined from the load-elongation curves [4, 171, 213]. The slope of the linear region of the curve such that $R^2 > 0.995$ was defined as the stiffness.

Figure 10. Femur-ACL-tibia complex mounted within custom clamps on a materials testing machine for uniaxial tensile testing.

4.4.3 Data analysis

Statistical analyses were done using SPSS software (Version 14.0, SPSS, Inc.). For all data, normality was checked using the Kolmogorov-Smirnov test [102]. If the data are not normally distributed, non-parametric tests replaced the parametric tests described below. For all tests, overall significance was set at $p<0.05$. If multiple comparisons were done, a Bonferroni correction was performed such that $p=0.05/n$, where n is the number of comparisons made.

For Specific Aim 1, the joint kinematics, in-situ forces, CSA, and biomechanical properties of the two treatment groups were compared to their respective control groups using a paired t-test and compared to each other using an unpaired t-test. For both parts of Specific Aim 2.1, a repeated measures ANOVA was utilized to compare joint kinematics and the in-situ forces in the tissues. To determine statistical differences between groups, a Bonferroni post-hoc was done. For Specific Aim 2.2, statistical comparisons were performed as in Specific Aim 1.

5.0 BIOLOGICAL AUGMENTATION OF THE ACL THROUGH EXTRACELLAR MATRIX BIOSCAFFOLDS

The suture repair technique characterized in Section 4.3 was utilized in Specific Aim 1, in which ECM bioscaffolds were applied to enhance healing of the ACL [67, 70, 71]. An ECM sheet was wrapped around the injury site, so as to completely enclose it (Figure 6). Then, an ECM hydrogel was injected, so as to fill the injury site (Figure 6).

5.1 JOINT STABILITY

All goats tolerated surgery well and were ambulating with a slight limp within a few hours following surgery. Daily inspection of the animals revealed that their weight-bearing had returned to normal within the first two weeks. Afterward, all animals were mobile and moved freely with no noticeable limping.

Figure 11A details the joint function, as represented by the curves for the A-P tibial translation (A-PTT) in response to the 67 N A-P tibial load at 30° of flexion as measured by the robotic/UFS testing system. To provide a consistent reference position for all stifle joints, the A-PTT began at the 67 N posterior tibial load. It could be seen that the curves for all groups were nonlinear. The amount of translation for the experimental groups was much higher, and the difference began at low loads. The suture repair group showed larger amounts of A-PTT than

the ECM-treated group. Similar results were observed with the stifle joint at 60° and 90° of flexion (Table 4). In all three groups, the A-PTT increased from 30° to 60° and then decreased at 90°. Both treatment groups had statistically higher A-PTT compared to those for the sham-operated controls at 30°, 60° and 90° of flexion ($p<0.05$). For statistical comparison of joint kinematics data between groups, it is suitable to normalize the A-PTT with respect to the sham-operated control groups of each animal to take into account the interspecimen variability (Figure 11B). Between treatment groups, the normalized values for A-PTT for the ECM treated group were 30%, 24%, and 13% lower than those for the suture repair group at 30°, 60° and 90° of flexion, respectively. However, these differences were not statistically significant ($p>0.05$).

A.

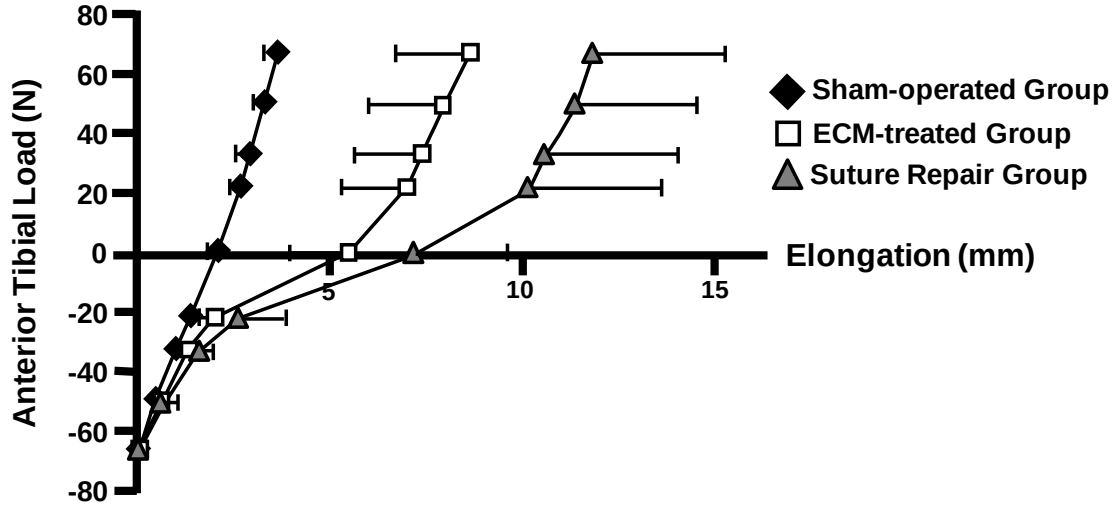

B.

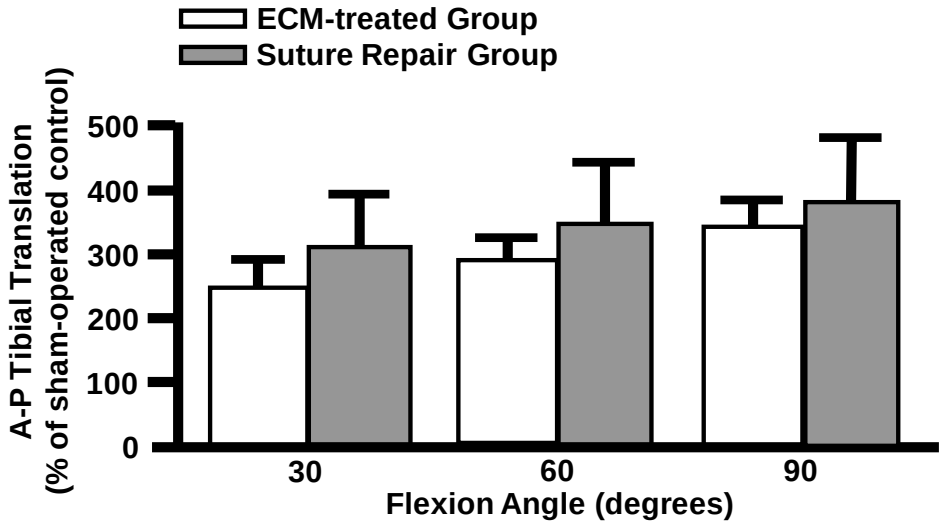

Figure 11. A) Average curves for the A-PTT in response to the 67 N A-P tibial load as measured by the robotic/UFS testing system at 30° of flexion for the sham-operated, ECM-treated, and suture repair groups. **B)** A-P tibial translation of the ECM-treated and suture repair groups in response to an 67-N anterior tibial load normalized to their respective intact joint controls (mean ± SD).

Table 4. Anterior-posterior tibial translations (mm) of the goat joints 30°, 60°, and 90° of joint flexion under an 67-N anterior-posterior tibial load (mean ± sd). *Indicates a statistically significant difference compared to the respective sham-operated controls ($p<0.05$).

	Joint Flexion Angle		
	30°	60°	90°
I. ECM-treated Group			
Sham-operated Control	3.4 ± 0.4	3.9 ± 0.5	3.0 ± 0.5
Experimental	8.6 ± 2.0*	11.3 ± 2.1*	10.2 ± 1.9*
II. Suture Repair Group			
Sham-operated Control	3.8 ± 0.2	4.1 ± 0.3	2.8 ± 0.4
Experimental	11.8 ± 3.4*	14.4 ± 4.2*	10.8 ± 3.3*

In terms of the in-situ force of the ACL under the 67 N anterior tibial load, its anterior component at 30° of flexion was plotted against the amount of A-PTT (Figure 12A). For consistency, the A-PTT for all groups was normalized to the respective sham-operated control group. In general, the sham-operated ACLs carried the vast majority of the applied anterior tibial load. A similar response was found for the ECM-treated healing ACLs; however, the suture repaired ACLs carried markedly lower anterior force. Similar findings were obtained at with the stifle joint at 60° and 90° of flexion.

A.

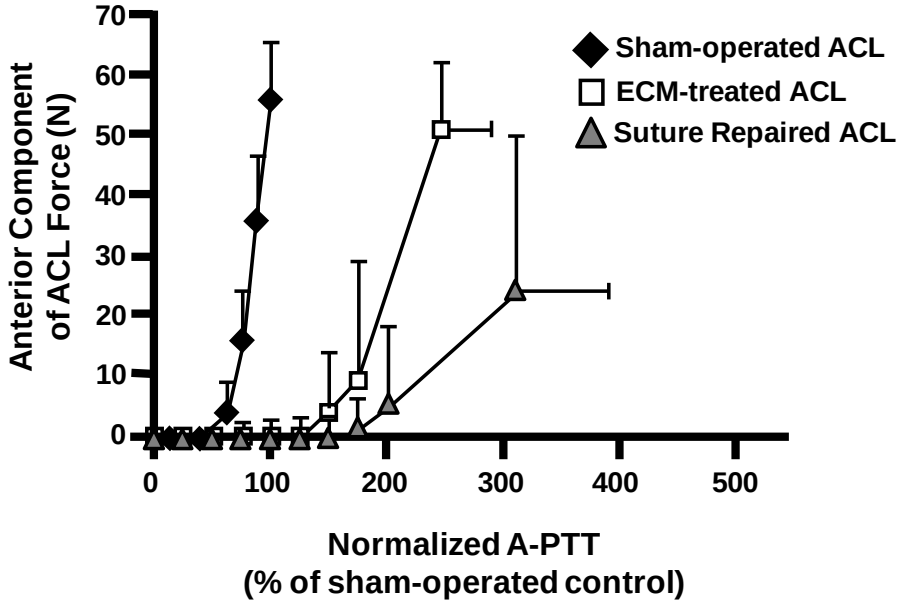

B.

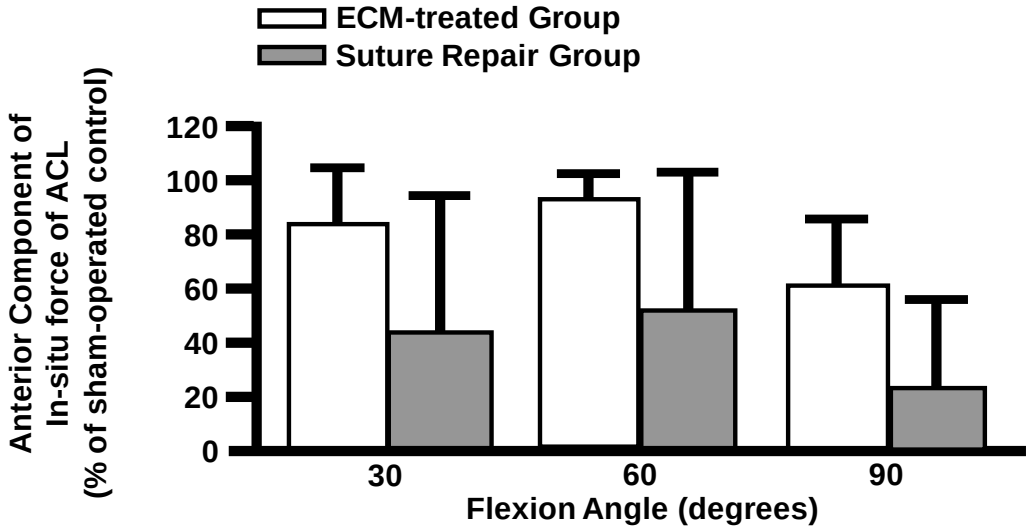

Figure 12. A) Anterior component of the in-situ force of the ACL as a function of the A-PTT at 30° of flexion for the sham-operated, ECM-treated, and suture repair groups. Note: Values of A-PTT are normalized to the A-PTT for the respective sham-operated control group. **B)** Anterior component of the in-situ force healing ACLs of the ECM-treated and suture repair groups normalized by the values for the sham-operated ACLs.

Table 5. Resultant in-situ force of the ACL (in N) at 30°, 60°, and 90° of joint flexion under a 67-N anterior tibial load (mean ± sd). *Indicates a statistically significant difference compared to the respective sham-operated controls ($p<0.05$).

	Joint Flexion Angle		
	30°	60°	90°
I. ECM-treated Group			
Sham-operated Control	62 ± 5	54 ± 6	53 ± 5
Experimental	52 ± 11	52 ± 8	31 ± 12*
II. Suture Repair Group			
Sham-operated Control	50 ± 12	51 ± 11	53 ± 7
Experimental	26 ± 24	29 ± 25	13 ± 15*

Quantitative data on the resultant in-situ force of the ACL are presented in Table 5. The intact ACL carried forces ranging from 50-62 N on average throughout joint flexion. For both treatment groups, the highest values of in-situ force of the healing ACL were found at 30° and 60° of flexion and were not statistically significant from their respective sham-operated controls ($p>0.05$). In fact, the ECM-treated group, the in-situ force in the healing ACL was found to be 84% and 96% of those for the sham-operated ACLs. At 90° of flexion, both treatment groups had significantly lower values than the sham-operated control groups ($p<0.05$). Similar to the joint kinematics, it is useful to normalize the anterior component of the in-situ force of the ACL with respect to the sham-operated control groups to compare treatment groups (Figure 12B). Following this step, the average values for the ECM-treated group were 92%, 76% and 142% larger than those for the suture repair group at 30°, 60°, and 90°, respectively. However, again, these differences were not statistically significant ($p>0.05$).

5.2 GROSS MORPHOLOGY AND DIMENSIONS

Gross observation revealed that the sham-operated ACLs were white and opaque, consisting of distinct bundles with clearly observable collagen fiber orientation (Figure 13A). In the ECM-treated ACLs, there was continuous neo-tissue formation for all specimens, with no noticeable concavities (Figure 13B). The neo-tissues were slightly reddish in color but were less opaque than the sham-operated control ACLs. Overall, a small amount of hypertrophy of the ECM-treated ACLs could be seen compared to the sham-operated controls. This observation was confirmed in the CSA measurement as the healing ACLs for the ECM-treated group were 29.0 ± 19.3 mm², whereas those for the sham-operated control group were 23.0 ± 4.6 mm². The difference was not statistically significant ($p>0.05$). It should be noted that one specimen in the ECM-treated group, did show significant hypertrophy with a CSA measuring 69.2 mm^2. Upon visual inspection, it was observed that the tissue on the anterior portion of the ACL was likely not contributing to the function of the ACL, as its appearance and quality were substantially lower than toward the posterior regions. However, this tissue was connected to the sutures as well as the rest of the healing tissue, and thus, could not be removed without potentially damaging the ACL. In the other specimens, little tissue hypertrophy was observed. In the suture repair group, however, there was only a small amount of neo-tissue found, most of which was directly attached to the repair sutures (Figure 13C). In total, four specimens showed some tissue formation, two had very little, and one had no tissue formation at all. Quantitatively, the values for the CSA of the healing ACLs were only 34% of those for the sham-operated control group (6.5 ± 4.3 mm² vs. 21.6 ± 5.6 mm², respectively), and the difference was statistically significant ($p<0.05$). When normalized by their respective sham-operated control of each animal, the

experimental/control values for the CSA from the ECM-treated group was four times those of the suture repair group (127 ± 90 % vs. 34 ± 25 %, respectively, $p<0.05$; Figure 14).

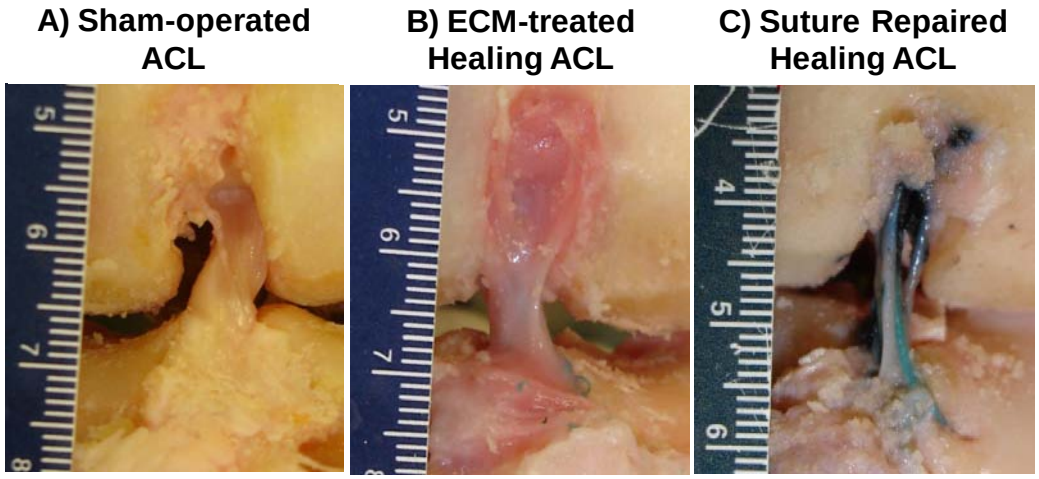

Figure 13. Gross morphology of (A) sham-operated ACL, (B) ECM-treated healing ACL, and (C) suture repaired healing ACL at 12 weeks of healing.

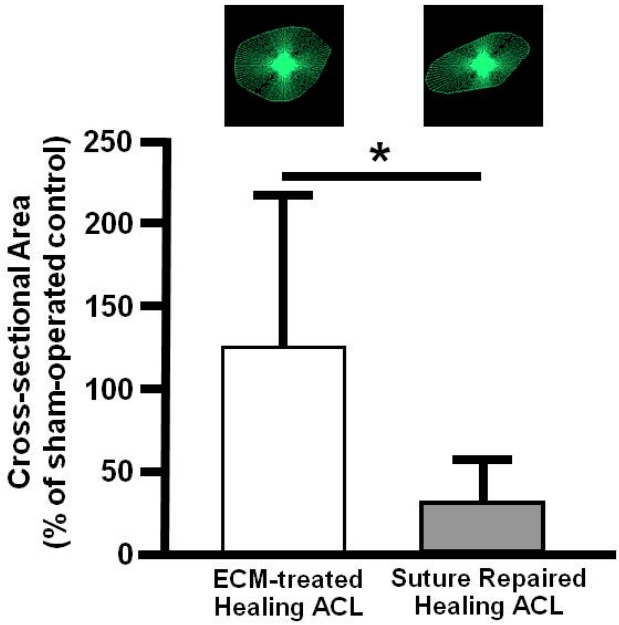

Figure 14. The cross-sectional area of healing ACLs for the ECM-treated and suture repair groups at 12 weeks post-surgery normalized by the values for the respective sham-operated ACLs. Examples of the cross-sectional shape are also shown above each bar graph. *Indicates a statistically significant difference ($p<0.05$).

5.3 HISTOLOGICAL EVALUATION

Histologically, the midsubstance of the ACL in the sham-operated group showed compact collagen fibers that were highly aligned with many regularly interspersed spindle-shaped cells (Figure 15A). For two of the four samples from the ECM-treated group and one of the two samples from the suture repair only group, aligned collagen fibers parallel to the longitudinal axis of the ligament were observed with many spindle-shaped cells oriented along the collagen fibers (Figure 15B). However, at this stage of healing, the matrix was not as dense as the sham-operated controls. In addition, there were more cells in the ECM-treated healing ACL, most of which were spindle-shaped. On the other hand, for the other two samples from the ECM-treated

group and one sample from the suture repair group, there were only sparse collagen fibers without clear alignment (Figure 15C). It should be noted that these two samples from the ECM-treated group were from the first two animals used in the study, and the poor results could be partially attributed to a lack of surgical skill. Nevertheless, the high variability in outcome was clear from the histological evaluation.

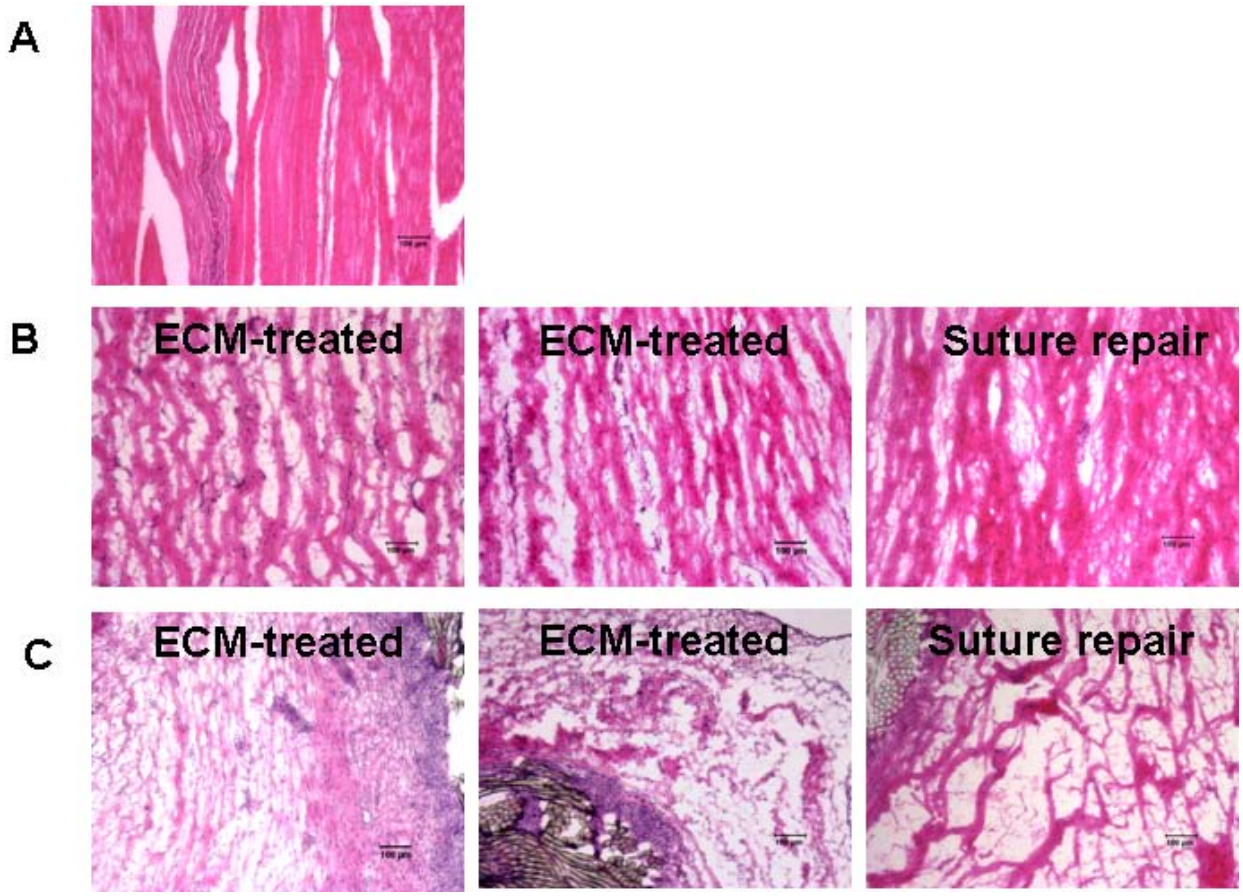

Figure 15. Histological appearance of the (A) sham-operated ACL as well as the ECM-treated and suture repaired healing ACLs at 12 weeks of healing showing (B) good tissue formation and (C) poor tissue formation (100x magnification).

5.4 TENSILE PROPERTIES

Figure 16 details the nonlinear load-elongation curves for the ECM-treated and suture repair groups. Typically, the toe region existed for up to 1-1.5 mm of elongation, followed by a linear region until failure. All specimens were found to fail in the tissue midsubstance of the healing ACL.

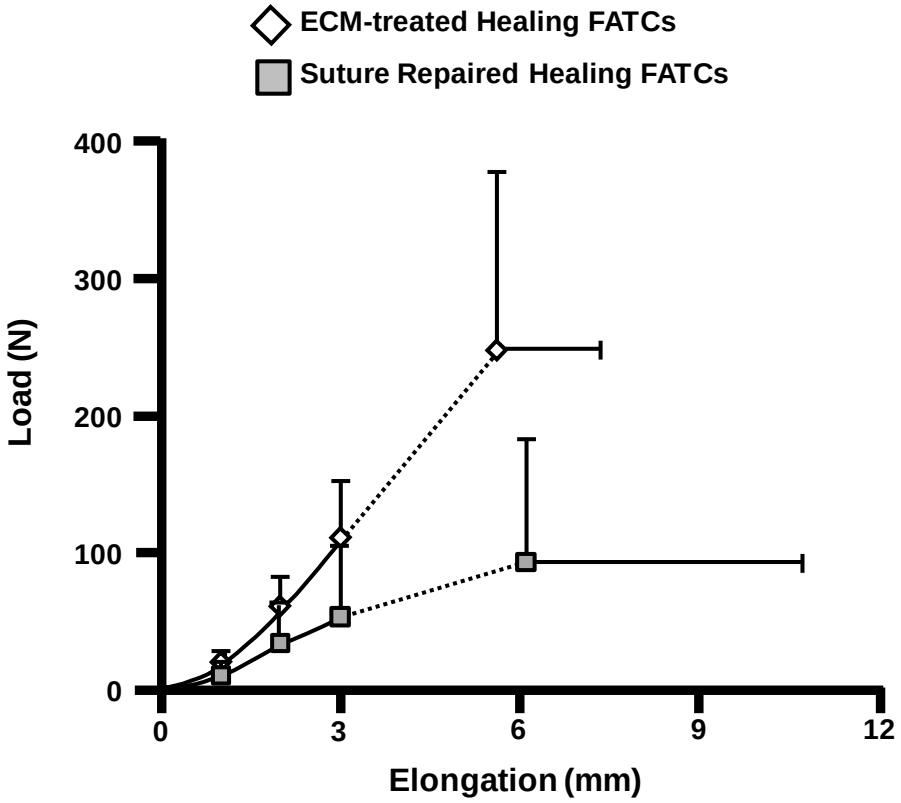

Figure 16. Average load-elongation curves of the ECM-treated and suture repair groups at 12 weeks post-surgery.

Data on the parameters representing these structural properties of the FATCs are detailed in Table 6. For both the ECM-treated and suture repair groups, the values for stiffness, ultimate load, and ultimate elongation were below the values for their respective sham-operated groups ($p<0.05$). Again, the data was normalized with respect to the sham-operated controls for

statistical comparisons between experimental groups (Figure 17). The linear stiffness of the ECM-treated FATCs was 140% greater than those for the suture repair group (experimental/control was 48 ± 19% vs. 20 ± 18%, respectively, $p<0.05$). Similarly, the mean values for the ultimate load were 90% higher with ECM-treatment (16 ± 9% vs. 9 ± 9%, respectively); however, these differences were not statistically significant ($p>0.05$). The ultimate elongation was similar between the two groups (38 ± 14% vs. 30 ± 19%, respectively, $p>0.05$).

Table 6. Parameters representing the structural properties of the femur-ACL-tibia complexes for the sham-operated control, ECM-treated and suture repair groups at 12 weeks post-surgery (mean ± sd). *Indicates a statistically significant difference compared to the respective sham-operated controls ($p<0.05$).

	ECM-treated Group		Suture Repair Group	
	Sham-operated Control	Healing	Sham-operated Control	Healing
Stiffness (N/mm)	112 ± 21	53 ± 19*	125 ± 23	24 ± 21*
Ultimate Load (N)	1624 ± 235	249 ± 129*	1385 ± 365	95 ± 90*
Ultimate Elongation (mm)	15.3 ± 2.9	5.6 ± 1.7*	19.0 ± 6.3	6.1 ± 4.6*

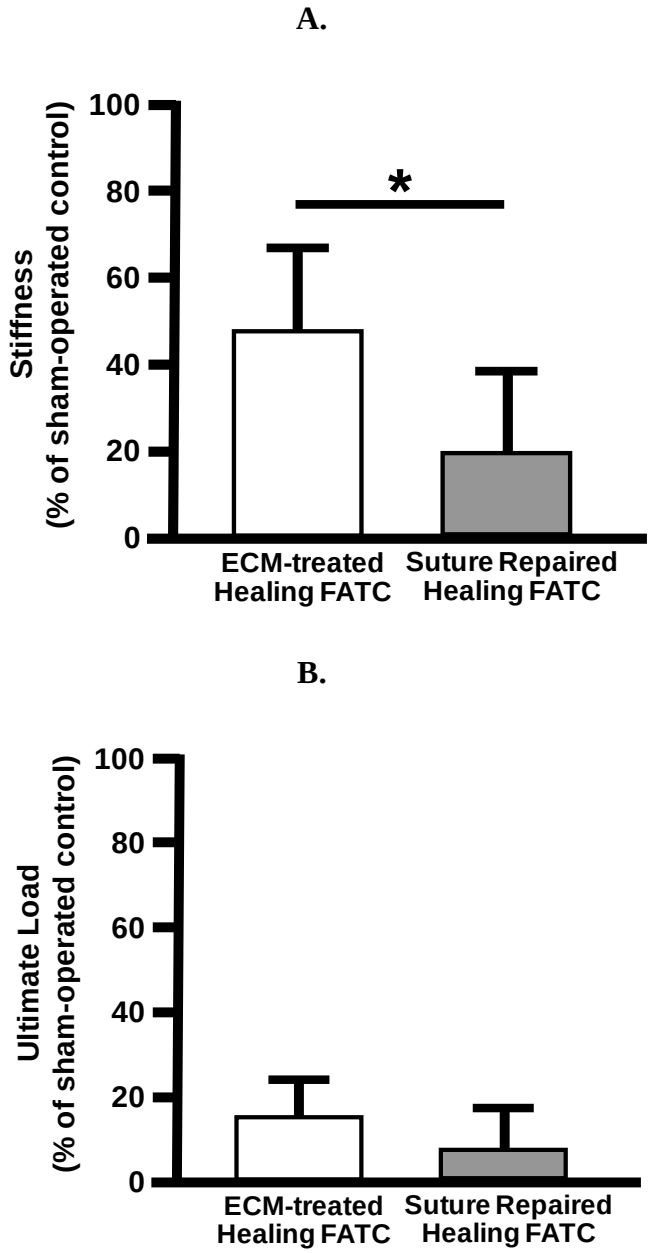

Figure 17. Stiffness (A.) and ultimate load (B.) of the healing femur-ACL-tibia complexes for the ECM-treated and suture repair groups as a percentage of the sham-operated controls at 12 weeks post-surgery. *Indicates a statistically significant difference ($p<0.05$).

6.0 MECHANICAL AUGMENTATION OF THE HEALING ACL THROUGH SUTURE TECHNIQUES

6.1 AIM 2.1- IN-VITRO EVALUATION OF SUTURE TECHNIQUES

In Specific Aim 2.1, the suture repair and suture augmentation techniques were compared in-vitro in a set of goat knees using the robotic/UFS testing system to determine their ability to restore initial joint stability as well as maintain in-situ forces similar to that of the normal ACL [67-69].

6.1.1 Effect of Tunnel Location for Suture Techniques on Joint Stability

Since both suture techniques required creating bone tunnels in the femur and tibia, it was important to first determine whether the locations of these bone tunnels had a significant impact on the resulting joint stability [69]. As described in Section 4.4.2.1(a), a two-way factorial design was used (Table 2). Suture augmentation was used for this study, since it is easier from a technical standpoint, as well as more repeatable than suture repair (which would require that since the ACL tissue to be repaired multiple times). Two femoral tunnels were created and compared: 1) a tunnel anterior to the ACL footprint at the femoral origin (F_A), and 2) a tunnel through the ACL footprint at the femoral origin (F_T) (Figure 7). For the tibial tunnel location, two groups were compared: 1) a single tunnel medial to the ACL footprint at the tibial insertion

(T_M), and 2) tunnels medial and lateral to the ACL footprint at the tibial insertion (T_{LM}) (Figure 7). We hypothesized that sutures placed through the ACL footprint at the femoral origin will better restore kinematics compared to a more anterior femoral tunnel placement because the location better replicates the footprint of the ACL. We further hypothesized that the effect of tibial tunnel location will be negligible since the tunnels are placed similarly in the sagittal plane while the slight difference in the frontal plane would result in a minimal shift in the line of action of the sutures.

6.1.1.1 Joint Kinematics and In-situ Forces under 67 N Anterior Tibial Load

The data on joint kinematics in response to a 67 N anterior tibial load as measured by the robotic/UFS testing system are detailed in Table 7. For all experimental conditions, values for ATT were higher at 30° and 60° and then decreased at 90°. For the intact joint, mean ATT was found to range from 1.9 to 2.5 mm for the three joint flexion angles tested. Corresponding values for the ACL-deficient joint were 12.8 to 15.5 mm, representing a very large increase of 6-7 fold ($p<0.05$). Following suture augmentation, the ATT was reduced to 2.5 to 5.2 mm and was 10.3-11.2 mm lower than the ACL-deficient joint throughout the joint flexion angles tested ($p<0.05$). More importantly, there was no statistically significant difference from those of the intact joint (maximum difference of means of 2.9 mm, 2.4 mm, and 1.3 mm) at 30°, 60°, and 90°, respectively ($p>0.05$). Statistical comparisons showed no significant differences between the four augmentation groups at all three flexion angles, with the largest difference in mean values of 0.8 mm between them ($p>0.05$).

In terms of the in-situ forces, the intact ACL carried mean forces ranging from 56 N to 69 N in response to the 67 N anterior tibial load throughout the range of flexion (Table 7). Similar values were found for the sutures in all of the four augmentation groups. The maximum

difference in means was only 11 N, 6 N, and 9 N from the intact ACL at 30°, 60°, and 90°, respectively ($p>0.05$). The only two exceptions were that Group 1 (F_A/T_M) and Group 2 (F_T/T_M) were statistically significantly lower than those for the intact ACL at 30° ($p<0.05$). When compared between the four experimental groups, the findings were the same as for ATT, as there were no significant differences in the in-situ forces between them ($p>0.05$).

Table 7. Anterior tibial translation (A) and in-situ forces carried by the intact ACL and augmentation sutures (B) of the goat joints in response to an 67 N anterior tibial load at 30°, 60°, and 90° of joint flexion (Mean ± SD).

	A. Anterior Tibial Translation (mm)			B. In-situ Force of ACL/Sutures (N)		
Flexion Angle (degrees)	30	60	90	30	60	90
Intact Joint	2.3 ± 0.5	2.5 ± 0.5	1.9 ± 0.6	69 ± 6	63 ± 4	56 ± 7
ACL-deficient Joint	15.3 ± 2.2*	15.5 ± 3.0*	12.8 ± 3.3*	NA	NA	NA
Suture Augmented Joint						
Group 1 (F_A/T_M)	5.2 ± 1.9	4.9 ± 1.9	2.8 ± 1.8	60 ± 4$^+$	57 ± 6	51 ± 6
Group 2 (F_T/T_M)	4.8 ± 1.8	4.5 ± 1.7	2.7 ± 1.7	58 ± 7$^+$	62 ± 5	52 ± 8
Group 3 (F_A/T_{LM})	4.4 ± 1.5	4.3 ± 1.4	2.5 ± 1.5	61 ± 5	60 ± 5	52 ± 10
Group 4 (F_T/T_{LM})	4.7 ± 1.7	4.6 ± 1.6	3.2 ± 1.6	62 ± 5	60 ± 6	47 ± 13

*$p < .05$ compared with all other joint conditions at the same flexion angle

$^+p < .05$ compared to intact joint at the same flexion angle

6.1.1.2 Joint Kinematics and In-situ Forces under 5 N-m Varus-Valgus Torque

The data on joint kinematics in response to a 5 N-m valgus torque are detailed in Table 8. The intact joint had higher values at 90° and lower values at 30°. The trends were opposite for both the ACL-deficient and suture augmented conditions. For the intact joint, mean values for ATT for the intact joint ranged from -0.3 to 0.2 mm for the three joint flexion angles tested. With ACL-deficiency, the range of mean values was 2.5 to 5.0 mm, although these increases were not statistically significant ($p>0.05$). Following suture augmentation, mean ATT was reduced to -0.4 to 1.3 mm. There was no statistically significant difference from those of the intact joint (maximum difference in means of 1.6 mm, 0.4 mm, and 0.4 mm) at 30°, 60°, and 90°, respectively ($p>0.05$). Further, there were no statistically significant differences between the four experimental groups, with the largest difference of only 0.3 mm in mean values between them ($p>0.05$).

In terms of the in-situ forces under the 5 N-m valgus torque, the intact ACL carried mean forces ranging from 19 N at 90° to 31 N at 30° (Table 8). Corresponding values for the augmentation sutures were not statistically different from the intact ACL and ranged from 13 to 16 N on average ($p>0.05$). When compared between the four experimental groups, there were no significant differences in the in-situ forces between them ($p>0.05$).

Table 8. Anterior tibial translation (A) and in-situ forces carried by the intact ACL and augmentation sutures (B) of the goat joints in response to an 5 N-m valgus torque at 30°, 60°, and 90° of joint flexion (Mean ± SD).

	A. Anterior Tibial Translation (mm)			B. In-situ Force of ACL/Sutures (N)		
Flexion Angle (degrees)	30	60	90	30	60	90
Intact Joint	-0.3 ± 0.4	0.2 ± 0.7	0.0 ± 1.2	31 ± 13	22 ± 10	19 ± 8
ACL-deficient Joint	4.7 ± 4.5	5.0 ± 6.1	2.5 ± 4.8	NA	NA	NA
Suture Augmented Joint						
Group 1 (F_A/T_M)	1.0 ± 1.3	0.4 ± 1.2	-0.4 ± 1.3	13 ± 8	13 ± 6	16 ± 12
Group 2 (F_T/T_M)	0.9 ± 1.1	0.4 ± 1.0	-0.3 ± 1.3	14 ± 7	15 ± 9	15 ± 10
Group 3 (F_A/T_{LM})	1.2 ± 1.5	0.6 ± 1.5	-0.4 ± 1.3	15 ± 6	13 ± 5	16 ± 7
Group 4 (F_T/T_{LM})	1.3 ± 1.5	0.6 ± 1.4	-0.1 ± 1.5	14 ± 8	15 ± 8	13 ± 9

The data on joint kinematics in response to a 5 N-m varus torque are detailed in Table 9. Similar to the 5 N-m valgus torque, the intact joint had higher values at 90° and lower values at 30°, while the opposite trends were observed for the ACL-deficient and suture augmented conditions. Mean values of ATT for the intact joint ranged from -0.2 to 0.5 mm for the three flexion angles tested. With ACL-deficiency, the corresponding range was 11.7 to 8.0 mm, which corresponded to an increase of 7.5 to 11.9 mm ($p<0.05$). After suture augmentation, the mean ATT was reduced to 1.4 to 4.2 mm. At 30°, the mean ATT for all augmentation groups were approximately 4.0 mm greater than that of the intact joint ($p<0.05$). At 60°, mean values of ATT for all groups were within 3.0 mm of that for the intact joint, with the only statistically significant difference between the intact joint and Group 3 (F_A/T2) ($p<0.05$). At 90°, all augmentation groups restored mean ATT to within 1.6 mm, and were not significantly different from the intact joint ($p>0.05$). At all flexion angles, the values after augmentation were significantly lower than the ACL-deficient joint ($p<0.05$). No significant differences were found between the augmentations, with a maximum difference in means of only 0.7 mm at 90° ($p>0.05$).

In terms of the in-situ forces under the 5 N-m varus moment, the intact ACL was found to carry mean forces ranging from 59 at 30° to 65 N at 90° (Table 9). At 30° of flexion, the mean in-situ forces of all augmentations were 12-16 N lower than those for the intact ACL ($p<0.05$); however, similar values were observed at 60° and 90° of joint flexion compared to those for the intact ACL ($p>0.05$). When comparing between the four experimental groups, there were no significant differences in the in-situ forces carried by the sutures ($p>0.05$).

Table 9. Anterior tibial translation (A) and in-situ forces carried by the intact ACL and augmentation sutures (B) of the goat joints in response to an 5 N-m varus torque at 30°, 60°, and 90° of joint flexion (Mean ± SD).

	A. Anterior Tibial Translation (mm)			B. In-situ Force of ACL/Sutures (N)		
Flexion Angle (degrees)	30	60	90	30	60	90
Intact Joint	-0.2 ± 0.3	0.3 ± 0.4	0.5 ± 0.5	59 ± 7	61 ± 13	65 ± 16
ACL-deficient Joint	11.7 ± 2.0*	11.2 ± 1.6*	8.0 ± 1.4*	NA	NA	NA
Suture Augmented Joint						
Group 1 (F_A/T_M)	4.0 ± 2.0$^+$	3.1 ± 2.2	1.4 ± 1.4	43 ± 4$^+$	51 ± 17	55 ± 10
Group 2 (F_T/T_M)	3.9 ± 1.8$^+$	3.0 ± 2.1	1.5 ± 1.2	44 ± 7$^+$	54 ± 14	56 ± 8
Group 3 (F_A/T_{LM})	3.9 ± 1.5$^+$	3.0 ± 1.6$^+$	1.7 ± 1.1	47 ± 10$^+$	52 ± 15	59 ± 14
Group 4 (F_T/T_{LM})	4.2 ± 2.4$^+$	3.4 ± 2.5	2.1 ± 1.6	43 ± 6$^+$	52 ± 10	52 ± 11

*$p < .05$ compared with all other joint conditions at the same flexion angle

$^+p < .05$ compared to intact joint at the same flexion angle

6.1.2 Discussion of Appropriate Tunnel Locations for Suture Augmentation

In Specific Aim 2.1, we first wished to examine the effects the location of the bone tunnels for suture augmentation on the stability of the joint. It was found that the tunnel locations chosen for this study had a minimal effect on joint stability.

We first hypothesized that the femoral tunnel location for the sutures would have a significant effect of joint stability and the in-situ force carried by the sutures. Contrary to our hypothesis, no differences were observed when the femoral tunnel was placed just anterior to the femoral insertion of the ACL or placed through the femoral insertion. In the ACL reconstruction literature, the effect of femoral tunnel position has been extensively studied in the human knee joint [8, 105, 124, 150, 226, 272]. Having an ACL graft placed within the ACL footprint at the femoral origin of the ACL has been found to be important as it better restores the knee stability. In the current study, the F_A tunnel was placed immediately anterior to the ACL footprint at the femoral origin, such that the location of the F_A and F_T tunnels only differed by a few millimeters, which may explain why no differences due to femoral tunnel location were discernable under either the anterior tibial load or the varus-valgus torque.

We further hypothesized that tibial tunnel location for the sutures would not play a role in joint stability and the in-situ force carried by the sutures. Our hypothesis was confirmed as no differences were found when the sutures were placed medial to the tibial insertion of the ACL or medial and lateral to the tibial insertion. For tibial tunnel location, passing within the anterior or middle portion of the ACL footprint at the tibial insertion in the sagittal plane has been shown to restore kinematics for both ACL reconstruction using a soft tissue graft [8, 105, 124] or suture augmentation [73]. In the frontal plane, ACL reconstruction grafts have been usually placed

within the ACL footprint at the tibial insertion [8, 99, 105, 124]. However, in the context of using FTE treatments to heal an ACL, it becomes necessary to place the tunnels adjacent to the ACL footprint in order to avoid further damage to the injured ACL and perhaps impede its healing process. In this study, sutures placed both medial and lateral to the ACL footprint showed no biomechanical advantage when compared to placing the augmentation sutures only medial to the ACL footprint. Thus, the location of the tibial tunnels in the frontal plane also had little influence on joint stability.

In summary, all four suture augmentation groups were similarly able to restore joint kinematics as well as the in-situ forces in the sutures close to levels of the intact joint and ACL, respectively. Nevertheless, statistical differences versus the intact condition were found for some suture augmentation groups, but not others. It should be noted that the use of a robotic/UFS testing system allowed data for the intact, ACL-deficient, and suture augmented conditions to be collected in the same set of goat stifle joints allowing repeated measures statistical analysis for increased statistical power. Thus, small and consistent differences in means can become statistically significant, even if the difference in the values of the means (~10 N) was small and on the same order of magnitude of the repeatability of our testing system.

Since there was no statistically significant change in anterior joint stability between these four suture augmentation procedures, the findings suggest that the sutures be placed anterior to the ACL footprint of the femoral origin and medial to the ACL footprint of the tibial insertion. Since this surgical procedure is relatively simple and avoids further injury to the ACL tissue, it was used in the remainder of the dissertation.

6.1.3 In-vitro comparison of suture repair and suture augmentation

In the second part of Specific Aim 2.1, suture repair and suture augmentation were compared in-vitro on a set of goat knees using the robotic/UFS testing system, according to the protocol in Section 4.4.2.1(a). After performing each procedure, external loads were applied to the joint, and the resulting joint kinematics as well as the in-situ forces in the sutures and other structures, such as the MCL and medial meniscus, were determined. The results were compared between suture techniques as well as to those for the intact and ACL-deficient conditions.

6.1.3.1 Joint Kinematics and In-situ Forces under 67 N Anterior Tibial Load

The data on knee kinematics in response to a 67 N anterior tibial load as measured by the robotic/UFS testing system are detailed in Table 10. For the intact joint, the amount of ATT was similar at 30° and 60° (2.1 mm and 2.4 mm, respectively) and then decreased slightly at 90° (1.8 mm). Corresponding values for the ACL-deficient joint ranged from 13.9 mm at 90° to 17.3 mm at 60°, representing an increase of 7-8 fold compared to the intact joint ($p<0.05$). With suture repair, the amount of ATT reached a maximum of 12.0 mm at 60° and a minimum of 10.8 mm at 90°. These values were still 5-6 times higher than the intact joint ($p<0.05$); however, they were 34%, 31%, and 22% lower than the ACL-deficient joint at 30°, 60°, and 90°, respectively ($p<0.05$). With suture augmentation, the amount of ATT ranged from 5.1 mm at 30° to 2.6 mm at 90°, and thus, was restored to within 3 mm of the intact joint throughout joint flexion ($p>0.05$). Furthermore, these values for 69%, 72%, and 81% lower than the ACL-deficient joint ($p<0.05$) and 54%, 59%, and 76% lower than the suture repair group, respectively ($p<0.05$).

Table 10. Anterior tibial translation (in mm) under a 67 N anterior tibial load (*p<0.05 compared to intact, +p<0.05 compared to ACL-deficient, #p<0.05 compared to suture repaired).

	Flexion Angle (degrees)		
	30	60	90
Intact Joint	2.1 ± 0.6	2.4 ± 0.6	1.8 ± 0.3
ACL-deficient Joint	16.6 ± 2.4*	17.3 ± 2.0*	13.9 ± 1.7*
Suture Technique			
Suture Repair	11.0 ± 3.5*+	12.0 ± 2.8*+	10.8 ± 2.4*+
Suture Augmentation	5.1 ± 2.2+#	4.9 ± 1.9+#	2.6 ± 1.5+#

In this study, all groups were compared within the same set of joints, and thus, had the same reference position. This allowed the amount of ATT to be directly compared between groups, so for this study statistical analyses were done using the values of ATT. However, when comparing to groups in another set of joints (i.e. data at 12 weeks of healing), it is necessary to standardize the data in order to allow an objective comparison. First, in order to eliminate dependence on the reference position, the amount of total A-PTT is calculated for each experimental condition under the 67-N anterior-posterior tibial load. As a reference for future studies, the values for A-PTT for this study are provided in Table 11. Further, for results at 12 weeks, it is important to limit interspecimen variability between experimental groups. Thus, the APTT of the experimental group can be normalized by the APTT of the intact control joint for each animal (%experimental/control) (Figure 20). The normalized values for A-PTT for the suture augmentation group (178 ± 66%, 163 ± 60%, and 123 ± 37%) were 43%, 48%, and 62% lower than those for the suture repair group (313 ± 106%, 313 ± 85%, and 319 ± 80%), at 30°,

60° and 90° of flexion, respectively. Further, these values were 60%, 62%, and 69% lower than the ACL-deficient joint (442 ± 105%, 429 ± 103%, and 397 ± 89%), respectively.

Table 11. Anterior-posterior tibial translation under a 67 N anterior-posterior tibial load.

	Flexion Angle (degrees)		
	30	60	90
Intact Joint	4.5 ± 0.9	4.8 ± 0.9	4.3 ± 0.8
ACL-deficient Joint	18.9 ± 2.1	19.6 ± 1.8	16.4 ± 1.2
Suture Technique			
Suture Repair	13.4 ± 3.3	14.4 ± 2.7	13.3 ± 2.3
Suture Augmentation	7.4 ± 1.6	7.3 ± 1.5	5.1 ± 1.2

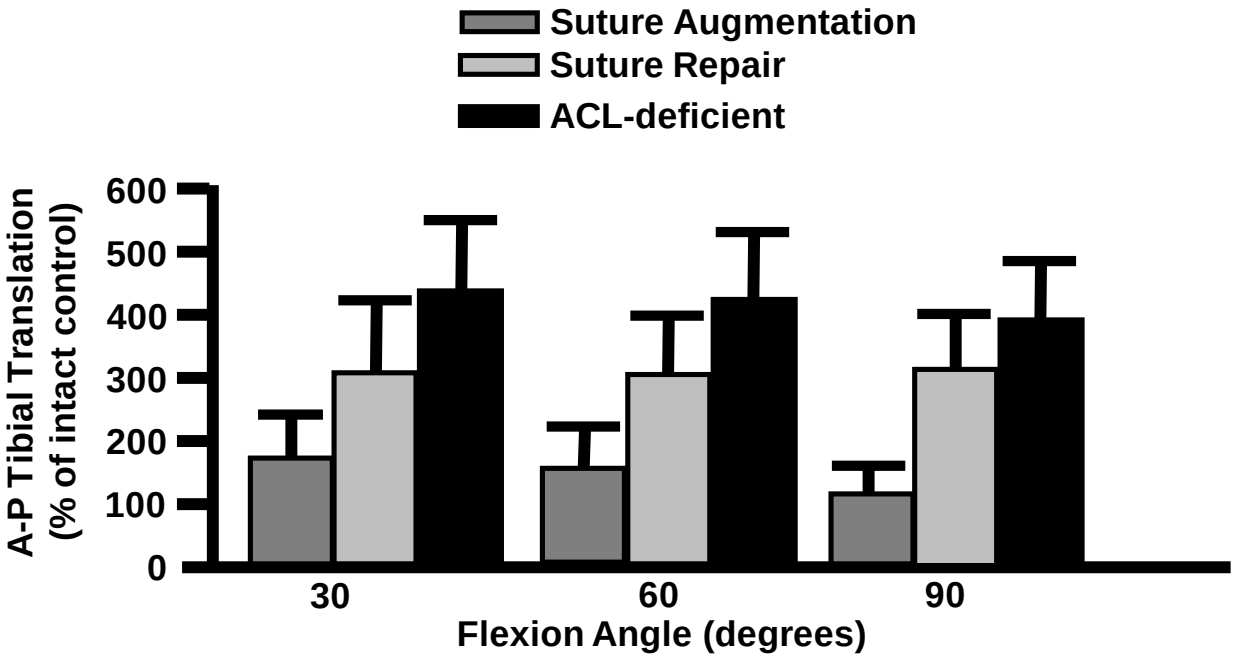

Figure 18. Anterior-posterior tibial translation normalized to intact joint (%experimental/control) under a 67 N anterior-posterior tibial load.

Under the 67 N anterior tibial load, the in-situ force of the intact ACL was similar at 30° and 60° and slightly lower at 90° of joint flexion, ranging from 62 N at 30° to 48 N at 90° (Table 12). These trends were similar for both the augmentation sutures and repair sutures. For both the suture repair and suture augmentation groups, the in-situ forces in the sutures were similar to those for the intact ACL ($p>0.05$). Interestingly, statistical analysis confirmed that the in-situ force of the augmentation sutures was 21% and 35% higher than the repair sutures at 30° and 90°, respectively ($p<0.05$).

Table 12. Resultant in-situ force of the ACL and sutures (in N) at 30°, 60°, and 90° of joint flexion under a 67-N anterior tibial load (mean ± sd). #Indicates a statistically significant difference compared suture repair ($p<0.05$).

	Flexion Angle (degrees)		
	30	60	90
Intact ACL	62 ± 5	60 ± 6	49 ± 6
Suture Technique			
Repair Sutures	50 ± 13	50 ± 13	36 ± 14
Augmentation Sutures	64 ± 10#	61 ± 5	55 ± 5#

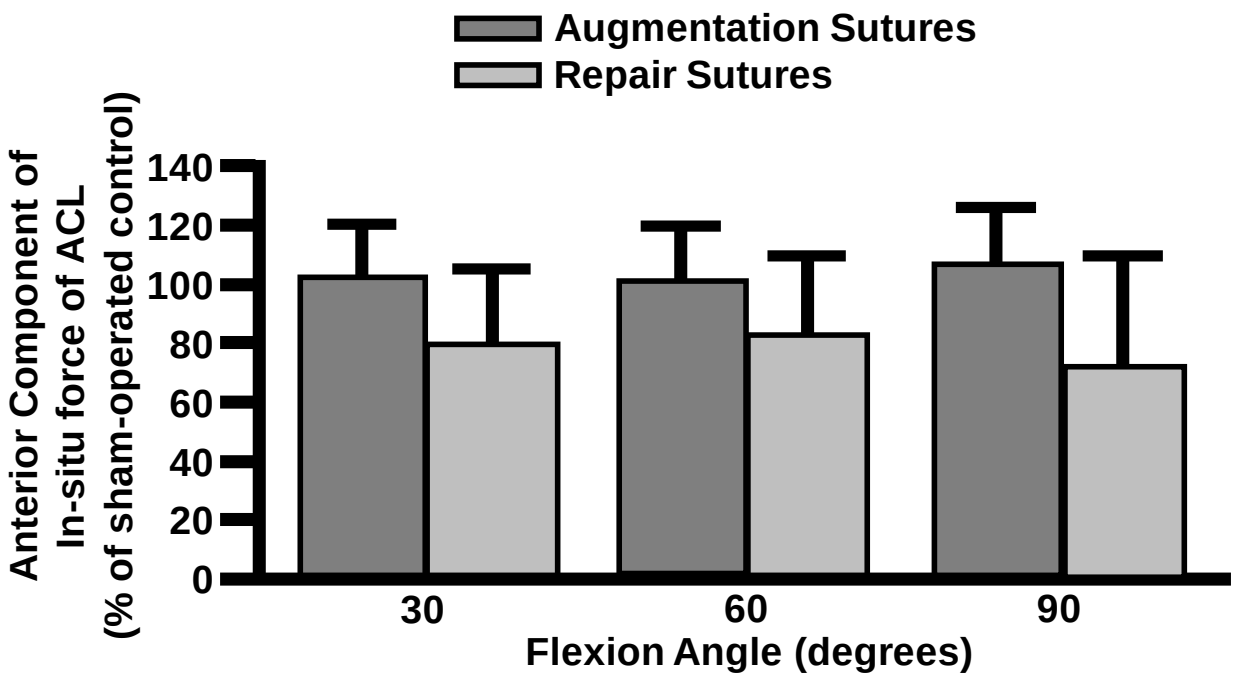

Figure 19. Anterior component of the in-situ force for the repair sutures and augmentation sutures normalized by the values for the intact ACLs under a 67 N anterior tibial load.

Again, similar to the joint kinematics, it is useful to normalize the in-situ force data with respect to the sham-operated control groups to compare treatment groups (Figure 19). Following this step, the values for anterior component of the in-situ force of the ACL for the suture augmentation group (103 ± 17%, 102 ± 17%, and 108 ± 18%) were 27%, 22% and 47% larger than those for the suture repair group (81 ± 23%, 84 ± 25%, and 73 ± 36%) at 30°, 60°, and 90°, respectively.

The in-situ forces of the other tissues of the knee under the 67 N anterior tibial load are also presented in Appendix A. These data are not directly relevant to the objectives of this dissertation, but are provided as a reference for future studies. In general, as the role of the ACL decreased, the in-situ forces in the other tissues, particularly the MCL and medial meniscus, increased.

6.1.3.2 Joint Kinematics and In-situ Forces under 67 N Anterior Tibial Load + 100 N Joint Compression

The data on joint kinematics in response to a 67 N anterior tibial load with 100 N axial joint compression are detailed in Table 13. For all groups, values were similar at 30° and 60° of joint flexion before decreasing at 90° of joint flexion. The data on ATT in response to a 67 N anterior tibial load with 100 N axial joint compression are detailed in Table 3A. Values for the intact joint ranged from 2.3 mm at 90° to 3.6 mm at 60°. Corresponding values for the ACL-deficient joint ranged from 15.0 mm at 90° to 18.9 mm at 30°, representing an increase of 5-7 fold ($p<0.05$). The suture repair group reached a maximum ATT of 16.6 mm at 30° and a mimimum ATT of 12.2 mm at 90°. These values were still 4-5 times higher than the intact joint ($p<0.05$), but were reduced by 12%, 14%, and 19% compared to the ACL-deficient condition at 30°, 60°, and 90°, respectively ($p<0.05$). With suture augmentation, the ATT ranged from 8.9 mm at 30° to 4.1 mm at 90°. These values were 5.5 mm and 4.4 mm higher than the intact joint at 30° and 60°, respectively ($p<0.05$), but were within 1.8 mm at 90° ($p>0.05$). Moreover, the ATT was reduced by 53%, 57%, and 73% compared to the ACL-deficient joint ($p<0.05$) and 46%, 50%, and 66% compared to the suture repair group at 30°, 60°, and 90°, respectively.

Table 13. Anterior tibial translation (in mm) under a 67 N anterior tibial load + 100 N joint compression (*p<0.05 compared to intact, +p<0.05 compared to ACL-deficient, #p<0.05 compared to suture repair).

	Flexion Angle (degrees)		
	30	60	90
Intact Joint	3.4 ± 0.7	3.6 ± 0.5	2.3 ± 0.5
ACL-deficient Joint	18.9 ± 2.7*	18.5 ± 2.7*	15.0 ± 2.7*
Suture Technique			
Suture Repair	16.6 ± 2.9*+	15.9 ± 2.6*+	12.2 ± 1.9*
Suture Augmentation	8.9 ± 1.7*+#	8.0 ± 2.0*+#	4.1 ± 1.4+#

As in Section 6.1.1.1, all analyses were done using the values of ATT; however, the data on A-PTT is also presented so that it could be compared to data from Specific Aims 1 and 2.2 (Table 14). Further, the data on A-PTT as a percentage of the intact control (%experimental/control) is depicted in Figure 20. The normalized values for A-PTT for the suture augmentation group (218 ± 57%, 173 ± 65%, and 150 ± 47%) were 36%, 0%, and 21% lower than those for the suture repair group (344 ± 79%, 171 ± 77%, and 191 ± 71%), at 30°, 60° and 90° of flexion, respectively. Further, these values were 45%, 8%, and 41% lower than the ACL-deficient joint (396 ± 85%, 186 ± 93%, and 253 ± 64%), respectively.

When comparing between external loading conditions, the amount of A-PTT for the intact joint slightly increased by 62%, 50%, and 28% with the additional 100 N compressive load compared to the 67 N anterior tibial load alone at 30°, 60°, and 90°, respectively. Slightly higher increases (75%, 63%, and 58%, respectively) were observed for suture augmentation, while slightly lower increases (51%, 33%, and 13%, respectively) were seen for suture repair. Interestingly, only small increases (14%, 7%, and 8%, respectively) occurred for the ACL-deficient joint. Moreover, the values for A-PTT for the suture augmentation, suture repair, and

ACL-deficient conditions were similar at 60° and 90°, in contrast to the results found under the 67 N anterior-posterior tibial load alone.

The differences in trends between loading conditions may have been due to a lack of stabilization in the ACL-deficient and suture repair groups. When applying the external loads to the joint, the robot first finds a new equilibrium position, that is, the position at which the forces and moments in the joint are minimized. In the case of the 67 N anterior tibial load with 100 N joint compression, the new equilibrium position is found after the compressive load is applied. In the case of the ACL-deficient and suture repair groups, the lack of anterior joint stability caused a large shift in the equilibrium position in the anterior direction. Then, the load is applied in both the anterior and posterior directions. However, because of the large shift in equilibrium position versus the other experimental conditions (e.g. intact and suture augmentation groups), the path of motion, and as a result, the relative amount of APTT can change drastically. Thus, these results require careful interpretation. In order to compare groups for the in-vivo studies on a more reliable basis, only the data for the 67 N anterior tibial load will be considered.

Table 14. Anterior-posterior tibial translation under a 67 N anterior-posterior tibial load + 100 N joint compression.

	Flexion Angle (degrees)		
	30	60	90
Intact Joint	5.1 ± 0.9	5.4 ± 0.9	4.5 ± 0.9
ACL-deficient Joint	19.9 ± 3.8	10.5 ± 6.5	11.6 ± 4.6
Suture Technique			
Suture Repair	17.3 ± 3.9	9.2 ± 4.5	8.7 ± 4.3
Suture Augmentation	10.8 ± 1.5	8.9 ± 2.1	6.4 ± 1.2

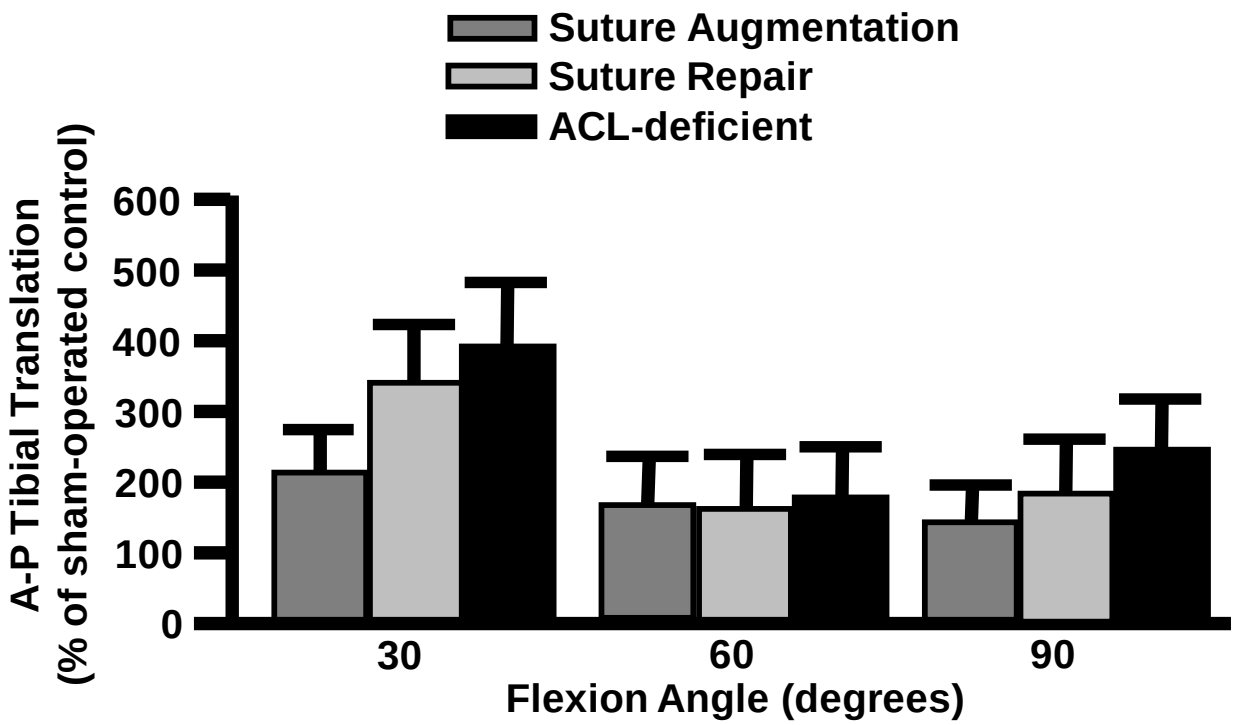

Figure 20. Anterior-posterior tibial translation normalized to intact joint (%experimental/control) under a 67 N anterior-posterior tibial load with 100 N axial compression

The data on in-situ forces in the ACL and sutures are presented in Table 15. With the added 100 N axial compression, the in-situ force in the intact ACL was 102 ± 16 N, 112 ± 10 N, and 95 ± 12 N at 30°, 60°, and 90° of joint flexion, respectively. Again, the ACL was largely responsible for carrying the anterior load. With suture repair, the in-situ force in the sutures were 2-3 times lower than the intact ACL ($p<0.05$). Following suture augmentation, the in-situ force of the sutures ranged from 78 N at 30° and 95 N at 60°. These values were significantly lower than the intact ACL at 30° and 60° ($p<0.05$), but were similar at 90° ($p>0.05$). Moreover, the in-situ forces of the augmentation sutures were 129%, 157%, and 90% higher than those of the repair sutures at 30°, 60°, and 90°, respectively ($p<0.05$).

Table 15. Resultant in-situ force of the ACL and sutures (in N) at 30°, 60°, and 90° of joint flexion under a 67-N anterior tibial load + 100 N axial compression (mean ± sd). *Indicates a statistically significant difference compared to the intact ACL ($p<0.05$). #Indicates a statistically significant difference compared to suture repair ($p<0.05$).

	Flexion Angle (degrees)		
	30	60	90
Intact ACL	102 ± 16	112 ± 10	95 ± 12
Suture Technique			
Repair Sutures	34 ± 13*	37 ± 28*	49 ± 27*
Augmentation Sutures	79 ± 11*#	95 ± 9*#	93 ± 11#

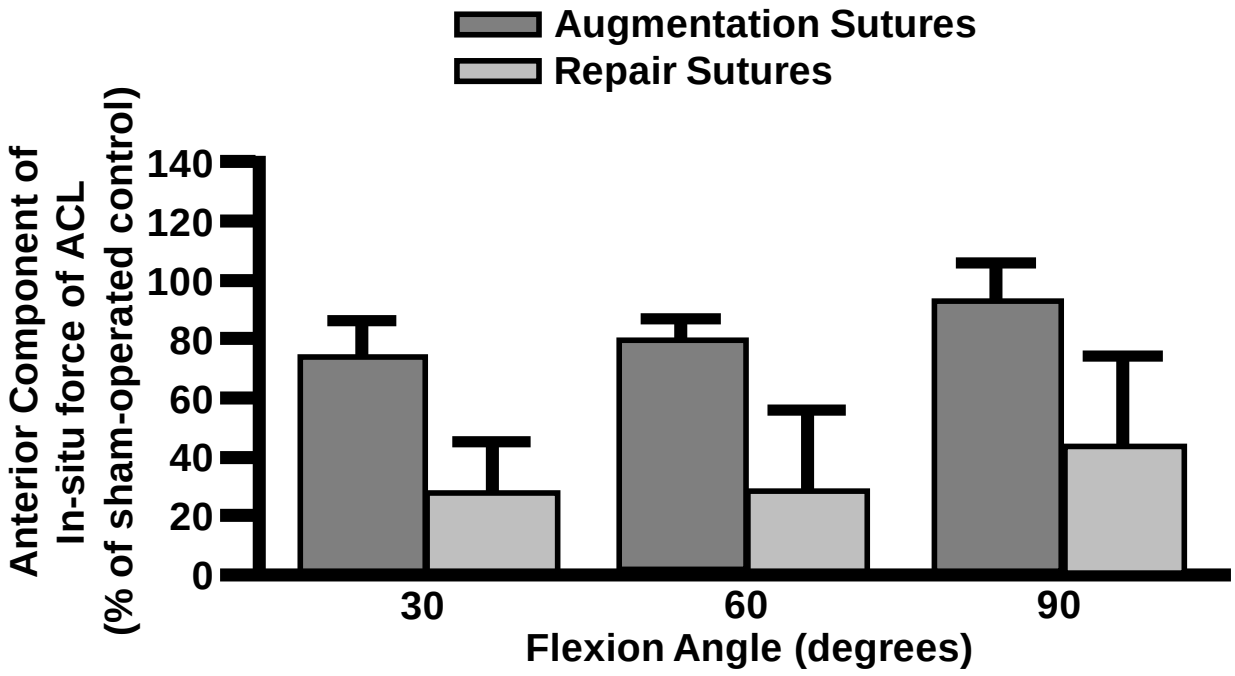

Figure 21. Anterior component of the in-situ force for the repair sutures and augmentation sutures normalized by the values for the intact ACLs under a 67 N anterior tibial load with 100 N axial compression.

Again, similar to the joint kinematics, it is useful to normalize the in-situ force data with respect to the sham-operated control groups to compare treatment groups (Figure 21). Following

this step, the values for anterior component of the in-situ force of the ACL for the suture augmentation group (75 ± 12%, 81 ± 6%, and 93 ± 13%) were 158%, 169% and 106% larger than those for the suture repair group (29 ± 16%, 30 ± 26%, and 45 ± 29%) at 30°, 60°, and 90°, respectively.

The in-situ forces of the other tissues of the joint are also presented in Appendix A as a reference for future studies. Like under the 67 N anterior tibial load, as the role of the ACL decreased, the in-situ forces in the other tissues, particularly the MCL and medial meniscus, increased. However, with the compressive load, the forces due to bony contact as well as the in-situ forces of the menisci were greatly increased.

6.2 AIM 2.2- IN-VIVO EVALUATION OF SUTURE TECHNIQUES

In Specific Aim 2.2, the suture repair and suture augmentation plus suture repair techniques were also compared in-vivo in the goat model after 12 weeks to evaluate these techniques in terms of their ability to allow healing of the ACL [67]. Biomechanical, histological, and morphological evaluations were done according to Section 4.4. For simplicity, the suture augmentation plus suture repair group will be denoted as the suture augmentation group hereon.

6.2.1 Joint Stability

As in Specific Aim 1, all goats tolerated surgery well and were ambulating within a few hours following surgery, with weight-bearing returning to normal within the first two to three weeks with no noticeable limping.

The curves for the A-PTT in response to the 67 N A-P tibial load at 30° of flexion as measured by the robotic/UFS testing system are detailed in Figure 22A. Similar to Specific Aim 1, the A-PTT began at the 67 N posterior tibial load to provide a consistent reference position for all stifle joints. The curves for all groups were nonlinear. The amount of translation was much higher for the experimental groups compared to the sham-operated controls and the difference began at low loads. The shapes of the curves for the suture augmentation and suture repair groups were remarkably similar, although the suture augmentation group showed lower amounts of A-PTT than the suture repair group.

Similar results were observed with the stifle joint at 60° and 90° of flexion (Table 16). In all three groups, the A-PTT increased from 30° to 60° and then decreased at 90°. Statistical analysis revealed that both experimental groups were significantly different than the sham-operated controls at all flexion angles tested ($p<0.05$).

For statistical comparison of joint kinematics data between groups, the data were again normalized with respect to the sham-operated control group (Figure 22B). Between treatment groups, the normalized mean value for A-PTT for the suture augmentation group (267 ± 48%, 297 ± 23%, and 341 ± 53%) was 21%, 21%, and 14% lower than those for the suture repair group (312 ± 79%, 350 ± 92%, and 382 ± 94%) at 30°, 60° and 90° of flexion, respectively. However, no statistically significant differences could be detected between these groups ($p>0.05$).

A.

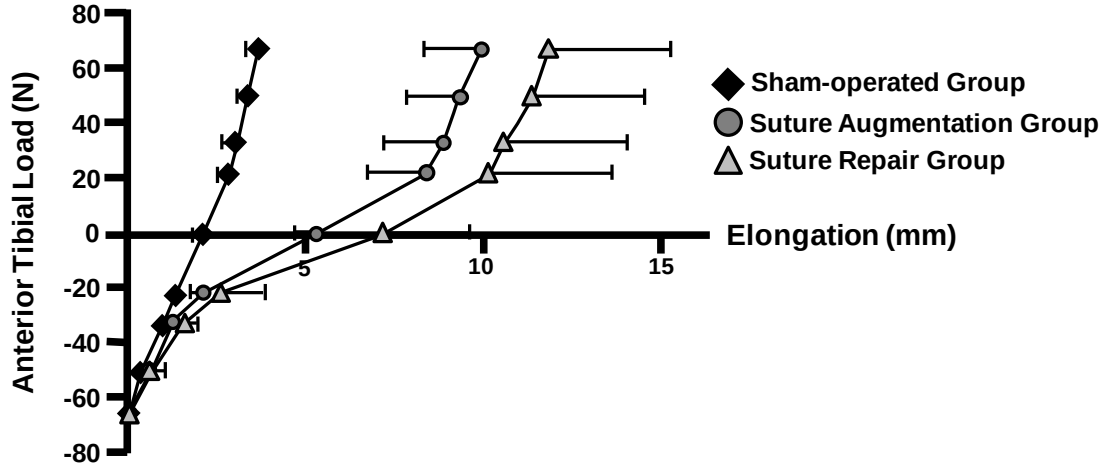

B.

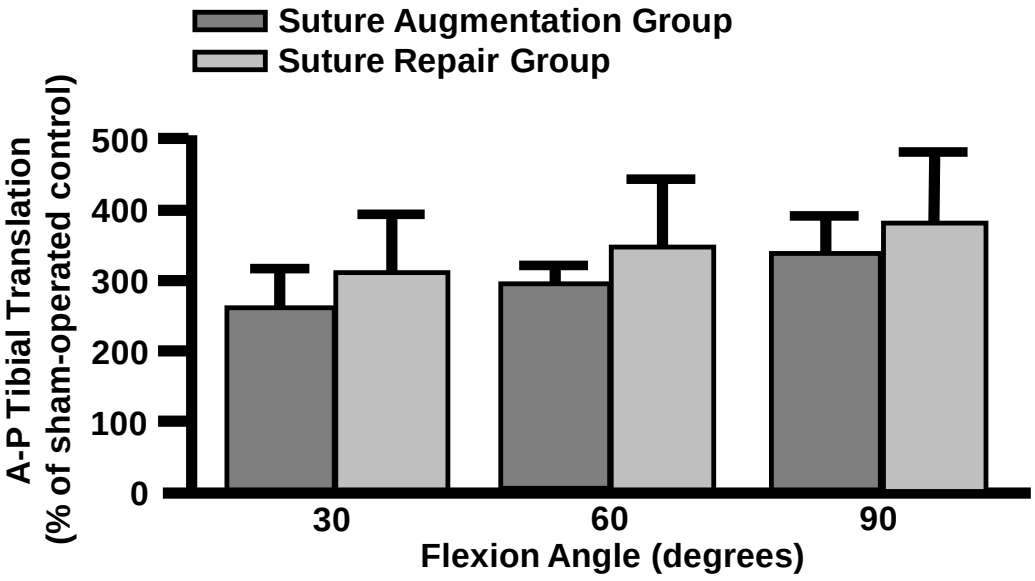

Figure 22. A) Average curves for the A-PTT in response to the 67 N A-P tibial load as measured by the robotic/UFS testing system at 30° of flexion for the sham-operated, suture augmentation, and suture repair groups. **B)** A-P tibial translation of the suture augmentation and suture repair groups in response to an 67-N anterior tibial load normalized to their respective intact joint controls (mean ± SD).

Table 16. Anterior-posterior tibial translations (mm) of the goat joints 30°, 60°, and 90° of joint flexion under an 67-N anterior-posterior tibial load (mean ± sd). *Indicates a statistically significant difference compared to the respective sham-operated controls ($p<0.05$).

	Joint Flexion Angle		
	30°	60°	90°
I. Suture Augmentation Group			
Sham-operated Control	3.7 ± 0.4	4.0 ± 0.5	2.9 ± 0.4
Healing	9.9 ± 1.6*	11.9 ±1.8*	9.8 ± 1.4*
II. Suture Repair Group			
Sham-operated Control	3.8 ± 0.2	4.1 ± 0.3	2.8 ± 0.4
Healing	11.8 ± 3.4*	14.4 ± 4.2*	10.8 ± 3.3*

In terms of the in-situ force of the ACL under the 67 N anterior tibial load, its anterior component at 30° of flexion was plotted against the amount of A-PTT (normalized to the respective sham-operated control group) in Figure 23A. Just as in Specific Aim 1, the sham-operated ACLs carried the vast majority of the applied anterior tibial load. The suture augmented healing ACLs carried approximately half of the applied load. Qualitatively, this was substantially higher than the suture repaired ACLs. Similar findings were obtained at with the stifle joint at 60° and 90° of flexion.

A.

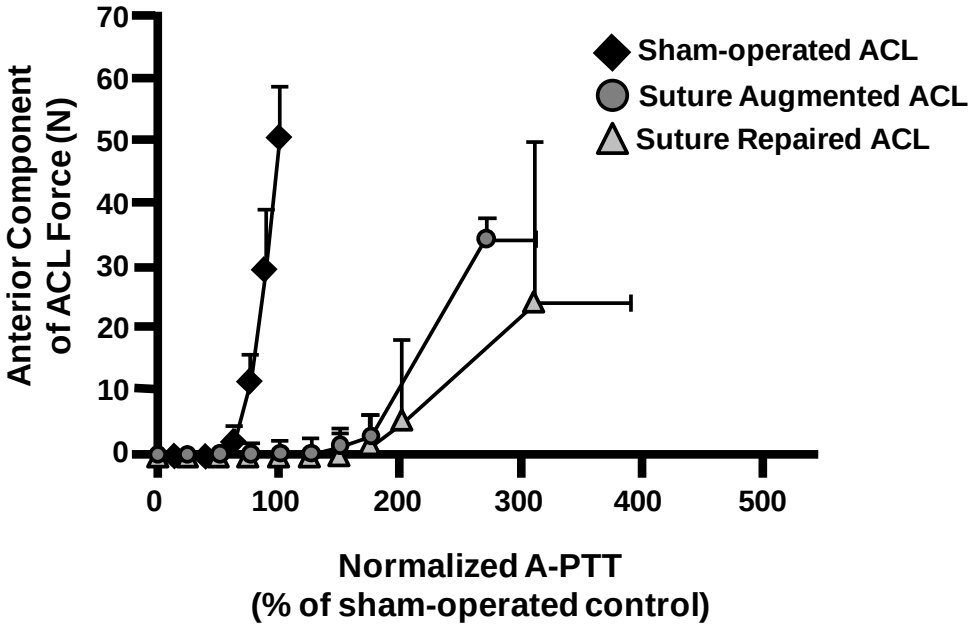

B.

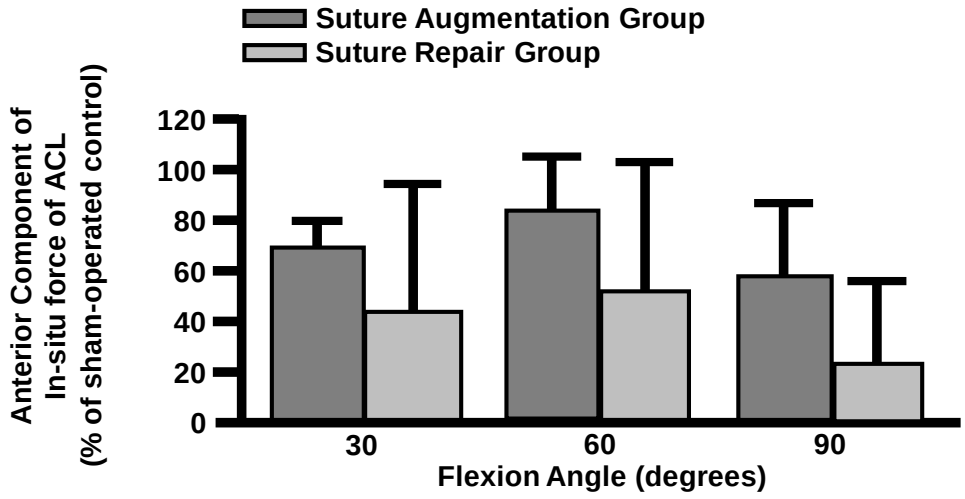

Figure 23. A) Anterior component of the in-situ force of the ACL as a function of the A-PTT at 30° of flexion for the sham-operated, suture augmentation, and suture repair groups. Note: Values of A-PTT are normalized to the A-PTT for the respective sham-operated control group. **B)** Anterior component of the in-situ force healing ACLs of the suture augmentation and suture repair groups normalized by the values for the sham-operated ACLs.

Table 17. Resultant in-situ force of the ACL (in N) at 30°, 60°, and 90° of joint flexion under a 67-N anterior tibial load (mean ± sd). *Indicates a statistically significant difference compared to the respective sham-operated controls ($p<0.05$).

	Joint Flexion Angle		
	30°	60°	90°
I. ECM-treated Group			
Sham-operated Control	50 ± 7	46 ± 8	43 ± 9
Healing	38 ± 6*	42 ± 7	22 ± 5*
II. Suture Repair Group			
Sham-operated Control	50 ± 12	51 ± 11	53 ± 7
Healing	26 ± 24	29 ± 25	13 ± 15*

Quantitative data on the resultant in-situ force of the ACL are presented in Table 17. For the intact joint, the ACL carried forces ranging from 43-53 N on average throughout joint flexion. For both treatment groups, the highest values of in-situ force of the healing ACL were found at 30° and 60° of flexion and were not statistically significant from their respective sham-operated controls ($p>0.05$). The only notable exception was that the in-situ force in the healing ACL for the suture augmentation group was significantly lower than those for the sham-operated ACLs at 30° ($p<0.05$). At 90° of flexion, both treatment groups had significantly lower values than the sham-operated control groups ($p<0.05$). Similar to the joint kinematics, it is useful to normalize the anterior component of the in-situ force of the ACL with respect to the sham-operated control groups to compare treatment groups (Figure 23B). Following this step, the value of the mean for the suture augmentation group (70 ± 10%, 86 ± 20%, and 58 ± 29%) was 54%, 60% and 131% larger than those for the suture repair group (45 ± 49%, 54 ± 50%, and 25 ±

32%) at 30°, 60°, and 90°, respectively. Nevertheless, these groups were not statistically different ($p>0.05$).

6.2.2 Gross Morphology and Dimensions

After dissection, the sham-operated ACLs at 12 weeks were white and opaque, consisting of distinct bundles with clearly observable collagen fiber orientation (Figure 24A). In the suture augmentation group, there was continuous neo-tissue formation for all specimens (Figure 24B). The neo-tissues were reddish in color and slightly translucent. The augmentation sutures could be seen immediately adjacent to the healing ACL tissue, but not within it. Further, the augmentation sutures appeared to be loosened within the intra-articular space compared to at the time of surgery. No remnants of the repair sutures could be found, and it is probable that they had fully degraded. The fixation of the sutures at both the femur and tibia remained good at 12 weeks of healing. The suture knot on the femoral side did not collapse into the bone tunnel or separate from the sutures in any animals. On the tibial side, the button was surrounded by a moderate amount of fibrotic tissue, but was still immediately adjacent to the tibial bone. No signs of rupture of the augmentation sutures were observed.

In the suture repair group, significant resorption of the ACL was observed (Figure 24C). Out of seven stifle joints, one ACL had completely resorbed in the synovial environment, four had only a small amount of tissue, while the remaining two still had some tissue concentrated around the sutures. Further, the repair sutures appeared to be loosened within the tissue compared to the time of surgery. The bone bridge at the tibia remained intact with no sign of suture rupture. At the femur, the bone bridge was not directly against the bone in some cases,

and rather, within the muscle tissue. This could have been from loosening over time with loading or a result of poor initial fixation during surgery.

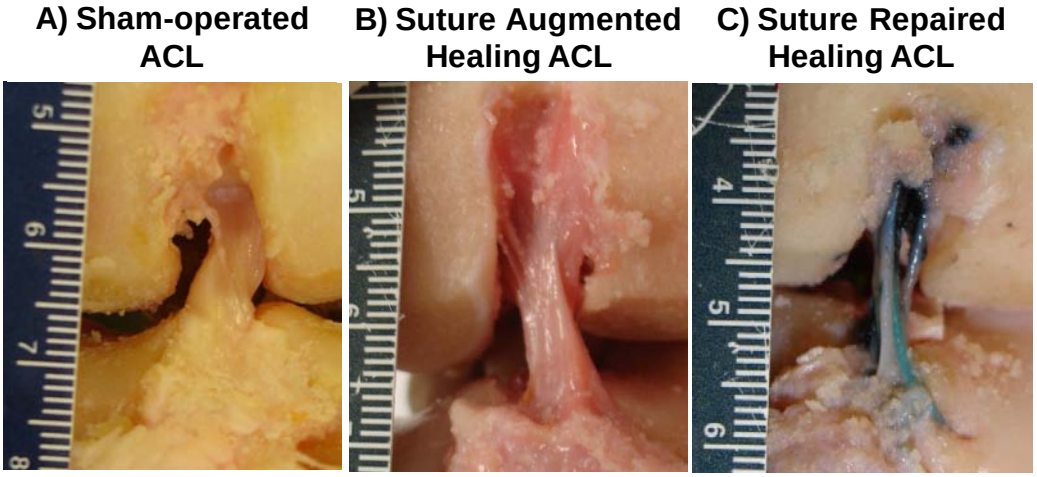

Figure 24. Gross morphology of (A) sham-operated ACL, (B) suture augmented healing ACL, and (C) suture repaired healing ACL at 12 weeks of healing.

These gross observations were confirmed in the CSA measurement of the ACLs. Values for the healing ACLs for the suture augmentation group were 19.9 ± 7.6 mm², whereas those for the sham-operated control group were 24.4 ± 1.8 mm². The difference was not statistically significant ($p>0.05$). For the suture repair group, the values for the CSA of the healing ACLs were only 34% of those for the sham-operated control group (6.5 ± 4.3 mm² vs. 21.6 ± 5.6 mm², respectively), and the difference was statistically significant ($p<0.05$). When normalized by their respective sham-operated control of each animal, the experimental/control values for the CSA from the suture augmentation group (80 ± 24%) was 2.3 times those of the suture repair group (34 ± 25%, $p<0.05$; Figure 25).

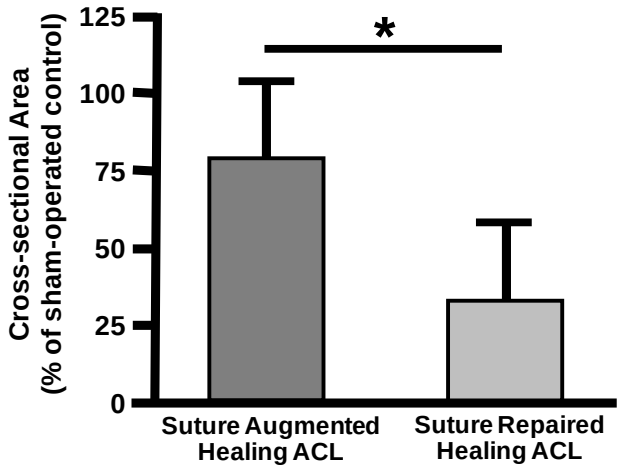

Figure 25. The cross-sectional area of healing ACLs for the suture augmentation and suture repair groups at 12 weeks post-surgery normalized by the values for the respective sham-operated ACLs. *Indicates a statistically significant difference ($p<0.05$).

6.2.3 Histological Evaluation

Histological examination of the midsubstance of the ACL in the sham-operated group showed compact collagen fibers that were highly aligned with many regularly interspersed spindle-shaped cells (Figure 26A). In both samples from the suture augmentation group and one of the two samples from the suture repair only group, significant neo-tissue was observed with aligned collagen fibers parallel to the longitudinal axis of the ligament and spindle-shaped cells oriented along the collagen fibers (Figure 26B). On the other hand, for one sample from the suture repair group, there were only sparse collagen fibers without clear alignment (Figure 26C).

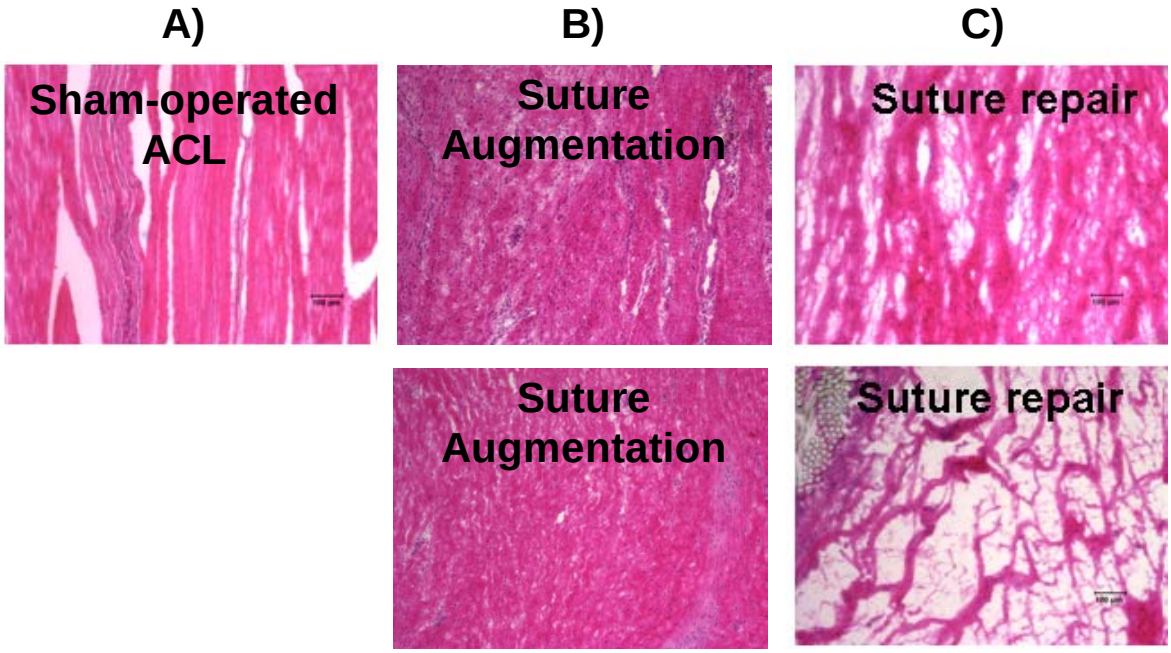

Figure 26. Histological appearance of the (A) sham-operated ACL as well as the (B) suture augmentation and (C) suture repaired healing ACLs at 12 weeks of healing (100x magnification).

6.2.4 Tensile Properties

Figure 27 details the nonlinear load-elongation curves for the suture augmented and suture repair groups. Typically, the toe region existed for up to 1-1.5 mm of elongation, followed by a linear region until failure. All specimens were found to fail in the tissue midsubstance of the healing ACL.

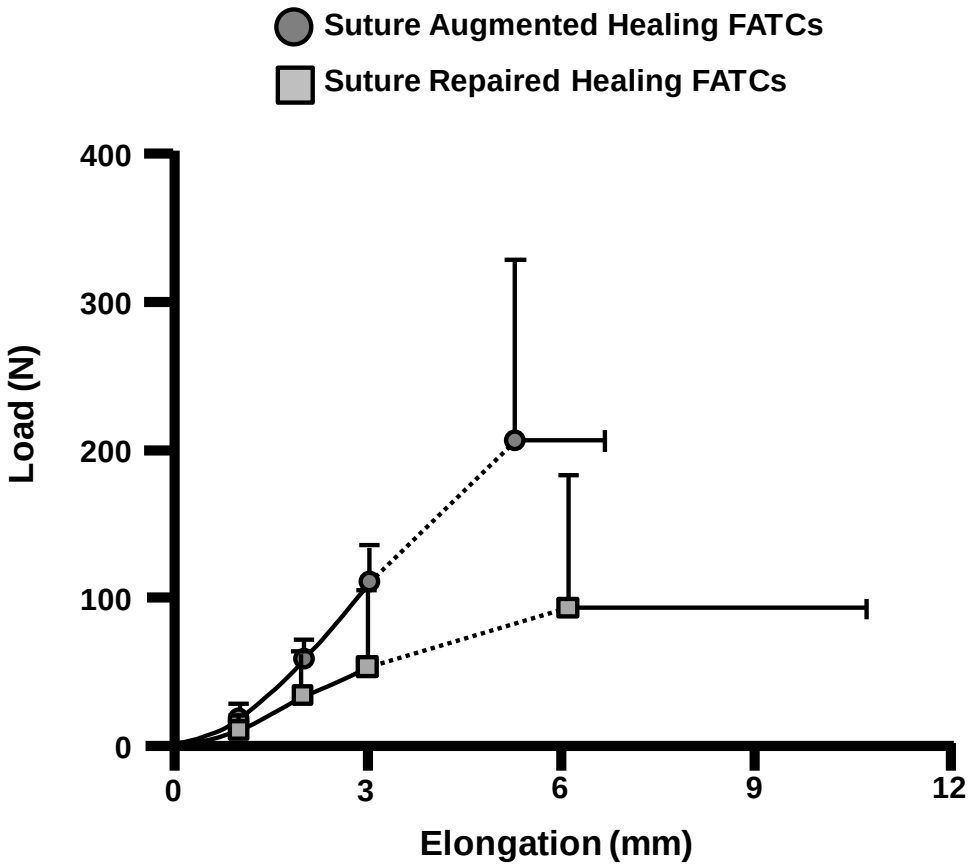

Figure 27. Average load-elongation curves of the suture augmentation and suture repair groups at 12 weeks post-surgery.

Data on the parameters representing these structural properties of the FATCs are detailed in Table 18. For both experimental groups, the values for stiffness, ultimate load, and ultimate elongation were below the values for their respective sham-operated groups ($p<0.05$). Again, the data was normalized with respect to the sham-operated controls for statistical comparisons between experimental groups (Figure 28). The mean value of the linear stiffness of the suture augmented FATCs was 75% greater than those for the suture repair group (experimental/control was 36 ± 15% vs. 20 ± 18%, respectively). However, this difference was not statistically significant ($p>0.05$). Similarly, the values for ultimate load were comparable between the two

groups (10 ± 9% vs. 9 ± 9%, respectively, $p>0.05$). Finally, the ultimate elongation was similar between the two groups (37 ± 8% vs. 30 ± 19%, respectively, $p>0.05$).

Table 18. Parameters representing the structural properties of the femur-ACL-tibia complexes for the sham-operated control, suture augmentation, and suture repair groups at 12 weeks post-surgery (mean ± sd). *Indicates a statistically significant difference compared to the respective sham-operated controls ($p<0.05$).

	Suture Augmentation Group		Suture Repair Group	
	Sham-operated Control	Healing	Sham-operated Control	Healing
Stiffness (N/mm)	152 ± 29	52 ± 21*	125 ± 23	24 ± 21*
Ultimate Load (N)	2033 ± 356	209 ± 122*	1385 ± 359	95 ± 90*
Ultimate Elongation (mm)	14.4 ± 2.9	5.3 ± 1.4*	19.0 ± 6.3	6.1 ± 4.6*

A.

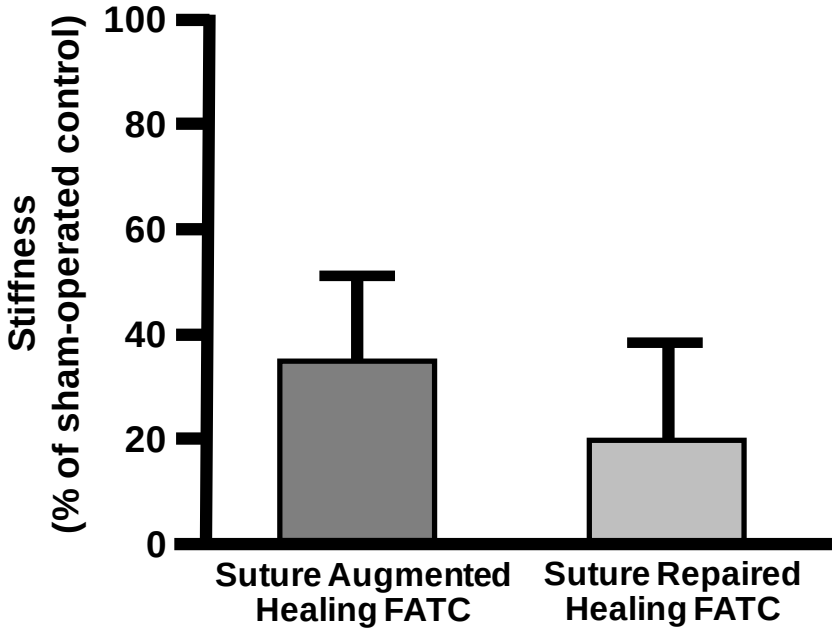

B.

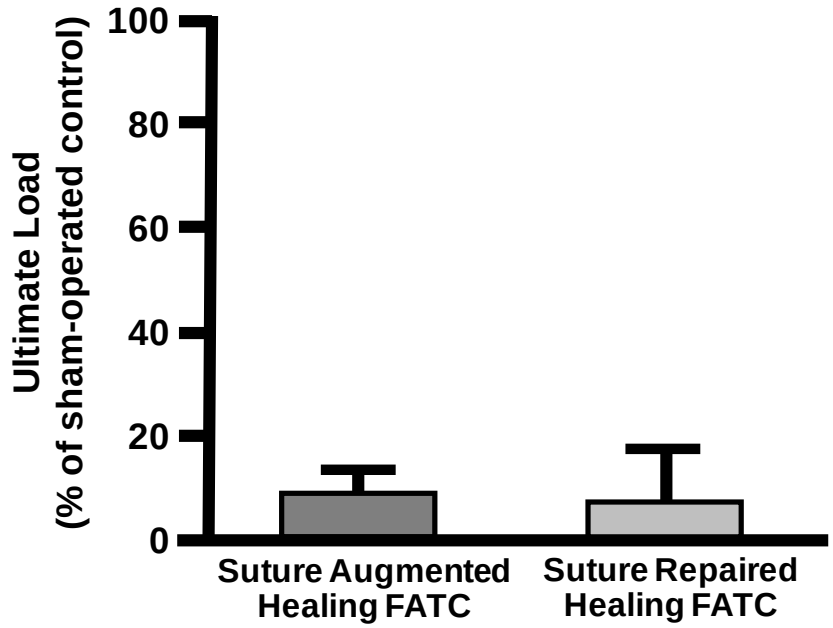

Figure 28. Stiffness (A.) and ultimate load (B.) of the healing femur-ACL-tibia complexes for the suture augmentation and suture repair groups as a percentage of the sham-operated controls at 12 weeks post-surgery.

7.0 MATHEMATICAL MODELING OF THE HEALING ACL

As described in Section 2.5.2, it is believed that ligaments modulate their size and biomechanical properties in response to applied strains above and below its homeostatic level. A similar case can be made for ligament healing especially during the remodeling phase. During healing, joint loading and movement results in stresses and strains within ligaments. In general terms, it is theorized that increased strains over a period of time will cause the tissue to remodel by either increasing its CSA or altering its biochemical composition to increase its mechanical properties, both of which impact the overall stiffness of the tissue. This is turn reduces the strain in the tissue for a given applied load. In the long-term, these changes in CSA and mechanical properties would return the tissue strains to the normal homeostatic levels. The opposite occurs under decreased strains, with a rapid reduction in size and/or mechanical properties.

In order to evaluate the strain-induced tissue remodeling in the healing ACL, we will first develop a general mathematical framework for evaluating growth and remodeling of healing ligaments (Section 7.1) and assess the sensitivity of the model to the parameters as well as perform some preliminary simulations as a proof-of-concept (Section 7.2). We will then apply the model to experimental data for the MCL, which is a well-established experimental model for ligament healing (Section 7.3). Finally, we will perform some preliminary analyses to gain insight on the healing of the ACL (Section 7.4).

7.1 MATHEMATICAL FORMULATION OF STRAIN-INDUCED GROWTH AND REMODELING

The formulation of the mathematical framework in this dissertation is an extension of the generalized structural constitutive model for hyperelastic soft tissues proposed by Sacks [206, 254], based on the work of Lanir [131], as well as the large body of theoretical and experimental work on growth and remodeling developed by Humphrey, Gleason, and others [46, 93, 106, 200]. These topics are described in Section 2.8.

7.1.1 Quasi-static Constitutive Model

As stated in Section 2.8.2, for the model developed by Sacks et al. [206, 254], the stress component along the axis of loading was represented as,

$$S_{11} = \int_{-\pi/2}^{\pi/2} R(\theta) S^{ens}(E^{ens}) \cos^2(\theta) d\theta \qquad 7\text{-}1$$

where S_{11} is the component of the 2nd Piola-Kirchoff stress along the direction of loading, R(θ) is a function representing the distribution of fibers in the tissue, and $S^{ens}(E^{ens})$ is the stress-strain relationship of the fiber ensemble at each θ. The constitutive relation for the fiber ensemble is

$$S^{ens} = \int_0^{E^{ens}} D(x) S_f(x) dx = k \int_0^{E^{ens}} D(x) \frac{E^{ens} - x}{(1+2x)^2} dx \qquad 7\text{-}2$$

where D(x) is a function which represents the fraction of fibers which are straightened at a given strain, and k is the effective modulus for the collagen fibers. In specifying the form of D(x), a beta distribution is useful, since it has a lower bound of zero and upper bound of one. It can be represented as

$$Beta_{PDF}(x;\alpha,\beta) = \frac{1}{B(\alpha,\beta)} x^{\alpha-1}(1-x)^{\beta-1} \qquad 7\text{-}3$$

where α and β are shape functions described in terms of the distribution mean, μ, and standard deviation, σ:

$$\alpha = \frac{\mu^2 - \mu^3 - \mu\sigma^2}{\sigma^2} \qquad \beta = \alpha\frac{1-\mu}{\mu} \qquad 7\text{-}4$$

and B(α,β) is

$$B(\alpha,\beta) = \frac{\Gamma(\alpha+\beta)}{\Gamma(\alpha)\Gamma(\beta)} \qquad 7\text{-}5$$

where Γ is the Gamma function. Within this model, the beta distribution is constructed with respect to E^{ens}, such that it exists only between 0 and E_*^{ens}, which represents an upper bound strain value for the recruitment function. Thus, $x = \frac{E^{ens}}{E_*^{ens}}$, where E^{ens} is the current strain of the fiber ensemble.

Going back to Equation 7-1, the tissue stress-strain data can be determined from the stress-strain response of individual collagen fiber ensembles and the fiber distribution. For the collagen fibers, four parameters make up the shape of the curve, μ^{ens}, σ^{ens}, k^{ens}, and E_*^{ens}. The distribution of the fibers, R(θ), can also be represented as a statistical distribution with a mean and standard deviation. For a transversely isotropic tissue (e.g. normal ligaments), the mean and standard deviation of R(θ) can be defined such that all of the fibers are aligned along the axis of loading. For comparison to experimental data, it is useful to also define the 1st Piola-Kirchoff stress (P) using the relation,

$$P = S \cdot F^T \qquad 7\text{-}6$$

because P relates forces in the in the current configuration with areas in the reference configuration, and thus is more easily calculated since the values for forces and CSA are experimentally determined in the current and reference configurations, respectively.

7.1.2 Application to Constitutive Model to Ligament Healing

7.1.2.1 What are ligaments trying to restore during healing?

As ligaments (such as the MCL) heal, their structural properties gradually increase with time (Section 2.5.1). For the MCL at 52 weeks, the load-elongation behavior of the FMTC during tensile testing was recovered at low levels of elongation, suggesting at least a partial restoration of normal function. At the same time, the CSA of the healing ligament remained higher than normal at all time points. Meanwhile, the mechanical properties, or stress-strain behavior, of the tissue remained inferior to normal and did not noticeably improve by 52 weeks compared to earlier time points. Thus, the recovery of the stiffness of the FMTC is largely the result of an increase in tissue quantity. Nevertheless, it is clear that the tissue is not attempting to restore its size (CSA) or its quality (mechanical properties) alone. Instead, on a tissue level, its function, as represented by its load-elongation behavior, is being restored.

However, the cells, which remodel the tissue, do not operate on a tissue-level scale, but on a micro-level (or fiber-level) scale. And thus, the restoration of tissue function may be a by-product of the restoration of some other homeostatic quantity which the cells can interpret. As noted in Section 2.5.2.1, the mechanisms by which cells interpret mechanical signals are complex, multi-factorial, and not well understood to date. However, there is a strong relationship between the level of tissue strain applied to the tissues and the resulting changes in tissue size, quality, and function.

For example, as a simple thought experiment, consider a linear, elastic, homogenous, transversely isotropic tissue. In such a case,

$$F_{11} = K_{11}x_{11} \tag{7-7}$$

where F_{11}, K_{11}, and x_{11} represent the force, stiffness, and displacement along the direction of the fibers, respectively. In addition, $x_{11}=\varepsilon_{11}*l_0$, where ε_{11} is the strain and l_0 is the initial length of the tissue. Also,

$$P_{11} = TM_{11}\varepsilon_{11} \tag{7-8}$$

where P_{11}, TM_{11}, and ε_{11} are the components of the 1st Piola-Kirchoff stress, tangent modulus of the tissue, and the infinitesimal strain, respectively, in the direction of loading. Given $P_{11}=F_{11}/A_{11}$ where A_{11} is the CSA of the tissue then Equation 7-8 can be written as

$$F_{11} = TM_{11}A_{11}\varepsilon_{11} \quad \text{or} \quad F_{11} = \frac{TM_{11}A_{11}}{l_0}x_{11} \tag{7-9}$$

In other words,

$$K_{11} = \frac{TM_{11}A_{11}}{l_0} \tag{7-10}$$

In terms of load-elongation behavior on a tissue level, the stiffness could be changed over time by altering either the modulus of the tissue, its CSA, or its initial length. Assuming the initial length of the tissue remains constant, then the tissue restores its function (load-elongation behavior) by altering its stiffness (K_{11}) by changing its quality (TM_{11}) or size (A_{11}). It could be said that the tissue is attempting to change its behavior such that for a given F_{11}, a homeostatic value of x_{11} is achieved. However, the mechanism by which tissue displacement would be interpreted on a cellular level is difficult to understand.

Alternatively, the restoration of function can be expressed as in Equation 7-9. In this case, function would be restored if the force-strain relationship remains the same. In other

words, it could be said that the tissue is attempting to change its TM_{11} and A_{11} such that a homeostatic value of ε_{11} is achieved for a given F_{11}. Further, by relating the tissue strain to some measure of fiber strain via affine deformation (See Equation **2-6**) or another mechanism, then we can relate the fiber strains at a cellular level to the overall tissue strain, which is easily measurable experimentally. We hypothesize then that these fiber strains could provide a measure of homeostasis on the cellular level.

7.1.2.2 Application of Growth and Remodeling Theory to Ligament Healing

As mentioned in Section 2.5 and 7.1.2.1, ligaments heal by both changing their size as well as intrinsic mechanical properties in an effort to restore function, i.e. load-elongation behavior. Thus, throughout time, new matrix is produced while some matrix is degraded within the healing ligament. In addition, the orientation of the matrix can change over time to become more aligned with the direction of loading. Further, through the process of collagen maturation, the intrinsic stress-strain behavior of collagen fibers can increase during tissue remodeling.

In order to model these time- and strain-dependent processes, it is imperative to keep track of the matrix produced at each time point separately. Extending the work presented in Section 2.8.3 by Humphrey and Gleason, we can consider the matrix produced at each timepoint to be separable such that

$$W(\varepsilon,t) = \sum_i \phi_i(t) \cdot W_i(\varepsilon,t) \qquad 7\text{-}11$$

In other words, the total strain energy of the tissue (W) at a given time and strain is simply the relative mass fraction of the matrix produced at each timepoint (Φ_i) multiplied by the strain energy of the matrix produced at that timepoint. Note that for ligaments, the collagen fibers are the only matrix constituent explicitly considered as they play the dominant mechanical response

to loading. The response of the remaining constituents were lumped into a term representing the ground substance of the tissue (Equation **2-2**), which was assumed not to be time-dependent.

An important parallel can be made with regard to the growth of the tissue such that

$$A_{11}(t) = \sum_i A_{11}^i(t) \qquad 7\text{-}12$$

Again, this represents the total CSA of the tissue (A_{11}) at any time as a sum of the CSA for the matrix produced at each timepoint (A_{11}^i). Note that as the matrix for a given time, t_i, degrades, the value for A_{11}^i will decrease.

In order to evaluate these properties over time, the next step is to find specific functions for W_i and A_{11}^i. For W_i of the collagen fibers, the constitutive relationship is found in Equations 7-1 and 7-2. The ground substance was represented as an isotropic, neo-Hookean material whose strain energy is given in Equation **2-2**. From the fiber ensemble stress-strain relationship, we can see there are four possible time-dependent parameters: μ^{ens}, σ^{ens}, E_*^{ens}, and k^{ens}. Further, the mean and standard deviation of $R(\theta)$ can also be time-dependent. However, for our simulations at late timepoints of healing, we will assume the matrix to be transversely isotropic along the direction of healing, and thus, $R(\theta)$ will remain constant throughout time, with a mean and standard deviation such that all fibers are aligned along the direction of loading. Nevertheless, the potential to allow $R(\theta)$ is still possible within the model for future studies. From Equation 7-12, A_{11}^i should also be time-dependent.

A number of forms for time-dependent stimulus functions have been proposed in the literature, and include linear, nonlinear, and exponential functions [46, 93, 239, 243]. For our applications, a linear function is the easiest for an initial analysis and is defined as

$$f(t+\Delta t)=\left(q_f\cdot\left(\frac{E_t^{ens}-E_h^{ens}}{E_h^{ens}}\right)\cdot\Delta t+1\right)\cdot f(t) \qquad 7\text{-}13$$

where f(t) and f(t+Δt) are the values of parameter f at time t and t+Δt, respectively. Further, E_t^{ens} is the fiber ensemble strain at time t for a given load and E_h^{ens} is the homeostatic fiber ensemble strain for a given load, which the tissue is trying to reach. Finally, q_f is the remodeling constant associated with parameter f with units of time^{-1}. It is clear that this function provides a linear, positive response to an applied strain. For example, if $E_t^{ens} > E_h^{ens}$, then $f(t+\Delta t) > f(t)$ provided $q_f > 0$. This is important, since it is assumed that these functions respond positively to applied strain. An example would be the modulus of the collagen fibers, which we would anticipate increasing in response to strains above E_h^{ens} and decreasing in response to strains below E_h^{ens}.

On the other hand, some parameters may decrease in response to strains above E_h^{ens}. A good example is E_*^{ens}. Typically, E_*^{ens} should decrease as the stress-strain behavior of the tissue improves in response to strain. As such, we set $q_f < 0$ for these functions such that $f(t+\Delta t) < f(t)$.

In the case of underloading ($E_t^{ens} < E_h^{ens}$), alternative rate constants must be used, since it is unlikely that tissues respond exactly the same as when $E_t^{ens} > E_h^{ens}$. For simplicity, we can assign a ratio, r_i, to each parameter, such that $r_i = \frac{q_i}{p_i}$, where q_i and p_i are the remodeling constants when $E_t^{ens} > E_h^{ens}$ and $E_t^{ens} < E_h^{ens}$, respectively. For the case of $E_t^{ens} < E_h^{ens}$, the linear function described in Equations 7-13 is modified as

$$f(t+\Delta t) = \left(\frac{q_f}{r_f} \cdot \left(\frac{E_t^{ens} - E_h^{ens}}{E_h^{ens}} \right) \cdot \Delta t + 1 \right) \cdot f(t) \qquad 7\text{-}14$$

In the case of healing ligaments, conditions in which the healing tissue is underloaded are not likely to occur due to the large decrease in the mechanical properties of the tissue. However, the model was formulated to include underloading for completeness.

7.1.3 Computational Approach

The computational algorithm was developed in Matlab (Version 7.9.0 (R2009b), The MathWorks, Inc.) and consists of several sections. First, the variables were defined and initial values were designated. Then, experimental data for the normal and healing tissues were fit by an algorithm described in Section 7.1.3.2 to obtain parameters describing the tissue stress-strain behavior. After, the initial parameters describing the fiber stress-strain relationship were estimated via the algorithm in Section 7.1.3.3 given the tissue stress-strain data and fiber distribution data. Then, an iterative technique described in Section 7.1.3.4 was used to simulate the healing of the tissue out to the time of interest. Finally, if the experimental data at the time of interest is known, the experimental and predicted data can be compared and the values of the remodeling constants can be adjusted accordingly until the two sets of data converge, as described in Section 7.1.3.5.

7.1.3.1 Initial Variables

The initial portion of the code sets up the variables, values, etc. used in the remaining portions. First, any known experimental data were read in and stored as inputs. Next, the time variables (initial timepoint, final timepoint, and time increment) were designated. The modulus of the

ground substance was set to 10 MPa based on data in the literature for ligaments and tendons [195]. The collagen content was set at 0.8 based on data in the literature [77]. Also, the number of distinct "fiber families" or "fiber ensembles" was set at 9; however, for simulations of transversely isotropic tissues, only one fiber family had non-zero values. Initial values for the remodeling constants for each parameter were also set to 5 as a default (units for the remodeling constants are per unit time). Remodeling ratios (q_i / p_i) were set at 100 for each parameter. Finally, the simulated in-vivo load was inputted as 25 N. It should be noted that the value for the simulated in-vivo load was arbitrary at this stage and not based in in-vivo measurements. However, providing a numeric value allows the calculation of E_t^{ens} and E_h^{ens} (as discussed later). With these values for the variables, matrices are set up to store the values of the parameters and their associated remodeling constants throughout time. Next, based on the fiber distribution at the initial timepoint and the number of fiber ensembles, the area at the initial timepoint for each fiber ensemble was calculated.

To model both the stress-strain behavior of the tissue as well as determine the remodeling rates, the strain of the tissue must be found. To do so, the deformation gradient, F, was defined as

$$F = \begin{bmatrix} \lambda & 0 & 0 \\ 0 & 1/\sqrt{\lambda} & 0 \\ 0 & 0 & 1/\sqrt{\lambda} \end{bmatrix} \qquad 7\text{-}15$$

Note that since the fibers were assumed to be incompressible, the determinant of F equals 1. Since $\det(F)=1=\lambda_{11}\lambda_{22}\lambda_{33}$ the stretches in the other directions (λ_{22}, λ_{33}) could be calculated. All other components of F were assumed to be negligible. Further, the right Cauchy-Green deformation tensor, C, was defined as

$$C = F^T F = \begin{bmatrix} \lambda^2 & 0 & 0 \\ 0 & 1/\lambda & 0 \\ 0 & 0 & 1/\lambda \end{bmatrix} \quad \text{7-16}$$

Then, the Green-Lagrangian strain tensor, E, was defined as

$$E = \frac{1}{2}(C - I) = \frac{1}{2}\begin{bmatrix} \lambda^2 - 1 & 0 & 0 \\ 0 & \frac{1-\lambda}{\lambda} & 0 \\ 0 & 0 & \frac{1-\lambda}{\lambda} \end{bmatrix} \quad \text{7-17}$$

The component E_{11} represented the tensile strain in the tissue along the direction of loading.

Using the parameter estimates (μ^{tiss}, σ^{tiss}, E_*^{tiss}, and k^{tiss}) for the normal tissue (Section 7.1.3.2) along with the input value for force and the CSA of the normal tissue, the value of E_{11} under homeostatic conditions could be calculated. Then, with Equation **2-6**, the fiber ensemble strain under homeostatic conditions (E_h^{ens}) could be calculated. The same process was done for the healing tissue at the initial timepoint to find E_t^{ens}. For the future curve-fitting algorithms, the matrix for E was defined from zero to E_t^{ens} at increments of ($30/E_t^{ens}$).

7.1.3.2 Algorithm to Fit Tissue Stress-Strain Data

In order to compare the experimental stress-strain data with those obtained from the model, it was necessary to describe the data in terms of a finite number of parameters. To do so, the constitutive model in Equation 7-2 was fit to the experimental stress-strain. In other words, the equation used to describe the fiber ensemble behavior was also used to fit the nonlinear tissue

stress-strain behavior. It is important to note that the parameters for the tissue behavior have no direct structural meaning, and are phenomenological in that sense. However, this approach provided ease for the optimization algorithm, and allowed estimation of four parameters (μ^{tiss}, σ^{tiss}, E_*^{tiss}, and k^{tiss}), which could then be compared to those produced by the model.

To accomplish this, a custom algorithm was written. Several values of E_*^{tiss} were chosen evenly throughout the data range. For each value of E_*^{tiss}, the stress-strain data above E_*^{tiss} were fit via a nonlinear least squares algorithm to obtain k^{tiss}. Then, sets of stress-strain data were created for individual values of the mean (μ) and standard deviation (σ) of the beta distribution via numerical integration of Equation 7-2. The values for μ and σ were chosen evenly throughout the range of possible values. For each set of parameter estimates, stress values were computed for each value of E_{11} from the experimental data. The sum of squared errors (SSE) between the experimental and computed stress values was calculated. The values of μ and σ which minimized the SSE were chosen as the best values. Then the range of μ and σ was decreased accordingly and process was repeated until the range for μ and σ was less than 0.01. The SSE between values of E_*^{tiss} were compared. The value of E_*^{tiss} with the lowest SSE was set as the new midpoint of the range of E_*^{tiss}, the range was decreased accordingly, and the process was repeated until the range for E_*^{tiss} was less than the difference in strain between two consecutive experimental data points for E_{11}. Using this algorithm, the values for μ^{tiss}, σ^{tiss}, E_*^{tiss}, and k^{tiss} for a tissue could be estimated using the stress-strain data.

7.1.3.3 Algorithm to Estimate Fiber Parameter Values Based on the Tissue Stress-Strain Data

With the initial values defined in Section 7.1.3.1 and the parameter estimates for the experimental data found in Section 7.1.3.2, the parameter estimates for the fiber stress-strain relationship could be found using a custom algorithm. Using Equation **2-6** and the fiber unit vector for each fiber ensemble, the fiber ensemble strain (E^{ens}) was calculated for each value of the Green-Lagrangian strain tensor, E, defined in Equation 7-17. Using the initial values of the fiber ensemble parameters (μ^{ens}, σ^{ens}, E_*^{ens}, and k^{ens}) along with E^{ens}, the fiber stress was calculated. Using Equation 7-1, this was then related to the 2nd Piola-Kirchoff stress for the tissue. Then, the 1st Piola-Kirchoff stress (P) was calculated using Equation 7-6.

This simulated data set was then fed into the algorithm defined in Section 7.1.3.2 to obtain parameter estimates (μ^{tiss}, σ^{tiss}, E_*^{tiss}, and k^{tiss}) for the simulated data. These were compared to the parameter estimates of the experimental data. If the difference between the simulated and experimental parameter estimates for any parameter was greater than 1% of the experimental parameter estimate, then the values for the initial values of the fiber ensemble parameters (μ^{ens}, σ^{ens}, E_*^{ens}, and k^{ens}) were updated based on the difference between the simulated and experimental values for the tissue-level parameters, and the process was repeated. This procedure was done until parameter estimates for the simulated data were within 2% of the experimental data. As such, estimates of the fiber ensemble parameters (μ^{ens}, σ^{ens}, E_*^{ens}, and k^{ens}) could be determined from the experimental data.

We wished to determine the sensitivity of the algorithm in terms of its ability to converge to a solution, even if the initial estimates for the fiber ensemble parameters were far from the actual values. To do so, a set of simulated stress-strain data was generated using a set of fiber

ensemble parameters (μ^{ens}=0.4965, and σ^{ens}=0.2646, E_*^{ens} =0.0336, and k^{ens}=387.0 MPa). Then these true values were multiplied by a random factor, and the resulting values were then used for the initial guesses for the fiber ensemble parameters. For k^{ens}, the range of random factors was 0.1-10. For μ^{ens}, σ^{ens}, and E_*^{ens}, the range of random factors was 0.5-2, based on the constraints of meaningful values for these parameters. The algorithm was run again with the new initial guesses and new sets of fiber parameters were obtained. This process was repeated ten times. For each trial, the absolute value of the percent error between the predicted and actual values was calculated. Across trials, the mean and standard deviation of the error were calculated. The coefficient of variation for each parameter was also calculated as the standard deviation of the parameter values divided by the mean of the parameter values multiplied by 100%.

All parameters converged to within 5% of the actual values. In terms of error, the values of k^{ens} were the lowest (0.4±0.3%). The error for μ^{ens}, σ^{ens}, and E_*^{ens} was 4.0±1.8%, 4.9±1.4%, and 3.8±3.0%. The coefficient of variation was also less than 5% for each parameter, and was 0.3%, 3.5%, 4.7%, and 3.4% for k^{ens}, μ^{ens}, σ^{ens}, and E_*^{ens}, respectively. Although these values for error and coefficient of variation were small, they do suggest the initial value for the fiber ensemble parameters could have some impact on the final estimation of the fiber parameters from the stress-strain curve of the tissue. This is due to the nonlinear nature of the function and the possibility of dependency between the parameters. Moreover, due to the nature of the constitutive model and experimental limitations, the micro-scale parameters are adjusted in the algorithm in order to create a macro-scale response which matches the experimental data. This creates an added difficulty in curve-fitting as opposed to if the parameters for the macro-scale response were being adjusted. Thus, to maintain consistency between simulations in future studies, the initial values for the microstructural parameters (μ^{ens}, σ^{ens}, E_*^{ens}, and k^{ens}) were set

equal to the corresponding values for the tissue (μ^{tiss}, σ^{tiss}, E_*^{tiss}, and k^{tiss}) found via the curve-fitting algorithm in Section 7.1.3.2.

7.1.3.4 Numerical Iteration to Simulate Growth and Remodeling

To simulate growth and remodeling in ligaments, an iterative technique was performed, beginning at a prescribed initial timepoint and advancing at a prescribed time increment (Δt). At each timepoint, the changes in the parameters for the fiber ensemble (μ^{ens}, σ^{ens}, E_*^{ens}, and k^{ens}) produced at each of the prior timepoints were calculated using Equations 7-13 and 7-14. Based on the amount of new tissue growth as well as the degradation of older tissue, the relative fraction of the matrix at each timepoint was recalculated. Using E, $\overline{E}_{11}^{t}$, and the new fiber ensemble parameters (μ^{ens}, σ^{ens}, E_*^{ens}, and k^{ens}), the overall stress response could be found in the same manner as in Section 7.1.3.3 and the tissue parameter estimates for μ^{tiss}, σ^{tiss}, E_*^{tiss}, and k^{tiss} could be obtained. Along with the new A_{11}, these parameter estimates were then used to determine E_{11} in response to the applied load at the current timepoint. Then, E_t^{ens} could be updated for the current timepoint as in Section 7.1.3.3. This process continued until the final timepoint was reached.

7.1.3.5 Algorithm to Adjust Remodeling Constants to Fit Experimental Data

For some simulations, the experimental data at the final timepoint were available. Thus, it was possible to compare the simulated data to the experimental data in terms of the estimated parameters. Based on the difference between the experimental and computed values for these

parameter, the associated remodeling constants were adjusted for each parameter via a custom algorithm. Then, the process in Section 7.1.3.4 was repeated. This procedure was continued until the parameter estimates of the simulated data were within 3% of the experimental data. In this manner, an estimation of the remodeling constants could be obtained.

7.2 PRELIMINARY MODEL AND SENSITIVITY ANALYSIS

7.2.1 Description of Preliminary Model

In order to demonstrate the general feasibility of the model, a parallel aligned tissue was simulated with a set of given input parameters and subjected to uniaxial tension along the direction of its fibers. Values for the parameters were based on those collected at our research center for the rabbit MCL at 12 weeks of healing as well as for the sham-operated control (Table 19) [171]. The parameters k^{ens}, A_{11}, and μ^{ens} were given positive rate constants, such that their associated parameters could increase with strains above the homeostatic strain. The rate constants for σ^{ens} and E^{ens} were given negative values. The input force was 25 N, resulting in a homeostatic strain (E_h^{ens}) of 0.014 in the normal tissue. This was within the toe region of the stress-strain curve. For this preliminary test, the time interval was set at 1 week. Healing was simulated from 12 to 26 weeks.

Table 19. Input data for preliminary model.

$q_{k^{ens}}$ (day^{-1})	0.3
$q_{\mu^{ens}}$ (day^{-1})	0.005
$q_{\sigma^{ens}}$ (day^{-1})	-0.0125
$q_{E_*^{ens}}$ (day^{-1})	-0.02
q_A (day^{-1})	0.1
$r_{k^{ens}}$	0.2
$r_{\mu^{ens}}$, $r_{\sigma^{ens}}$, $r_{E_*^{ens}}$, r_A	0.02
Force (N)	25
Δt (days)	7
E_h^{ens}	0.014
μ^{tiss} at 12 weeks	0.5023
σ^{tiss} at 12 weeks	0.2487
E_*^{tiss} at 12 weeks	0.068
A_{11} (mm^2) at 12 weeks	6.0
k^{tiss} (MPa) at 12 weeks	133.2
μ^{ens} at 12 weeks	0.5182
σ^{ens} at 12 weeks	0.2551
E_*^{ens} at 12 weeks	0.0638
k^{ens} (MPa) at 12 weeks	144.7

Figure 29 shows the simulated stress-strain behavior (P_{11} vs. E_{11}), CSA (A_{11}), and fiber ensemble strain under loading (E_t^{ens}) throughout healing. In general the stress-strain behavior increased over time, with the largest increases seen at the earlier timepoints of healing. The same was true for the A_{11}. Both of these trends correlated well with E_t^{ens}, which decreased in a nonlinear fashion. The steepest decrease in E_t^{ens} occurred at the early time points, and these changes became less apparent at the strain approached its homeostatic level.

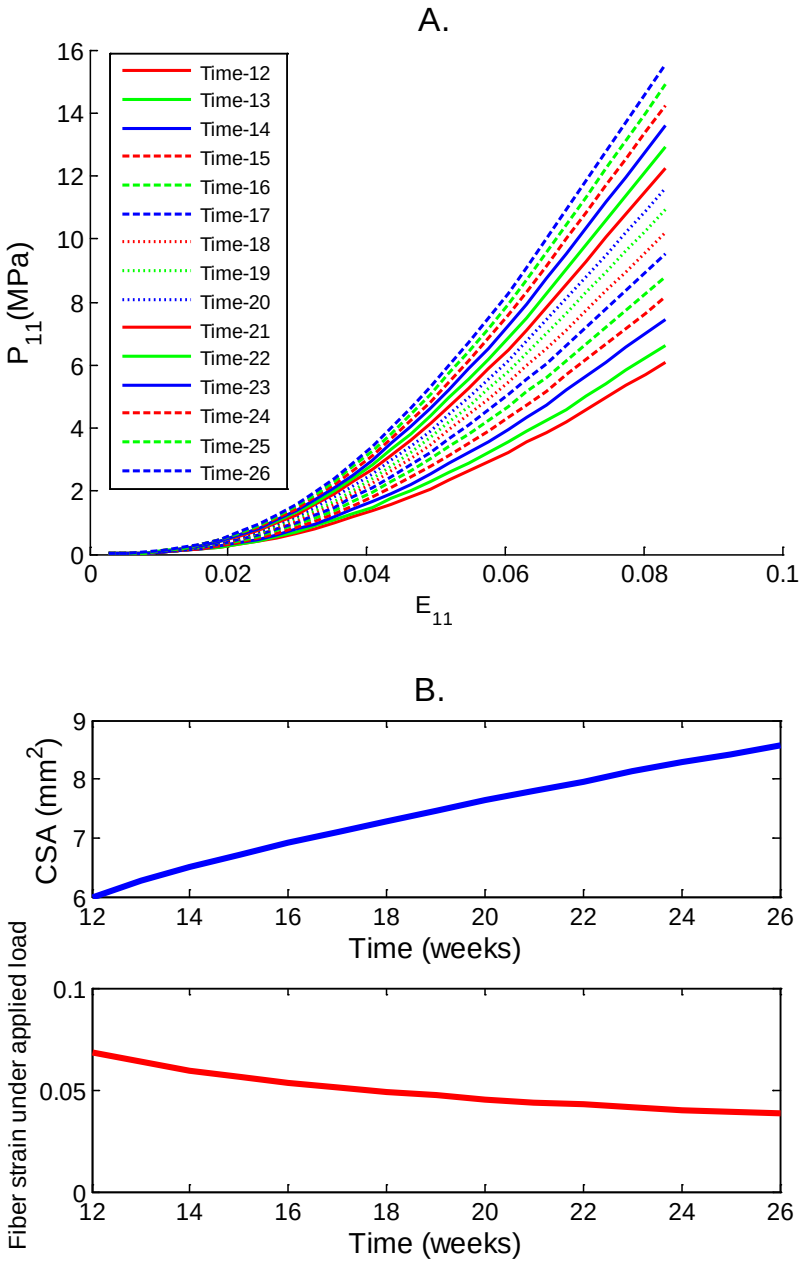

Figure 29. Simulated stress-strain data (A), cross-sectional area, and fiber ensemble strain under loading (B) as a function of time for preliminary model.

Based on these positive results, and noting the nonlinear nature of these changes throughout time, we next wanted to perform a simple sensitivity analysis to determine the impact of varying the time interval.

7.2.2 Sensitivity to Time Interval

Due to the highly nonlinear nature of the model, simulation of the data through time required numerical iteration at a given time interval (Δt). Thus, one important question is how the time interval impacts the obtained parameter values for the simulated data. Given the same set of initial data as in Section 7.2.1, the healing process was simulated from 12 to 26 weeks of healing. Separate simulations were conducted while varying only Δt from 1 day to 98 days. The simulated parameters at 26 weeks were obtained and compared between values of Δt. For example, the E_t^{ens} is shown in Figure 30. Percent error was calculated for each parameter with respect to the respective value when Δt=1 day (Table 20). In general, the largest errors were observed for Δt=98 days, and these errors decreased as Δt became smaller. At Δt= 7 days, the errors for all parameters were 1% or less of those for Δt=1 day. It is important to note that in general these differences were on the order or lower than our experimental accuracy for obtaining the original data. We also observed a drastic increase in the computational time with lower values of Δt. Considering both the error in parameter calculations and computational time, Δt=7 days was selected for all simulations in the next sections.

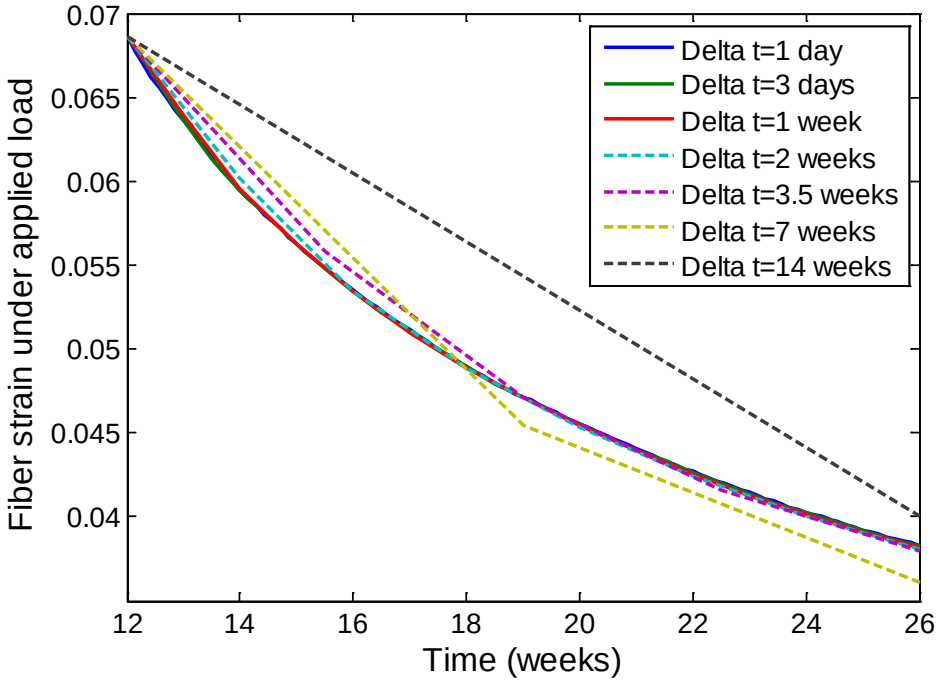

Figure 30. Fiber ensemble strain under applied load as a function of the time interval at which parameters are updated for remodeling.

Table 20. Error in parameter values at 26 weeks for the time interval sensitivity study (relative to Δt=1 day).

		Time interval (Δt in days)					
		98	49	14	7	3	1
Tissue Parameters	μ^{tiss}	3.2%	0.8%	-5.0%	0.0%	0.0%	0%
	σ^{tiss}	0%	-0.8%	-5.5%	0.5%	0.3%	0%
	k^{tiss}	-29.0%	-1.8%	-1.6%	-0.8%	-0.3%	0%
	E_*^{tiss}	-8.9%	-42.9%	4.4%	0.0%	0.0%	0%
	A_{11}	17.2%	16.9%	2.6%	1.2%	0.5%	0%
Fiber Parameters	μ^{ens}	1.5%	1.2%	0.2%	0.1%	0.0%	0%
	σ^{ens}	-4.2%	-3.2%	-0.5%	-0.2%	-0.1%	0%
	k^{ens}	4.8%	18.9%	2.2%	1.0%	0.4%	0%
	E_*^{ens}	-6.9%	-5.1%	-0.7%	0.3%	0.0%	0%
	E_t^{ens}	4.7%	-5.7%	-0.8%	-0.3%	-0.3%	0%

7.2.3 Relationship between Rate of Change in Area and Rate of Change in Modulus

We next wanted to ensure that the model could capture the interplay between the change in fiber ensemble properties (k^{ens}) and overall tissue growth (A_{11}). As a first example of this model, we evaluated the effect of varying the remodeling rates for A_{11} and k^{ens} (q_A and $q_{k^{ens}}$, respectively) for a parallel aligned tissue under uniaxial tension. Again, the representative values for the rabbit MCL at 12 weeks of healing were used as a basis. The Δt was 7 days, and the applied load was 25 N.

First, q_A was varied from 0.001 day^{-1} to 10 day^{-1}. The E_t^{ens} and stress-strain behavior of the tissue for each value of q_A is shown in Figure 31. Clearly, as q_A increases the strain under loading decreases more rapidly. At the same time, since the strain under loading decreases so rapidly, the ability of the matrix to remodel by changing its stress-strain behavior was limited. When q_A is much lower than $q_{k^{ens}}$, almost the entire decrease in strain under loading was due to alterations in the stress-strain behavior.

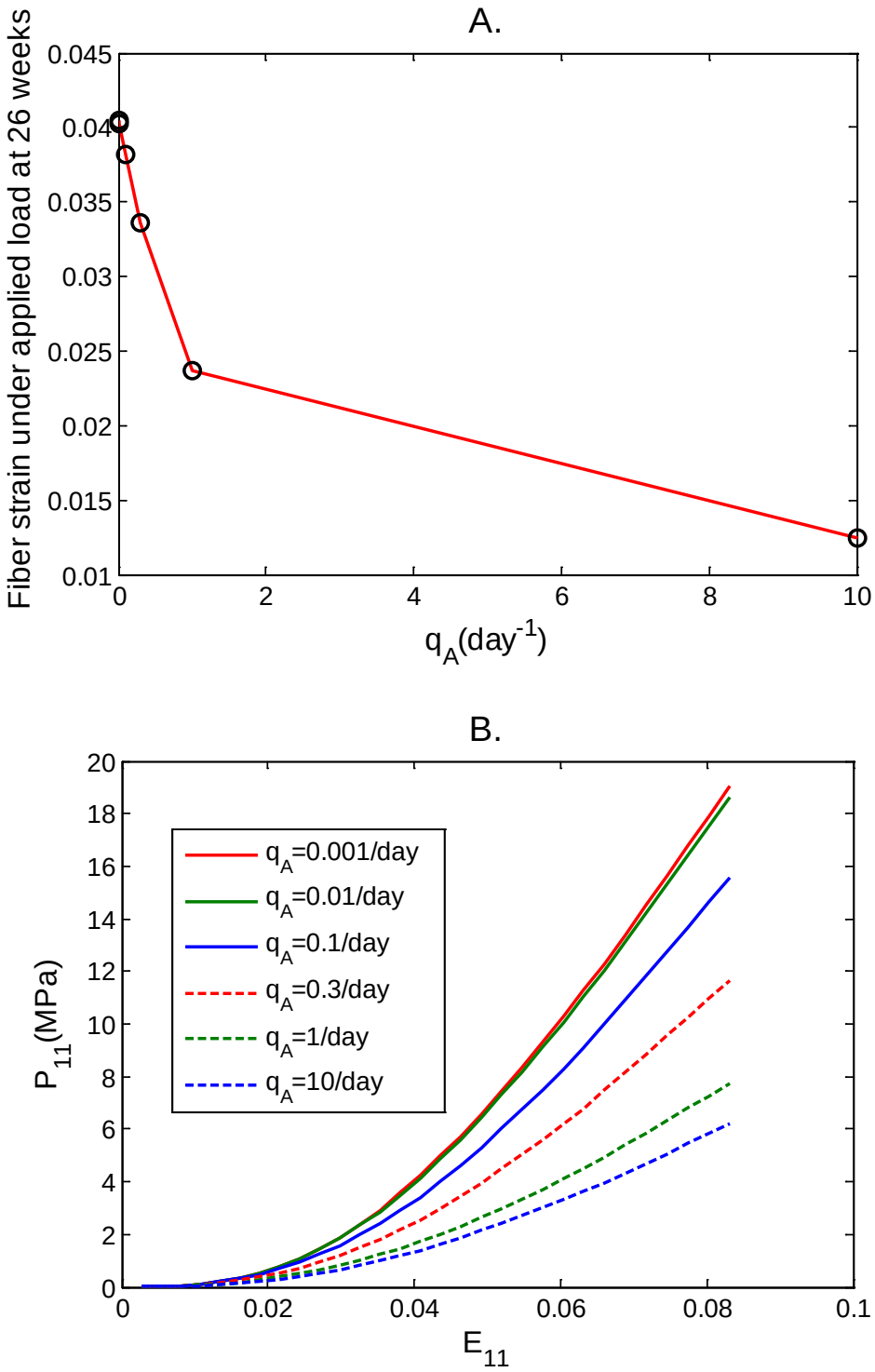

Figure 31. Fiber ensemble strain under loading (A) and stress-strain behavior (B) as a function of varying the rate of CSA growth (q_A).

Next, $q_{k^{ens}}$ was varied from 0.001 day^{-1} to 10 day^{-1}. The strain under loading and A_{11} of the tissue are shown in Figure 32. Like for q_A, the strain under loading also decreased with increasing values of $q_{k^{ens}}$. In fact, when the $q_{k^{ens}}$ was 10 day^{-1}, the final strain of the tissue under loading (0.014) was at its homeostatic value (0.014). As the rate of fiber modulus rate increased, the ability of the matrix to grow in size was limited. Also, under this condition, the matrix did not have to change in size, since the strain under loading decreased so rapidly due to the changes in k^{ens}.

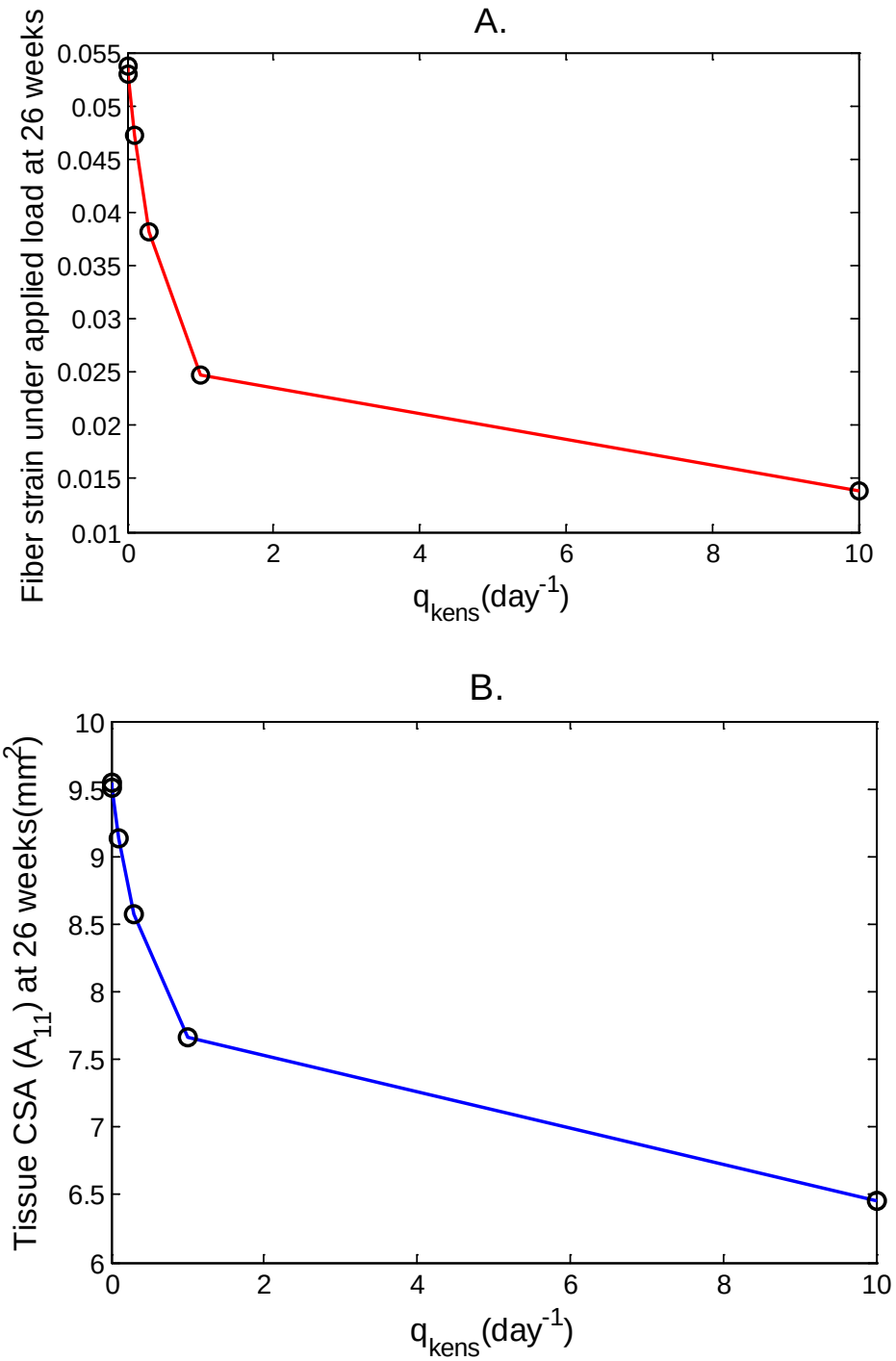

Figure 32. Fiber ensemble strain under loading (A) and cross-sectional area (A_{11}) (B) as a function of varying the rate of fiber modulus ($q_{k^{ens}}$).

7.3 APPLICATION TO MEDIAL COLLATERAL LIGAMENT HEALING

Next, we wished to determine if the model could be used to describe the healing MCL and predict the behavior of those treated with an ECM bioscaffold using data obtained for the non-treated healing MCL. First, parameters describing the tissue stress-strain behavior were first estimated to obtain a better idea of the differences between the ECM-treated and non-treated groups.

The experimental data for the normal and healing MCL have been previously reported [143, 171]. It should be noted that the experimental protocols differed for the data collected at 12 and 26 weeks of healing. For the data at 12 weeks (including the sham-operated controls), each specimen was preloaded to 1 N, preconditioned for ten cycles from 0 to 0.75 mm, before loading to failure at 5 mm/min. For the data at 26 weeks (including the sham-operated controls), each specimen was preloaded to 2 N, preconditioned for thirty cycles from 0 to 1.5 mm, before loading to failure at 10 mm/min. Each test was performed using a materials testing machine (Instron, Model 4502, Canton, MA) in a saline bath kept at 37ºC. From the load-to-failure test, the load-elongation and stress-strain data could be obtained [143, 171]. In this dissertation, these original data files were used to obtain the parameters describing the tissue stress-strain behavior. Since the difference in preload between the protocols at 12 and 26 weeks may have led to inconsistency in evaluating the "zero position" of the specimens, the "zero strain" condition was set as 2 N for all specimens. The difference in elongation rates may have also limited comparisons between timepoints; however, it has been shown that ligaments are generally strain-rate insensitive, even when the strain rate changes by a few orders of magnitude [266]. Since the load-to-failure test was performed at least one hour following preconditioning, it was also assumed the differences in the level of elongation and number of cycles was also negligible.

Thus, it was assumed that the stress-strain behavior of the tissue was comparable between time points.

The algorithm was able to fit all curves with R^2>0.999. The values for the obtained parameters for the healing MCLs and sham-operated MCLs are presented in Table 21 and Table 22, respectively. For the sham-operated controls, the most interesting value is that for E_t^{ens} at 25 N of load. For all sham-operated MCLs, this value was fairly consistent at about 1-2%. For the both treated groups at 12 weeks, this value was higher than the sham-operated controls. Also, at 12 weeks, the value for the ECM-treated group (0.035) was almost 55% lower than for the non-treated group (0.077). Interestingly, by 26 weeks, these values were similar to each other (0.044 vs. 0.043), which implies that both treatment groups had reached the same level of strain for a given load, suggesting that they are remodeling to reduce the strain to similar levels. However, since the ECM-treated group had a k^{tiss} at 12 weeks of healing, its properties did not need to change as much as the non-treated group (in which k^{tiss} rose rapidly). The implications of this can be tested in the model.

Table 21. Average parameter values for the tissue stress-strain behavior for the healing MCLs for the non-treated (NT) and ECM-treated (ECM) groups.

	k^{tiss} (MPa)	μ^{tiss}	σ^{tiss}	E_*^{tiss}	E_t^{ens}	A_{11} (mm^2)
NT-12 weeks	133 ± 66	0.50 ± 0.05	0.24 ± 0.01	0.068 ± 0.028	0.077 ± 0.011	7.2 ± 4.7
NT-26 weeks	321 ± 136	0.53 ± 0.04	0.22 ± 0.02	0.055 ± 0.014	0.043 ± 0.012	6.4 ± 1.4
ECM-12 weeks	277 ± 116	0.52 ± 0.04	0.26 ± 0.02	0.035 ± 0.019	0.035 ± 0.022	7.9 ± 3.4
ECM-26 weeks	378 ± 108	0.52 ± 0.05	0.23 ± 0.02	0.054 ± 0.014	0.044 ± 0.012	5.0 ± 1.3

Table 22. Average parameter values for the tissue stress-strain behavior for sham-operated rabbit MCLs for the non-treated (NT) and ECM-treated (ECM) healing groups.

	k^{tiss} (MPa)	μ^{tiss}	σ^{tiss}	E_*^{tiss}	E_t^{ens}	A_{11} (mm^2)
ShamNT-12 weeks	1115 ± 436	0.44 ± 0.14	0.22 ± 0.03	0.019 ± 0.007	0.013 ± 0.005	5.1 ± 1.0
ShamNT-26 weeks	1124 ± 457	0.42 ± 0.05	0.22 ± 0.02	0.037 ± 0.010	0.021 ± 0.008	4.2 ± 0.4
ShamECM-12 weeks	1152 ± 217	0.46 ± 0.09	0.23 ± 0.01	0.020 ± 0.007	0.014 ± 0.004	4.2 ± 0.8
ShamECM-26 weeks	1191 ± 439	0.44 ± 0.05	0.22 ± 0.03	0.032 ± 0.009	0.018 ± 0.004	4.1 ± 0.6

For this simulation, all remodeling rates except for $q_{k^{ens}}$ and q_A were held constant for simplicity. The experimental and simulated stress-strain data are plotted in Figure 33. The model was able to match the shape of the curve for the experimental data at 26 weeks (R^2>0.999). The values for the modulus of the tissue at 26 weeks for the experimental and simulated data sets were identical (321 MPa and 321 MPa, respectively). Further, the simulated A_{11} could match the

experimental value to within 0.5% (6.40 mm^2 vs. 6.43 mm^2, respectively). For the non-treated group to reach the average modulus value at 26 weeks, $q_{k^{ens}}$ was found to be 0.25 day^{-1}, while q_A was -1.52 day^{-1}.

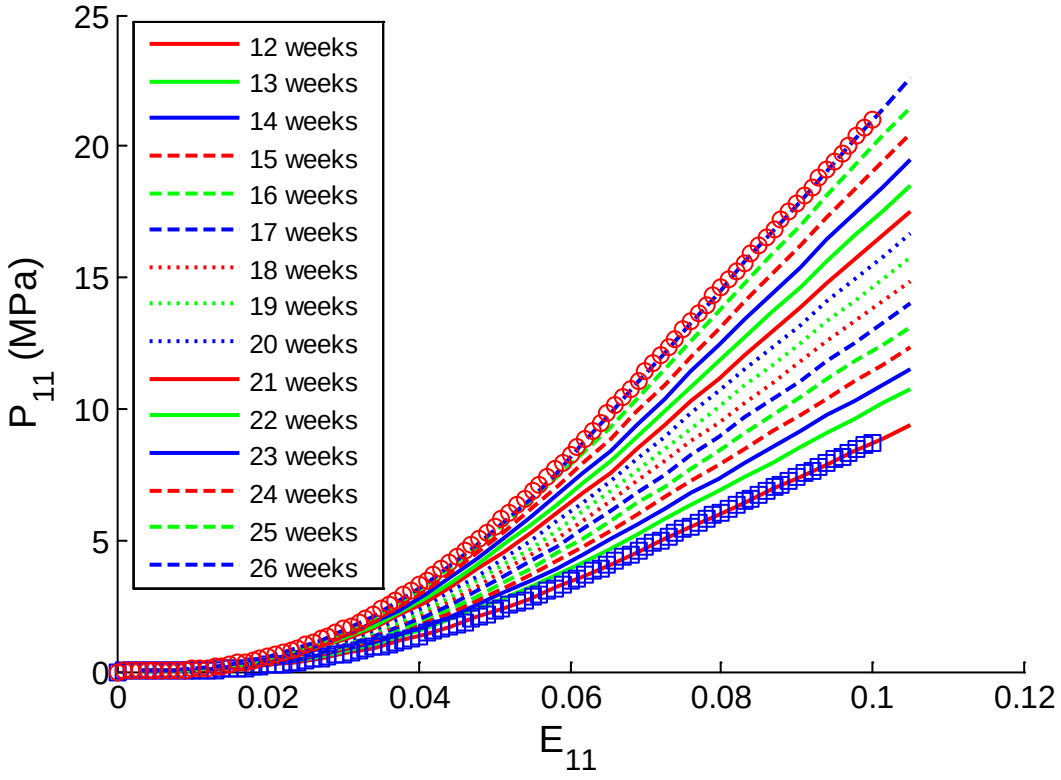

Figure 33. Experimental and simulated stress-strain data for non-treated healing rabbit MCLs from 12 to 26 weeks of healing.

We then wished to see whether the rate constants found for the non-treated group could be used to predict the results for the ECM-treated group. The same rate constants found above were used along with the average ECM-treated data at 12 weeks to a set of simulated data out to 26 weeks. The experimental and simulated stress-strain data are plotted in Figure 34. In this case, the model over predicted the stress-strain behavior of the ECM-treated healing tissue at 26 weeks. In fact, the model predicted a value for k^{tiss} of 449 MPa, which was 19% greater than the actual mean value of the experimental data (378 MPa).

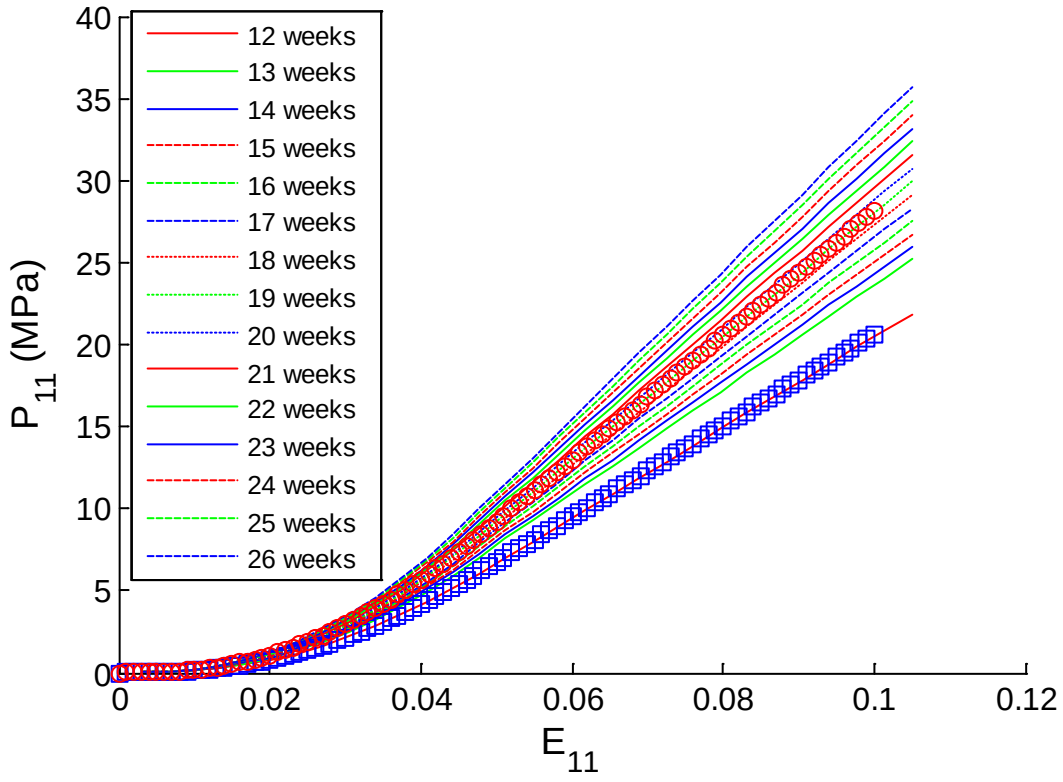

Figure 34. Experimental and simulated predicted stress-strain data for ECM-treated healing rabbit MCLs. The simulated stress-strain curves were created using the rate constants for the non-treated group.

Even though the model could not predict the results of ECM-treatment, we could still separately fit the ECM-treated group to the model to obtain $q_{k^{ens}}$ and q_A. Again, there was good agreement between the model and experimental data at 26 weeks (Figure 35, R^2>0.999). To reach the experimental modulus value at 26 weeks, $q_{k^{ens}}$ was found to be 0.13 day^{-1}, while q_A was -8.8 day^{-1}. The value for $q_{k^{ens}}$ was lower than the corresponding value for the non-treated group, while the value for q_A was much higher. These trends correspond to the experimental data as the relative increase in modulus was smaller and the relative decrease in A_{11} was larger

for the ECM-treated group from 12 to 26 weeks. As an additional note, for the model to match the experimental value for A_{11} at 26 weeks, a negative value for q_A was needed for both experimental groups, since the values for A_{11} decreased for both from 12 to 26 weeks. This topic is discussed in Section 8.3.

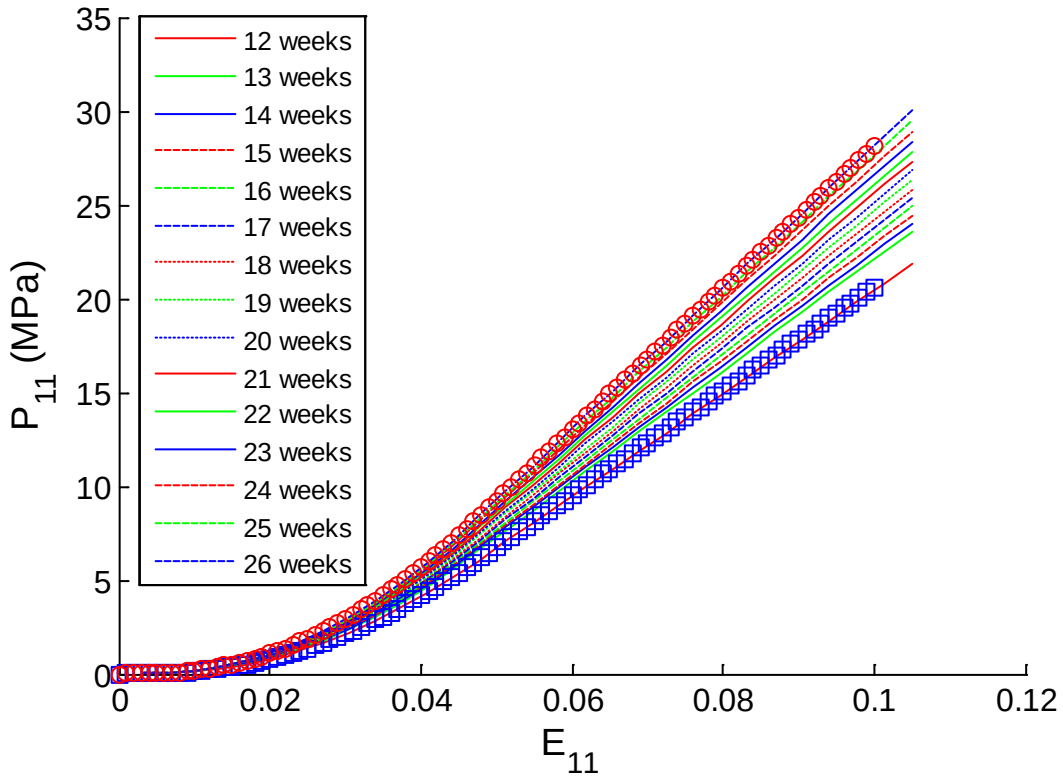

Figure 35. Experimental and simulated stress-strain data for ECM-treated healing rabbit MCLs from 12 to 26 weeks of healing.

To further illustrate the differences between the two healing groups, E_t^{ens} is presented as a function of time (Figure 36). In the non-treated group, E_t^{ens} decreases steadily as healing progresses. This matches the experimental data in Table 21 which showed large increases k^{tiss}

with only a slight reduction in A_{11}, which allows E_t^{ens} to decrease. On the other hand, E_t^{ens} for the ECM-treated group slightly increased over time. This also matched the experimental data in that E_t^{ens} increases from 12 to 26 weeks. With the sharp decrease in A_{11} within the ECM-treated group, E_t^{ens} should increase. Meanwhile, the matrix is remodeling to a better quality tissue such that E_t^{ens} should decrease. These counteracting mechanisms result in the relatively flat value of E_t^{ens} in Figure 36. Clearly, trends in the non-treated and ECM-treated tissues are quite different, so it is not surprising that the rate constants from the non-treated group could not predict the results for the ECM-treated group. Interestingly, the two plots appear to be converging to a similar value of E_t^{ens}.

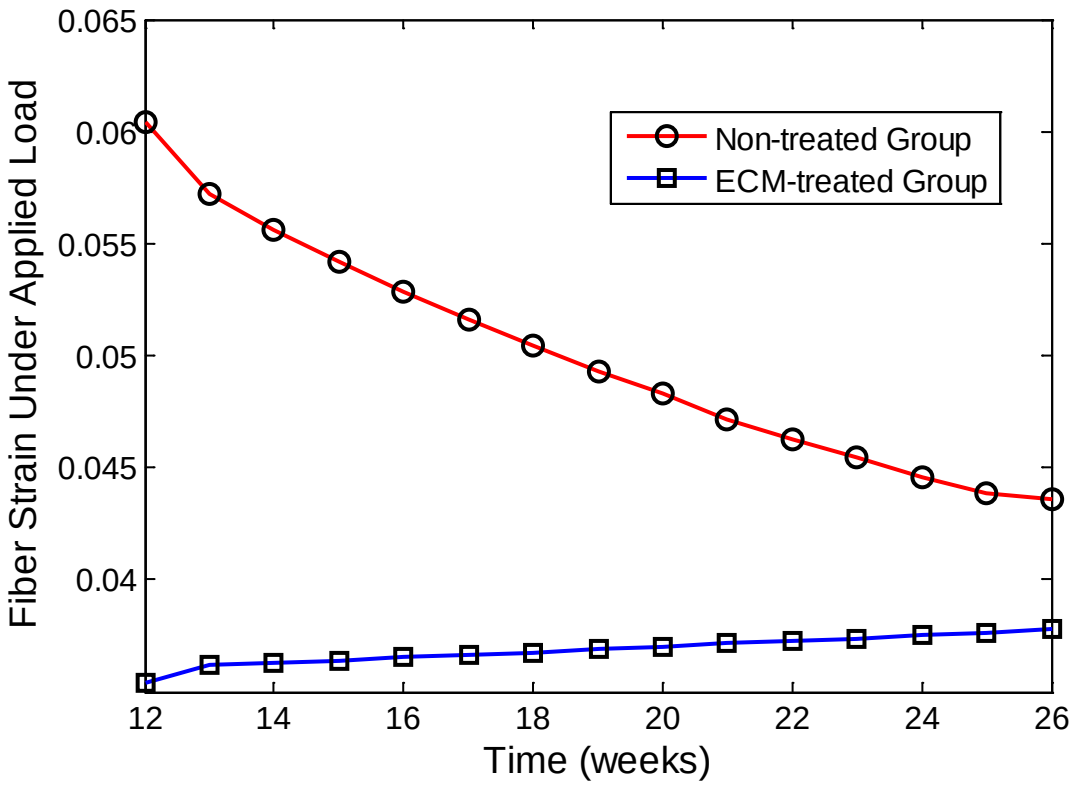

Figure 36. Fiber ensemble strain under applied load for the non-treated and ECM-treated groups as a function of time of healing.

7.4 IMPLICATIONS FOR ANTERIOR CRUCIATE LIGAMENT HEALING AND PRELIMINARY RESULTS

The previous section highlighted the importance of the level of strain on the remodeling response. The model suggests that the ECM-treated group experienced lower strains at 12 weeks compared to the non-treated group. Thus, its stimulus to grow and/or remodel was reduced. As such, its E_t^{ens} did not change over time. For the ACL, there is currently a lack of multiple time point data necessary to make comparisons like in the case of the MCL. Only three treatment groups have been completed at a single time point in Specific Aims 1 & 2. Further, due to the complex geometry of the ACL, determining its mechanical properties is a challenge, since neither a uniform cross-section nor a uniform strain distribution, could be assumed.

Alternatively, the computation model could be used to perform some simple simulations to supplement and explain the experimental findings to date. All initial values were kept the same as in Section 7.3, with the following exceptions: 1) force=50 N, 2) $q_{k^{ens}}$=0.05, 3) q_A=0.025, and 4) E_h^{ens}=0.0233. Based on the values of stiffness of the healing FATCs and CSA of the healing ACL in Specific Aim 1, we can estimate the tangent modulus of the tissue at 12 weeks. The modulus of the ECM-treated group was estimated as 60 MPa, while the value for the suture repair group was 100 MPa. Notice that the value for the suture repair group was higher, since the CSA of the ECM-treated group was more than 4x the suture repair group, while the stiffness of the healing FATC was only 2.5x greater.

With the simulation of healing to 26 weeks, the healing ACL for the ECM-treated group still had a lower stress-strain response compared to the non-treated group (Figure 37A), resulting in lower values of tangent modulus(k^{tiss}, 78 MPa vs. 149 MPa, respectively). On the other hand,

the CSA of the healing ACL was 4.1 times higher for the ECM-treated group versus suture repair (32.5 mm^2 vs. 7.9 mm^2, respectively). As a result, the simulated load-elongation behavior of the healing ACL for the ECM-treated group was much greater compared to the suture repair group (Figure 37B). In fact, the linear stiffness was 115% greater for the ECM-treated group (76 N/mm vs. 35 N/mm, respectively). Moreover, the stiffness for the suture repair group at 26 weeks was similar to the value achieved by the ECM-treated group at 12 weeks. This clearly shows the delay in the function of the healing ACL with suture repair alone.

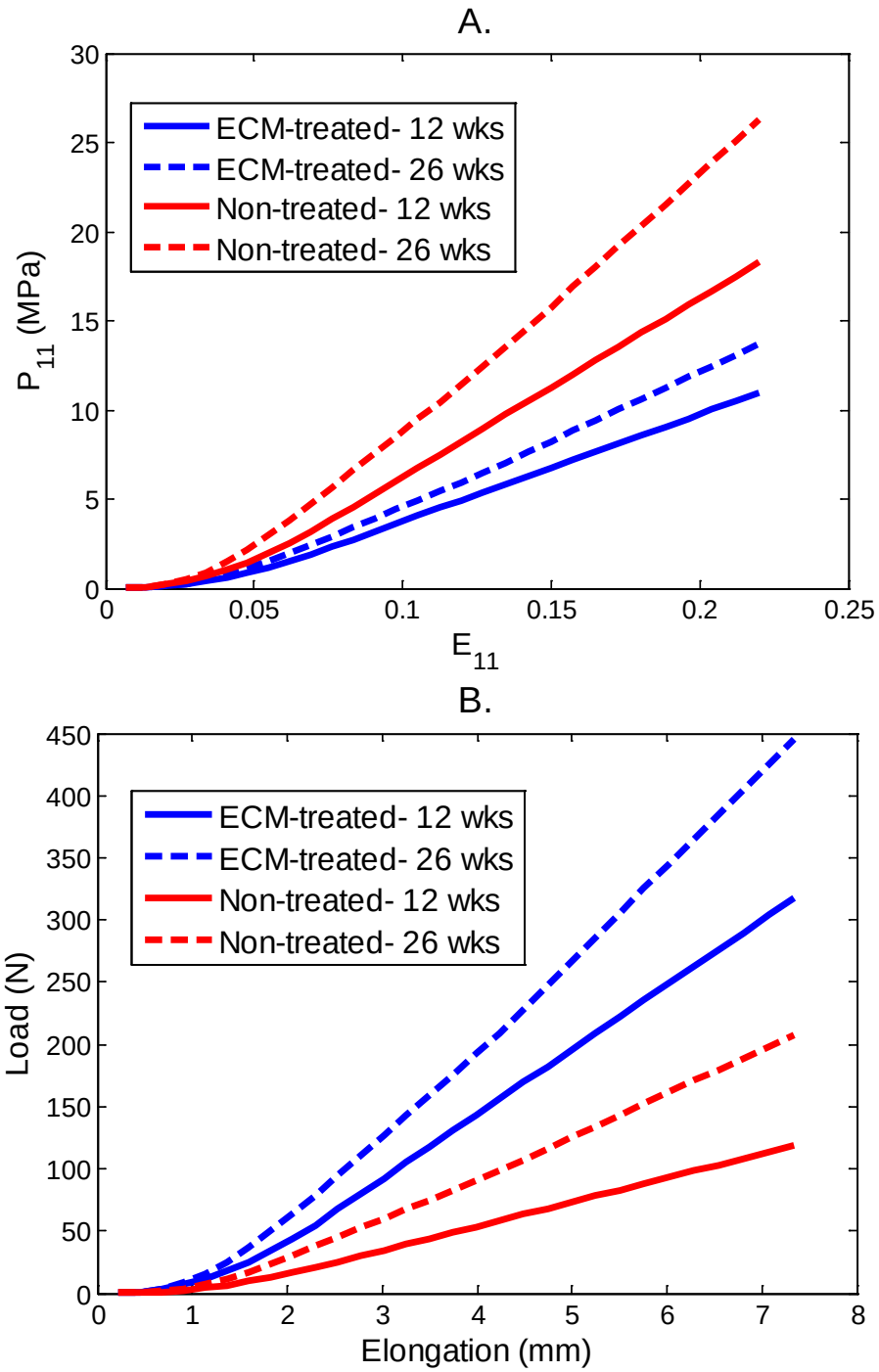

Figure 37. Simulated stress-strain behavior (A) and load-elongation behavior (B) for the healing ACL for the ECM-treated and suture repair groups at 12 and 26 weeks of healing.

Another item of interest is the effects of hypertrophy of the tissue, i.e. excessive CSA, on the growth and remodeling of the healing ACL. We again considered the healing ACL as a transversely isotropic tissue, and two conditions were simulated from 12 to 26 weeks: 1) a healing tissue with a CSA of 29 mm^2 (CSA29 group), similar to the ECM-treated group in Section 5.0 , and 2) a healing tissue with a CSA of 58 mm^2 (CSA58 group), double that of the CSA29 group. The initial modulus of the fibers (k^{ens}) was adjusted such that the two groups would have similar load-elongation behavior at 12 weeks (60 MPa and 30 MPa for CSA29 and CSA58 groups, respectively). The simulated force was 50 N. All other initial parameters were held constant between simulations and were similar to those found in Section 7.2.1. At both 12 and 26 weeks, the mechanical behavior of the CSA29 group was higher than that of the CSA58 group (Figure 38A). Interestingly, the relative change in tangent modulus (k^{tiss}) for both groups at 26 weeks compared to 12 weeks was about 31% and 34% for the CSA29 and CSA58 groups, respectively (79 MPa and 40 MPa at 26 weeks, respectively). The estimated load-elongation behavior of the tissue was similar at both 12 and 26 weeks. However, because the CSA of the CSA58 group was larger, the E_{11} under the applied load was lower at all time points (Figure 38B). This suggests that the CSA29 tissue retains a greater capacity to remodel its mechanical behavior in the long-term and highlights the importance of limiting hypertrophy at early phases of healing in order to obtain better quality tissue in the long-term.

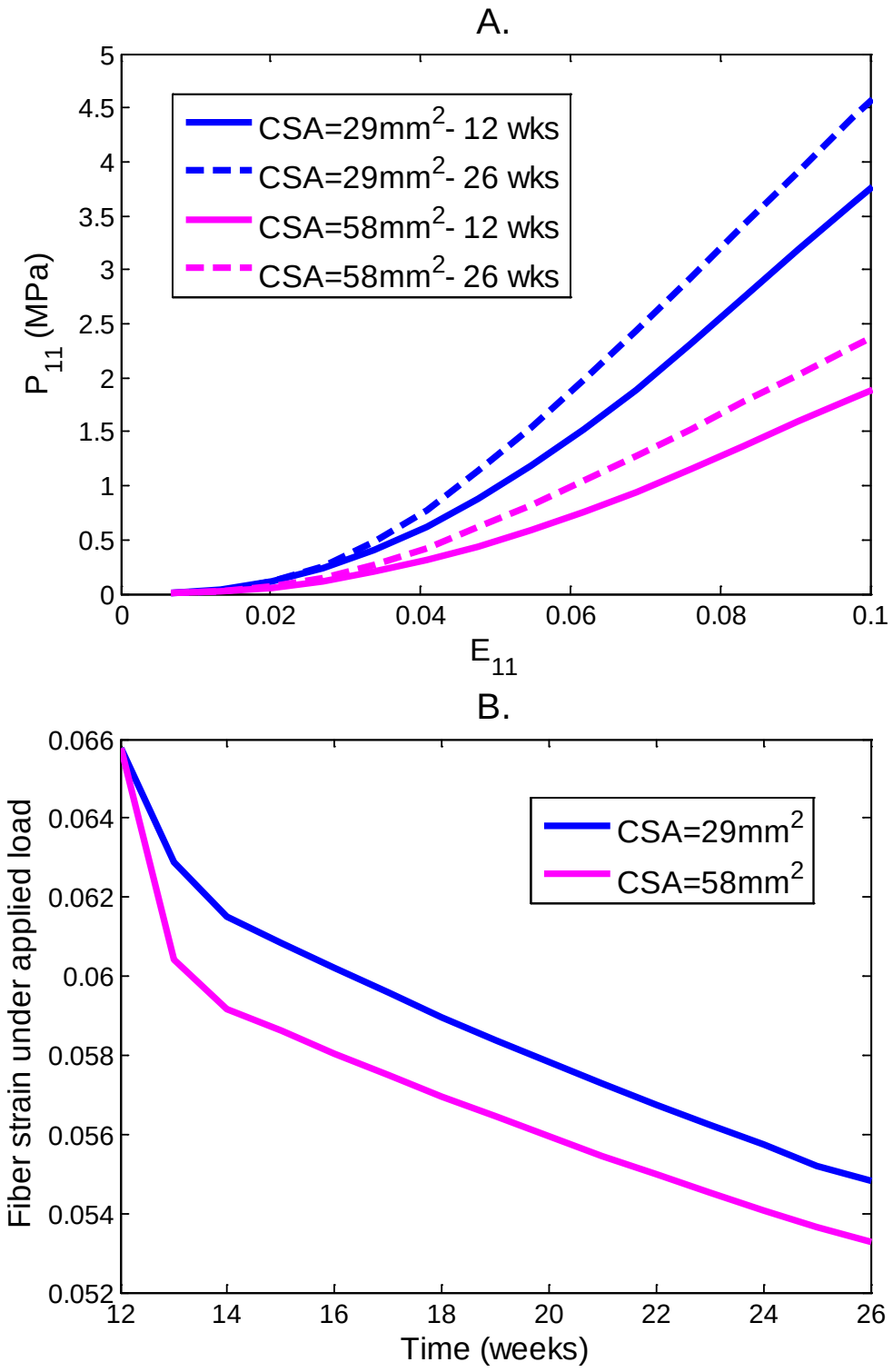

Figure 38. Simulated stress-strain behavior (A) and strain under applied load over time (B) for healing ACLs of varying CSA.

Finally, we considered the effects of the levels of loading on the healing tissues. The same tissue with a CSA of 6 mm^2 was simulated from 12 to 26 weeks of healing with either 25 or 50 N of applied load (Figure 39). Compared to the 25 N loading condition, the tissue was able to achieve superior stress-strain and load-elongation behavior under the 50 N loading condition. In fact, by 26 weeks, the predicted tangent modulus was 12% higher (149.4 MPa vs. 133.9 MPa, respectively), while the predicted stiffness was 19% higher (35.2 N/mm vs. 29.6 N/mm, respectively) for the 50 N loading condition compared to the 25 N loading condition. This highlights the importance of the applied load on the remodeling of the tissue, although the effects were not as drastic as the results due to changing the CSA. A discussion of these topics can be found in Section 8.3.

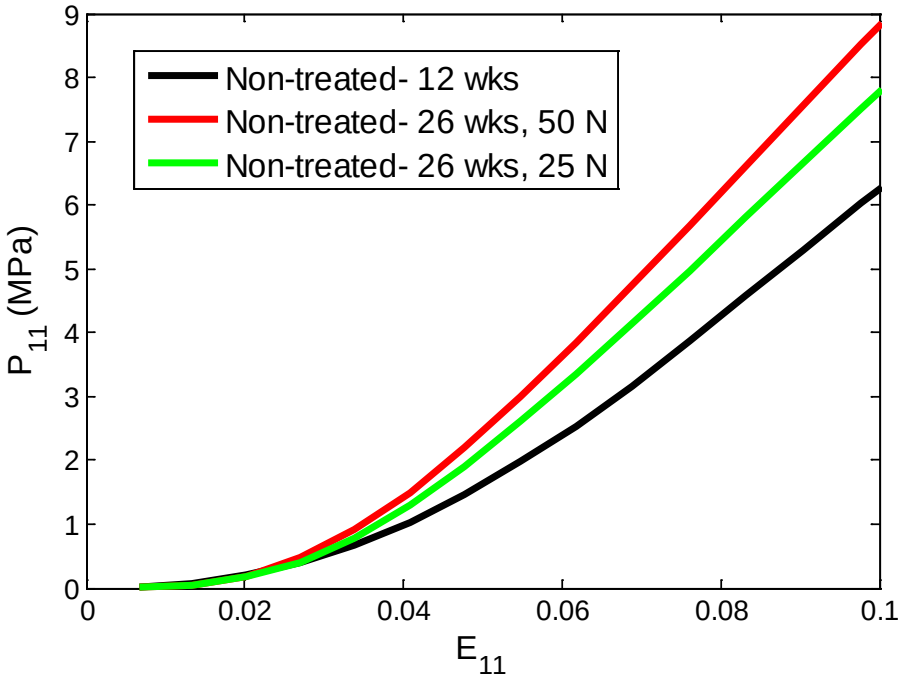

Figure 39. Simulated stress-strain behavior at 12 weeks (B) for healing ACL tissues under different loading conditions from 12 to 26 weeks.

8.0 DISCUSSION AND CONCLUSIONS

In this dissertation, we were able to demonstrate the positive impact of biological and mechanical augmentation on the healing of an injured ACL through a combined experimental and computational approach. First, the ability of an ECM bioscaffold in combination with an ECM hydrogel to enhance ACL healing following suture repair was demonstrated in the goat model at 12 weeks. ECM-treatment led to improved biomechanical properties and histological appearance of the healing ACL compared to suture repair alone. Second, a suture augmentation procedure was developed to provide additional mechanical augmentation to the healing ACL. Improved joint stability was shown at time-zero versus suture repair. These positive changes were also found at 12 weeks of healing, although to a lesser extent. Interestingly, suture augmentation with a simple suture repair led to a marked increase in neo-tissue formation as well as biomechanical properties of the healing ACL compared to suture repair alone. Finally, as a first step toward predicting long-term outcomes following these biological and mechanical augmentation procedures, a mathematical model was developed to describe the remodeling process of healing ligaments. Its ability to quantify changes in tissue biomechanical properties and CSA were shown in a generalized model of a healing ligament. Then, data for the healing MCL were used to test the validity of the model and provide insight as to an appropriate mathematical formulation to describe the changes in the healing ligament. Finally, the model

was used to provide some early implications of the healing of the ACL following biological and mechanical augmentation.

8.1 IMPACT OF ECM TREATMENT ON THE HEALING OF THE ACL

In Specific Aim 1, we were able to demonstrate that a combination of ECM-SIS bioscaffold coupled with its hydrogel form could improve the healing of a transected ACL following suture repair. We first hypothesized that the bioactive degradation byproducts of ECM-SIS [22, 247] would stimulate cells to produce more matrix for increased neo-tissue formation. In fact, gross observation showed abundant tissue formation compared to suture repair alone. In terms of the CSA of the ACL, ECM-treatment led to four times as much healing tissue formation compared to suture repair alone. These results are similar to previous studies in our research center using ECM-SIS to treat a 6mm MCL gap injury and central third PT defect injury [123, 143, 267]. In both cases, significant tissue formation was observed at 12 weeks of healing.

We further hypothesized that an ECM sheet could act as a temporary synovium to protect the injury site and allow tissue formation. Following injury of the ACL, the synovium, which surrounds the ACL, is disrupted. This allows synovial fluid to enter the injury site and prevent healing tissue formation. Since the ECM sheet surrounded the injury site, it could have functioned to prevent excessive tissue growth, ultimately making it a tissue of better quality. In fact, the values for CSA of the ECM-treated ACL were not significantly different from the sham-operated controls. These results are similar to our previous results for the rabbit MCL which noted that values for CSA of the ECM-treated healing tissue at 26 weeks were closer to the normal MCL compared to those in the non-treated group [143, 267].

Further, the structural properties of the healing FATC were improved with ECM-treatment versus suture repair alone. More specifically, the stiffness of the healing FATCs following ECM-treatment was more than double those of the suture repair group. In the case of the MCL, these increases were observed in terms of the mechanical properties of the tissue, i.e. tissue quality. However, due to the complex geometry of the ACL, an accurate description of its mechanical properties was not experimentally possible.

The impact of these improvements in the biomechanical properties of the healing ACL with ECM-treatment on joint stability was determined using a robotic/UFS testing system. Interestingly, under loads simulating a clinical exam for ACL function, statistical significance compared to the suture repair group could not be obtained for measures of joint kinematics and the contribution of the healing ACL (i.e. its in-situ force), despite obvious differences in the behavior of these two groups. For these tests, the relative levels of loading were lower compared to those during tensile testing. Thus, although improved joint function could be qualitatively observed with ECM-treatment compared to suture repair alone, higher levels of loading (tensile testing) were necessary to definitively show quantitative differences. If higher loads were applied, the differences in joint kinematics likely would have been more apparent.

The suture repair technique chosen in this study was based on studies in the clinical literature for repair of an injured ACL [61, 120, 248]. In these studies, up to an 80% rate of failure was observed at five year post-operatively in terms of joint stability. Nevertheless, the clinical outcomes following suture repair are quite variable, as a small percentage of patients do not need secondary surgery or have premature osteoarthritis following suture repair. Similarly, in the current study, large amounts of variability were seen in the amount of joint stability as well

as the neo-tissue formation, CSA of the healing ACL, and stiffness and ultimate load of the healing FATC.

The impact of ACL injuries on joint function cannot be understated. In clinical studies, following ACL injury with no surgical treatment, there is persistent instability as well as an increased risk for damage to the other structures of the knee, such as the medial meniscus, as well as development of premature OA [13, 40, 61, 119, 120, 183, 185, 220, 237, 281]. Furthermore, animal studies have documented both degenerative changes of the articular cartilage and hypertrophy of the medial meniscus could be observed at 12 weeks post-operatively following ACL transection [113]. Thus, for FTE approaches to be fully successful, joint stability must be maintained during healing. Further, the effectiveness of such approaches must be determined in terms of overall joint function, including changes to structures other than the ACL, such as the medial meniscus (See Future Directions, Section 9.0).

Our data compare favorably to those healing ACLs treated with a collagen-platelet composite scaffold following suture repair in a porcine model, which is tthe current standard for FTE treatment of the injured ACL [118]. After the same period of healing (3 months), the stiffness of the healing FATCs from the ECM-treated group had values reaching 53 ± 19 N/mm compared to 40.2 ± 21.8 N/mm following collagen-platelet composite treatment. However, it should be noted that there are differences in the animal model, surgical procedures, and methods of biomechanical evaluation that prevent a direct statistical comparison between these studies.

When comparing our results to those for ACL-reconstruction using the goat model [5, 48, 114, 175, 190], the A-PTT for the ECM-treated group was well within the range for those in the ACL-reconstructed knees, which could be 2-6 times higher than the intact knees on average at 12 weeks of healing. Further, a previous study from our research center has shown the in-situ force

of ACL replacement grafts in the goat model to be ~25-45 N at 6 weeks of healing in response to a 67-N anterior tibial load [5, 190]. Similar in-situ force levels (from 31-53 N) were seen in the ECM-treated ACLs. Further, the stiffness of the healing FATCs from the ECM-treated group (53 ± 19 N/mm) were also comparable to those with ACL-reconstruction at 12 weeks post-operatively (37.2 ± 22.0 N/mm) [175]. Interestingly, in the same study on ACL-reconstruction, the stiffness of the healing graft reached 33% and 50% of normal at 1 and 3 years, post-operatively. In the current study, the stiffness of the healing FATC reached 48% at 12 weeks, which may suggest that the remodeling process of the healing ACL may be accelerated compared to that of an ACL-reconstruction graft. However, data at longer-term time points will be necessary to confirm this hypothesis. The findings of using ECM treatment for ACL healing in the goat model show promise as the data are comparable to those following ACL reconstruction, which is the current clinical standard for treatment of ACL injuries.

Another important contribution of this study was the use of genetically-modified ECM, which could help to address the clinical concerns of chronic inflammation found in some patients following implantation of the porcine ECM [109, 154]. A significant part of the inflammatory response can be attributed to the existence of the αGal epitope [21, 153]. However, since the ECMs degrade rapidly in-vivo, the impact of the αGal epitope for ECM-related applications has been debated. A recent study using porcine-derived ECM to treat an abdominal wall defect in a primate model showed that the αGal epitopes did increase the presence of αGal antibodies in the serum, but otherwise did not negatively affect the remodeling of the tissue [51]. Nevertheless, there are still concerns among clinicians regarding the implantation of porcine materials for orthopaedic applications, and ECMs from these αGal(-) pigs may offer promise for more widespread use in the future.

In summary, Specific Aim 1 demonstrated the potential application of ECM bioscaffolds and hydrogels in combination with suture repair for ACL healing. However, it was noted that even with ECM-treatment, a considerable amount of joint instability was found at 12 weeks of healing. This motivated the development of alternative suture techniques for mechanical augmentation of the healing ACL in Specific Aim 2.

8.2 MECHANICAL AUGMENTATION OF THE HEALING ACL VIA SUTURE TECHNIQUES

In Specific Aim 2, we wished to compare the effectiveness of a newly developed suture augmentation technique to the suture repair technique utilized in Specific Aim 1. Before making these comparisons, we first assessed whether the tunnel locations selected for the suture augmentation would have an effect on the joint stability (Section 6.1.1). Since there was no statistically significant change in joint stability due to the tunnel locations chosen, the findings suggested that the sutures be placed anterior to the ACL footprint of the femoral origin and medial to the ACL footprint of the tibial insertion since it was simpler and avoided further injury to the ACL. This procedure was used in the remainder of Specific Aim 2.

8.2.1 Impact of Suture Augmentation on Initial Joint Stability Compared to Suture Repair

In Specific Aim 2.1, we utilized a robotic/UFS testing system to apply external loads to a set of goat stifle joints to assess the ability of suture techniques to restore joint stability as well as the relative contribution of the ACL. We found that suture augmentation could restore the joint kinematics near the levels of the intact joint, while the in-situ forces in the sutures were closer to the ACL compared to suture repair. These results supported our hypothesis that bone-to-bone fixation provided by suture augmentation could allow better stability compared to the soft tissue-to-bone fixation with suture repair.

As in Specific Aim 1, the suture repair technique chosen in this study was based on studies in the clinical literature for repair of an injured ACL [61, 120, 248]. Our results in the goat model mirrored these clinical findings, as the amounts of ATT following suture repair were much larger than the intact joint.

As an alternative, mechanical augmentation techniques, such as the used of additional sutures, have been developed as a means to better restore initial joint function [73, 218]. It is useful to compare the current results to those of Fleming et al., who examined the influence of suture augmentation versus suture repair in the porcine model [73]. In their study, suture augmentation could restore joint kinematics to within 1 mm on average under a 30 N anterior tibial load, while suture repair could only restore kinematics to within 6 mm on average. These changes are on the same order of magnitude as the current work; however, in general, the procedures by Fleming et al. were found to be closer to the intact joint. There are a few explanations for these differences. First, the porcine stifle joint has a natural laxity much greater than the goat stifle joint [270]. Thus, differences in kinematics compared to normal will be more

apparent in the goat stifle joint. Second, the level of applied load (30 N) was less than half of the current study (67 N). If similar loads were applied, it is possible that increases in joint kinematics may be found versus the intact joint. Third, during loading of the porcine stifle joints, all other translations and rotations of the joint were fixed except for anterior-posterior tibial translation. It is well-known that the joint undergoes coupled motions during in-vivo activities. For example, internal-external and varus-valgus rotations can occur during an applied anterior-posterior tibial load. Studies from our research center showed that constraining these other motions can lead to inaccurate joint kinematics and altered contribution of the structures of the joint [147]. For example, in the human joint, allowing unconstrained motion led to a 30-40% increase in anterior-posterior tibial translation compared to a constrained motion allowing only anterior tibial translation. A significant advantage of the robotic/UFS testing system is that these coupled motions can be allowed to achieve a better sense of 6-DOF joint stability.

Even with suture augmentation, the complex function of the ACL could not be completely replicated. In ACL reconstruction procedures, restoration of joint kinematics to within 2 mm of the intact joint at the time of surgery under an anterior tibial load is a common metric for a successful surgery [9, 81, 230]. The results for suture augmentation in this study were similar to those for ACL reconstruction in the goat model [5, 152, 189], as both procedures had values for ATT which were within 2-3 mm on the intact joint.

In summary, suture augmentation shows promise to better maintain joint function compared to suture repair alone under externally applied loads. In conjunction with simple suture repair (to reapproximate the torn ends of the ACL), this approach could maintain initial joint stability during the early healing process to allow better tissue remodeling and achieve

better long-term results. Thus, for our in-vivo studies in Specific Aim 2.2, suture augmentation was combined with a simple suture repair procedure.

8.2.2 Impact of Suture Augmentation on ACL healing at 12 weeks

In Specific Aim 2.2, we noted an increase in the amount of healing ACL neo-tissue at 12 weeks with additional suture augmentation compared to suture repair alone. This supports our hypothesis that suture augmentation could provide stability to the joint and limit excessive loading to the ACL. Further, with a simple suture repair, the gap between the injured ACL stumps is reduced, which gives the ACL a better chance to heal. Indeed, with suture augmentation and suture repair, the intrinsic healing potential of the ACL was sufficient to bridge the gap and form continuous tissue.

Despite the increased neo-tissue formation with additional suture augmentation, improvements in the biomechanical properties of the healing ACL and joint function, could not be demonstrated through statistical analyses. Qualitatively, in terms of joint kinematics, the suture augmentation group had a different response to an applied load and the healing ACL carried higher in-situ forces than for suture repair alone. Moreover, the average value of the stiffness of the healing FATC was 75% higher with suture augmentation. The inability to obtain statistical significance is likely due to a lack of statistical power as a result of the limited sample sizes. This topic is discussed in more detail in Section 8.5.

In both the suture repair and suture augmentation groups, the amount of A-PTT relative to the sham-operated controls increased at 12 weeks of healing versus time-zero. These differences were most dramatic in the suture augmentation group, which went from providing good initial joint stability at time-zero to allowing a large amount of instability at 12 weeks.

Although the amount of joint instability also increased with suture repair, the relative increase was lower. Since suture repair had significant joint instability at time-zero, there was a limit to how much these values could increase throughout healing.

Interestingly, the augmentation sutures carried minimal loads when an anterior tibial load was applied via the robotic/UFS testing system at 12 weeks of healing. Closer inspection revealed that the sutures were permanently elongated in all specimens (Figure 24), which implies that the sutures were no longer contributing to joint stability. However, it was not possible to determine the length of time in which the augmentation sutures could contribute to joint stability. In any case, by 12 weeks, the healing ACL carried a significant portion of the applied anterior tibial load. Compared to the suture repair group, the healing ACLs in the suture augmentation group could have experienced higher loads during joint motion, allowing for more positive remodeling and improved biomechanical function by 12 weeks of healing. This is a topic for discussion in Section 8.4.

Since the augmentation sutures did become considerably elongated over time, the in-vivo loading conditions could have been higher than our initial estimations. A previous study using force transducers applied to the normal ACL in the goat model found that an average anterior load of approximately 70 N was applied during walking [103]. Thus, the loading levels for our gfin-vitro tests were selected accordingly. However, in the same study, peak ACL forces could reach approximately 150-200 N. If a significant number of high loading cycles occurred, it is possible that the augmentation sutures could have permanently elongated early during healing, and not provided the appropriate amount of joint stability. In any case, elongation of the sutures is inevitable and even desirable once the ACL heals, so a careful design of the suture technique is important. A more detailed discussion of this topic is presented in Section 8.4.

In summary, suture augmentation could be a useful technique to provide initial joint stability superior to suture repair alone. This technique could used in combination with FTE treatments to further enhance healing of the ACL, while better maintaining joint stability throughout healing.

8.3 USE OF MATHEMATICAL MODELING TO STUDY ACL HEALING

In Specific Aim 3, we developed a model to capture the changes in CSA and biomechanical properties of a healing ligament via a mechanism of strain-based homeostasis. The model is advantageous to the study of the mechanisms of ligament healing since it incorporates a general constitutive model for soft tissues based on the tissues microstructure as well as allows the parameters at the fiber level (assumed to be on the same order of size as the cells present in the matrix) to remodel and ultimately dictate the tissue level biomechanical properties. This model was able to demonstrate how the stress-strain behavior of the tissue and its CSA would change in order to restore the level of homeostatic fiber strain in a generalized model of a ligament. Moreover, the interplay between the modulus of the tissue and its CSA based on the relative level of their rate constants was shown.

Furthermore, we were able to utilize the idea of strain-based homeostasis to describe experimental data for the rabbit MCL. The general changes in the stress-strain behavior and CSA of the non-treated and ECM-treated groups were captured in the rate constants of these parameters. In addition, the model was able to match the experimental finding that the fiber strain in the tissue under a given load did not change much in the ECM-treated group from 12 to 26 weeks. The response for the non-treated group was quite different, as the fiber strain for a

given load decreased substantially over the same time interval. This suggests that the two experimental groups are remodeling differently over this time period. At 12 weeks, the ECM-treated group had a notably higher tangent modulus as well as CSA. Thus, for any given load, the fiber strains in the ECM-treated tissues would be lower than their non-treated counterparts. This would lead to less of a stimulus to restore the homeostatic fiber strain in the ECM-treated group. Interestingly, even though the fiber strain in response to an applied load did not change over this time period, the CSA did decrease considerably, while the tangent modulus increased. This could imply that even if the tissue is not moving toward its homeostatic fiber strain, there could be significant alterations in its CSA and biomechanical properties over time. Thus, further mechanisms for growth and remodeling will need to be explored in the future.

The data sets chosen for the healing MCL were those collected and reported by our research center in recent years [143, 171]. It is interesting to note that for the non-treated group, the value for tangent modulus of the healing MCL reported in these studies almost doubled from 12 to 26 weeks (149 ± 77 MPa and 291 ± 123 MPa, respectively). Similar increases were observed in the ECM-treated group. These data are at odds with earlier studies from our research center examining the healing MCL out to 52 weeks after injury [186, 250, 262]. In these studies, the modulus of the healing tissue did not increase substantially between 6, 12, and 52 weeks of healing (230 ± 97 MPa, 269 ± 97 MPa, and 230 ± 158 MPa, respectively). However, the values for all of these groups are within a small range 150-300 MPa, suggesting that they are similar. It is also important to note that these data were collected by different researchers, and thus, differences in specimen preparation, data analysis, etc. may preclude direct comparison between groups. The data used for this dissertation were chosen in part because the raw data files were available which allowed for uniform data analysis across all data sets.

However, differences in the experimental techniques may have contributed to differences in the obtained data. In the future, it is important that multiple time point data be collected by the same investigators so as to reduce these effects. Additional methods to reduce inter-specimen variability are discussed in Section 9.0 .

Furthermore, we used the model to supplement the experimental findings in Specific Aims 1 & 2. First, the healing of the ACL was simulated to 26 weeks for both the ECM-treated and suture repair groups. It was found that the stiffness of the healing FATC remained 115% higher for the ECM-treated group, and the stiffness for the suture repair group at 26 weeks was similar to the value achieved by the ECM-treated group at 12 weeks, which clearly showed the delay in the function of the healing ACL with suture repair alone. Next, we could show that hypertrophy of the healing ACL at 12 weeks in terms of increasing its CSA would lead to a slower increase in its mechanical properties by 26 weeks. As such, the importance of limiting hypertrophy of the healing tissue at early time points was shown. Cases of hypertrophy have been observed in FTE treatment of the healing ACL using platelet-rich plasma (See Section 2.6.2). With ECM-treatment, hypertrophy of the healing tissue was limited, suggesting an increase in its quality. Finally, we noted that if the stimulus, i.e. load, was decreased, the stress-strain and load-elongation behavior by 26 weeks would also be negatively impacted, demonstrating the need for appropriate loading of the healing ligament in order to achieve biomechanical properties closer to normal. Once rigorously developed and validated, this type of model could be powerful in that it would allow prediction of long-term outcome with the use of short-term data.

However, it is clear that further development is needed. This stimulus function chosen for these studies was a simple linear relation to fiber strain, which may or may not have a direct

basis in terms of the stimuli observed at the cellular level. More complex relationships may need to be explored as noted in Section 8.5.

In these preliminary simulations, a transversely isotropic model could not explain the decrease in CSA for the healing MCL from 12 to 26 weeks within the context of strain-based homeostasis. A negative value for q_A was needed for both experimental groups, since the experimental values for CSA decreased for both from 12 to 26 weeks, which is counterintuitive to our assumption of strain-based homeostasis. If tissues experience strains above their homeostatic strain, we would expect them to want to increase size, not decrease. Thus, further exploration of the assumptions of the current model is needed.

These results highlight the need for an accurate description of the fiber alignment during healing. Histological evaluation of the healing rabbit MCL has revealed that some degree of fiber alignment does exist at 12 weeks; however, the degree of alignment was not similar to those of the normal MCL [77, 171]. In our model, under the assumption of affine deformation, as the fiber direction moves further away from the axis of loading, the strains in the fibers decrease. Thus, our model would predict a lower strain stimulus on these fibers. If the strains are below the homeostatic strain level, the degradation of matrix for that fiber family would become greater than its production, causing an overall loss in mass. If a sufficient percentage of the total area of the tissue consists of these fiber families, then a decrease in CSA could be expected, while maintaining a positive value for q_A. Using our model, we could simulate this scenario by including multiple fiber families in future studies. Further, the distribution of fibers in the healing tissue could be directly measured using a small angle light scattering (SALS) device [207] and directly implemented within the model.

Although still in its preliminary phases, it is easy to see how this model could impact both basic science as well as the clinical arena. A more robust treatment of this model will require a significant amount of carefully obtained data. However, once validated, it could be used to answer many research questions in a time- and cost-efficient manner.

8.4 MECHANISMS OF BIOLOGICAL AND MECHANICAL AUGMENTATION APPROACHES FOR ACL HEALING

In Specific Aims 1 & 2, we were able to show that both biological and mechanical augmentation could improve healing of the ACL versus suture repair alone. In light of these findings, it is interesting to explore the potential mechanisms by which each one acts.

A depiction of the natural biologic healing process of the ACL with an ideal mechanical augmentation technique is given in Figure 40. The vertical axis on the left-hand side represents the level of joint stability ranging from normal to ACL-deficient conditions. The vertical axis on the right-hand side represents the relative contribution, i.e. loads carried, by both the mechanical augmentation and healing ACL, ranging from the normal ACL to zero contribution. Both are plotted versus healing time on the horizontal axis ranging from early to late. In order to maintain joint stability near the levels of the normal joint (represented by the solid line), the mechanical augmentation (represented by the long dashed line) must provide a similar contribution to stability as the normal ACL, since the contribution of the injured ACL is zero (represented by the short dashed line). Over time, the contribution of the mechanical augmentation can decrease as the contribution of the healing ACL increases. This is essential, since healing ligaments respond

positively to loading. In an ideal case, this process occurs such that joint stability is maintained throughout the healing process.

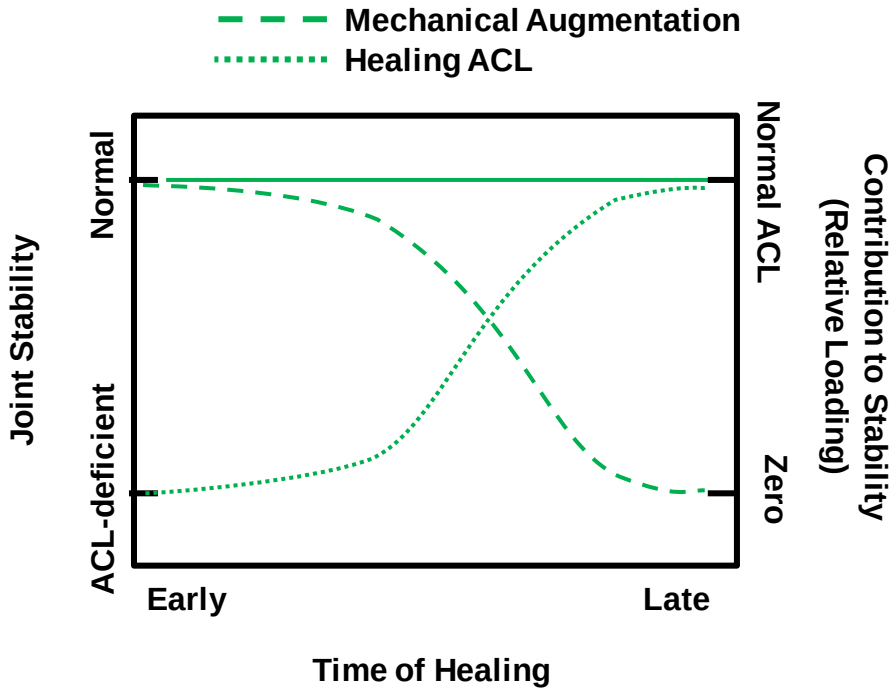

Figure 40. Schematic depicting the ideal ACL healing with appropriate mechanical augmentation.

Next, it is useful to depict the results of suture repair alone, which was used as a control in Specific Aims 1 & 2. In this case, suture repair could not restore initial joint stability. Thus, even though a small amount of healing ACL tissue could form, the joint stability was already lost. As a result, the tissue was likely not properly loaded and could not remodel to effectively contribute to stability.

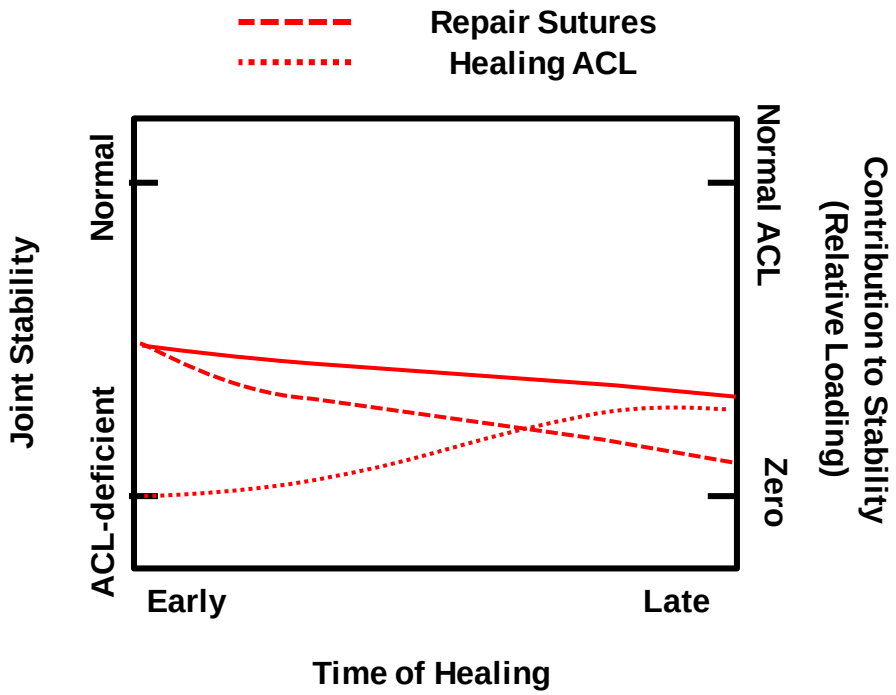

Figure 41. Schematic depicting ACL healing following suture repair alone.

In Specific Aim 1, ECM-treatment was able to accelerate tissue formation such that it could contribute to joint stability sooner, as depicted in Figure 42. In other words, it shifted the curve for the healing ACL in Figure 40 to the left. This allowed joint stability to be better maintained over time versus suture repair alone since the healing could bear more load and positively remodel (as modeled in Specific Aim 3) to more effectively contribute to stability. Nevertheless, since suture repair could not restore initial joint stability, even the positive effects of ECM-treatment could not restore joint stability following healing.

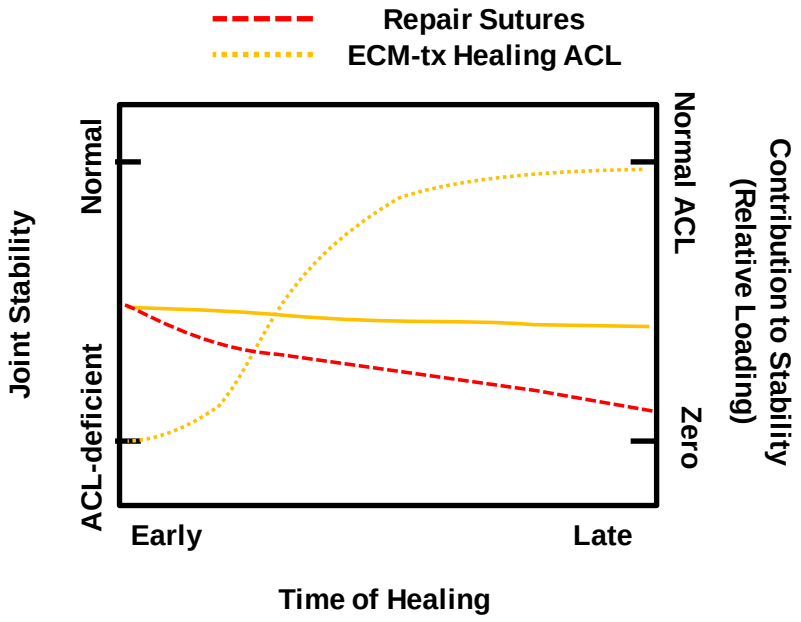

Figure 42. Schematic depicting ACL healing following ECM-treatment with suture repair.

In Specific Aim 2, we showed that suture augmentation could provide initial joint stability (Figure 43). Additionally, suture augmentation with simple suture repair provided sufficient protection to allow a substantial amount of healing tissue to form. However, as with suture repair alone, the natural healing process of the ACL would be slow. Thus, as the contribution of the augmentation sutures decreased with time, the healing ACL was not yet capable of contributing the amount necessary to maintain joint stability since it did not have the needed biomechanical properties. But, because the healing tissue was able to form, it could positively remodel to accept a greater contribution of loading. Thus, the values for joint stability decrease over time during the early phase, but reach a steady state once the ACL has sufficient biomechanical properties.

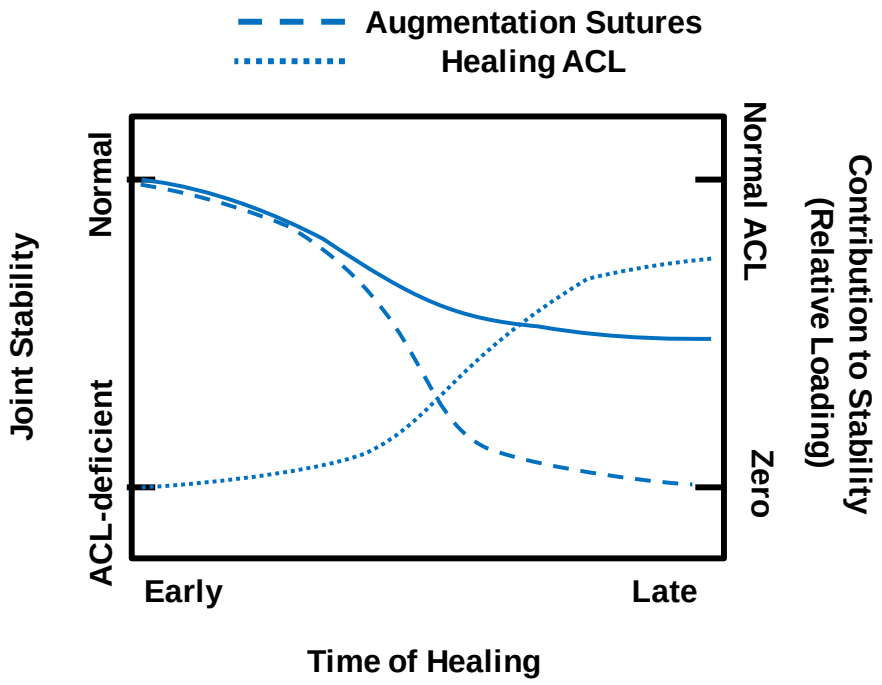

Figure 43. Schematic depicting ACL healing following suture augmentation with simple suture repair.

A promising extension of this dissertation would be to combine the advantages found in Specific Aims 1 & 2, which is presented graphically in Figure 44. The combined approach is represented by the purple curves, while the ideal curve from Figure 40 is represented by the green curves. Both sets of curves maintain joint stability throughout healing. However, since ECM-treatment allows for accelerated healing of the ACL, it could contribute to stability earlier in the healing process, reducing the demand for suture augmentation to maintain stability for a long period of time. The overall end result is a shift in the time when the healing ACL contributes the majority to maintaining joint stability from a later time point in the case of natural healing to an earlier time point with FTE treatment. This theoretical result will need to be verified in future experimental studies.

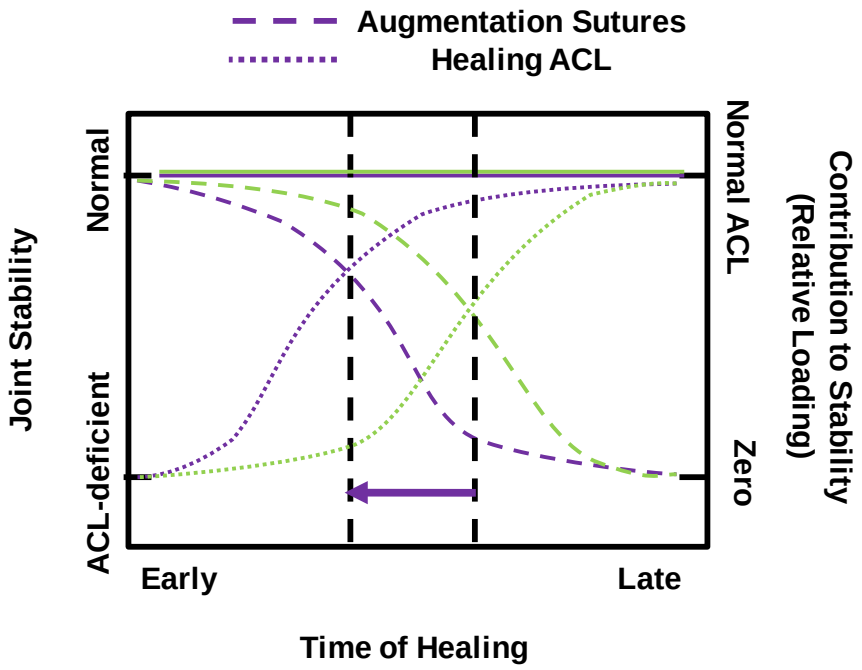

Figure 44. Schematic showing ACL healing following hypothetical combination of results from Specific Aims 1 & 2.

This thought experiment highlights an area of rising importance within the field of orthopaedic sports medicine, namely post-operative rehabilitation and care following FTE treatments. With the use of platelet-rich plasma and other biological stimuli already in practice, the question of how soon patients should return to normal activities is still open-ended. Theoretically, FTE treatments should allow for a more aggressive rehabilitation protocol, since the biomechanical properties of the healing ACL would be higher at earlier time points compared to the natural healing process. Also, the time at which patients return to normal activities should theoretically decrease. Since this area is still in its nascent stages, the specific type and duration of rehabilitation following FTE treatment has not yet been well-studied.

8.5 LIMITATIONS

There are a number of limitations to the work in this dissertation. First, the in-vivo experiments were limited by the sample sizes for each group, due to the costs and difficulties associated with performing large animal studies. In terms of biomechanical testing, we were limited to n=7 in the ECM-treated group and n=5 both in the suture repair group and suture augmentation group. In our study design, we initially planned for seven goats for the suture repair group; however, given the clearly poor and largely variable results observed in terms of tissue formation and biomechanics, we did not perform surgery on the remaining animals for this study due to ethical concerns. More practically, the high variability of the suture repair group almost certainly would have prevented determination of statistical significance for the data on joint kinematics and in-situ force of the healing ACL in Specific Aims 1 & 2, even if the extra animals were included in the study. Post-hoc power analyses suggest that a substantial number of animals would be needed to show statistical significance. For example, to show statistical significance in terms of A-PTT at 30º of flexion between the ECM-treated and suture repair only groups, 46 animals per group would be required. The same problem existed for Specific Aim 2.2 and the comparisons to the suture augmentation group. Clearly, the number of animals needed would be unfeasible experimentally.

Second, the experimental studies on joint kinematics used externally applied loads that were selected on data collected by Holden et al. for the average load applied to the ACL as well as the average ground forces during normal walking gait in the goat [103]. Thus, the true in-vivo function of the healing ACL could not be determined in this dissertation, but a methodology to potentially achieve this goal is highlighted as a future direction in Section 9.0 .

Third, although novel αGal(-) ECMs were utilized in this dissertation, the use of the goat model prevented a direct evaluation of their immunological advantages. As with all non-primate animal models, caprine tissues contain the αGal eptiope, and thus, goats do not have anti-αGal antibodies. To study the immune reaction due to the αGal(-) ECM, additional studies are warranted.

Fourth, the results were obtained for the goat model and may not yet be extrapolated to the human condition. Once the basic science of using FTE approaches for ACL healing is better established, other clinically relevant questions such as the best mode of application, rehabilitation, etc. can be addressed. Clearly, there are a number of scientific and practical challenges in moving FTE treatments to the clinic, which are outside the scope of this dissertation.

Fifth, the computation model could not predict experimental results for the ACL due to a lack of appropriate experimental data as well as the simplistic form of the model. Moreover, even if all groups were performed at multiple time points, the interspecimen variability of in-vivo studies was quite high. Paired data would be ideal to eliminate this variability; however, the techniques to obtain the necessary information, without euthanizing the animals, are either unavailable or difficult to perform experimentally.

Sixth, the computational model is a very simplified representation of the healing process and makes a number of assumptions, as described in Section 7.1.3. In the future, some of these assumptions, like the distribution of fibers in the healing tissue, could be directly measured using a SALS device or another similar experimental method [207]. Furthermore, more data are needed to identify appropriate functions for a strain-based remodeling response. A linear function was chosen in this dissertation for simplicity; however, more complex functions, e.g.

exponential, may be necessary to better describe these behaviors. Moreover, alternative stimuli could be chosen. For instance, in the field of bone remodeling, many have suggested that strain rate as opposed to strain is a more appropriate choice as a stimulus to cells [46, 47]. Along these lines, additional studies on the mechanisms of how ligament fibroblasts feel and interpret forces could provide insight on how to model the tissue level response to applied strains.

In our biomechanical studies, a preload (or prestress) is applied to provide a gauge length for the remainder of the testing protocol. It also offers a way to consistently compare the mechanical properties between experimental groups. This differs from the "zero position" of normal and healing ligaments in-vivo. For instance, it is well-known that normal ligaments are "pre-strained", and upon transection of the MCL or ACL, it is common to observe significant retraction of its torn ends. Thus, since ligaments remodel according to their in-vivo conditions, these in-vitro assessments may not give an accurate description of remodeling. Another major assumption in the model is that the reference length for the collagen fibers did not change over time. Many have suggested that the reference length is indeed an important aspect of growth and remodeling in soft tissues [93, 96, 106, 197, 243, 244]. During healing, the reference length of the fibers could be altered compared to the normal ACL as new matrix is produced. These issues will need to be considered in future models of ACL healing.

8.6 CONCLUSIONS

8.6.1 Clinical Significance

This dissertation illustrated the positive impact FTE approaches, such as ECMs, can have on the healing of ligaments, even ones with limited natural healing capacity, like the ACL. Such novel treatment approaches are attractive as they would have many advantages over ACL reconstruction, including preserving the complex anatomical features of the ACL as well as eliminating the complications associated with the graft donor site. A properly healed ACL would have the potential to better maintain multidirectional knee stability. Additionally, it would also allow recruitment of an appropriate set of muscles to prevent muscle atrophy and further improve joint function. In the end, these improvements could lead to a reduction in the incidence of premature osteoarthritis. Also, some of these technologies, such as ECMs, are already FDA approved, removing one barrier toward their clinical use.

This dissertation also highlights the need for appropriate mechanical stabilization of the joint even with FTE treatment. No matter what biological agent is applied, poor initial joint stability will all but guarantee a less than satisfactory outcome. Also, as stated in Section 8.4, it requires that surgeons and engineers rethink what an ideal repair or augmentation may be, in light of the accelerated formation of neo-tissue. More appropriate rehabilitation protocols may need to be developed for these new technologies. Mathematical modeling could offer a highly controlled way to answer some of these questions. Although the model of the healing ACL is still in the early stages, it could potentially be implemented within finite element models to predict the stresses and strains in the ligament at different phases of healing. As such,

rehabilitation protocols could be designed in order to prevent excessive stresses and strains in the healing ACL, while also providing positive mechanical stimuli for positive tissue remodeling.

In the end, successful scientific data obtained from this low cost, potentially high yield translational research has the potential to significantly impact the clinical management of ACL injuries. The results will provide a scientific basis for sports medicine knee surgeons to consider the many advantages of inducing ACL healing. Finally, the techniques described offer the potential to extend this technology to other intra-articular ligaments and tendons in the musculoskeletal system, e.g. the posterior cruciate ligament of the knee, rotator cuff tendons in the shoulder, and so on, which have difficulty to heal. It is our hope that multidisciplinary studies like those done in this dissertation can lead to significant advances in new knowledge to help the improvement of the clinical management of ligament and tendon injuries.

8.6.2 Scientific/Engineering Significance

The methodologies utilized in this dissertation offer a platform from which to compare the efficacy of FTE treatments to enhance ACL healing (Figure 45). At both the joint and tissue levels, the function of the healing ACL was quantitatively assessed. By developing rigorous experimental protocols and taking advantage of highly accurate tools, such as the robotic/UFS testing system, the best FTE approaches can be delineated. Further, the robotic/UFS testing system offers the capability to determine the role of the healing ACL within the intact joint by determining the in-situ force of the ACL under an externally applied load.

Nevertheless, long-term animal studies are costly and time consuming. By developing a mathematical model with the ability to predict long-term experimental data, better FTE approaches could be logically and rapidly developed, thereby accelerating the rate of basic

science research. These models could then be implemented within more complex finite element models to determine the stress and strain distribution within the healing ligaments throughout healing which would provide a major step forward toward understanding the healing process of ligaments.

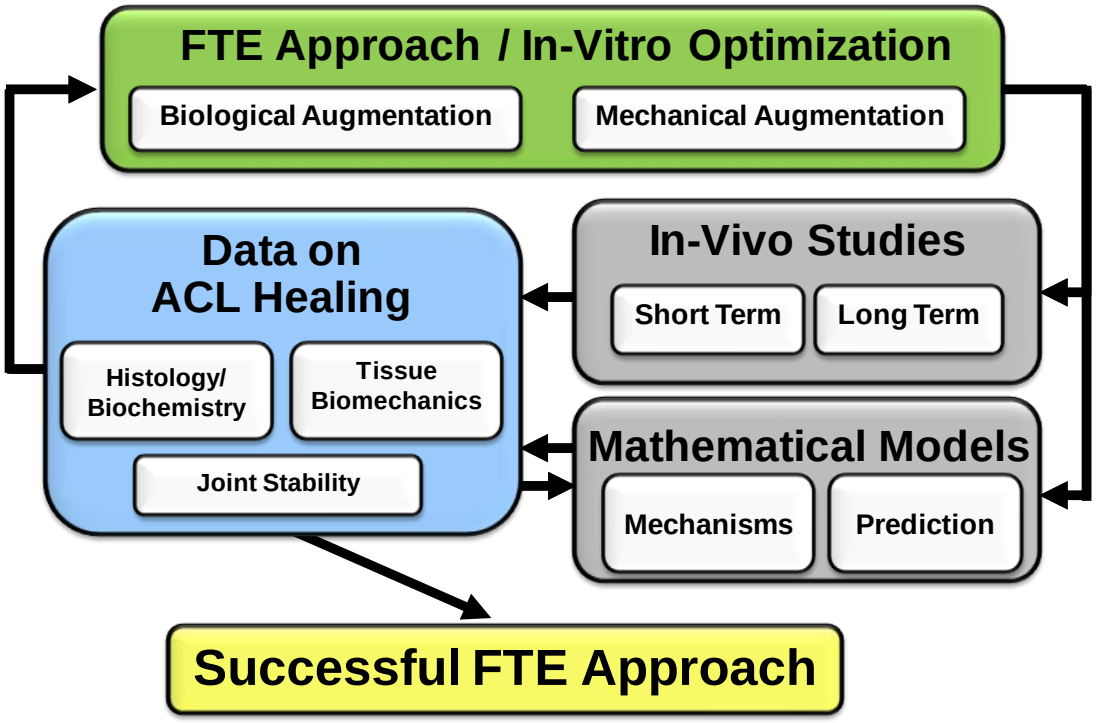

Figure 45. Schematic for the proposed platform to evaluate functional tissue engineering strategies to enhance healing of the ACL.

9.0 FUTURE DIRECTIONS

The overall goal of the proposed thesis work is to provide a quantitative approach by which FTE treatments used to heal the ACL could be quantitatively evaluated. Needless to say, there are a wide range of FTE techniques which could be pursued. Hopefully, they could be evaluated based on our findings and the unique methodologies developed in this thesis. The use of platelet-rich plasma combined with a collagen scaffold [162, 165, 167] or the controlled release of growth factors, such FGF and VEGF, are viable possibilities. It would be useful to directly compare these approaches with ECM treatment, so as to determine their effectiveness.

At the same time, it is still necessary to refine the current approaches. For the ECM bioscaffold treatment, our experience has told us that ECM-SIS can yield positive results for ligament and tendon healing [21, 121, 142, 143]. However, it is possible that ECM bioscaffolds derived from other tissue sources could be even more beneficial for ACL healing. For example, urinary bladder matrix (UBM) has a basement membrane layer, which could possibly function better as a synovium. UBM has shown positive results in other applications due to its unique bioactive characteristics [49, 193]. Slower degrading alternatives, including the use of more than a single layer of ECM (lyophilized together in order to create a multi-layer construct) could be used in an attempt to sustain its effect on ACL healing. Moreover, the ECM could be used together with other scaffolds, such as electrospun poly(ester urethane urea) (PEUU) [232].

In terms of suture augmentation, modifications, such as changing the suture material or amount of suture, can be done to improve results. These techniques should be rigorously tested using our robotic/UFS testing system under multiple loading conditions. Also, they should be subjected to repetitive loading cycles in order to obtain a better description for how their properties change over time.

Another future direction could be to quantify the impact of a loss of ACL function on the other structures of the joint. It is well known that the structures of the knee joint in humans or stifle joint in animals, such as the goat, work in concert to maintain joint function. For example, Jackson and colleagues monitored the changes of the stifle joint in terms of both the degeneration of the articular cartilage as well as the hypertrophy of the medial meniscus in the goat model following ACL transection [113]. Thus, if one structure is injured, the others must increase their relative contribution in response to an applied load. This is easily observed for the data found in Appendix A. Thus, monitoring the changes in these other structures within the joint could provide another method to evaluate the efficacy of FTE treatments.

This is particularly true for long-term results in which the degenerative changes in the articular cartilage would be observed. Clinically, the causes for premature osteoarthritis following ACL injury have been debated and are likely multi-factorial. One key question is whether even prefect restoration of joint stability could prevent these negative changes. In other words does degeneration of the articular cartilage result from changes in loading due to joint instability or from damage during the initial injury. In the case of the latter, no matter how well the function of the ACL is restored through FTE treatment, premature OA would still occur. In fact, there are many clinical cases which document concomitant injuries to the bone, cartilage,

and menisci with ACL injury [7, 37, 107, 115, 122, 157, 158, 191, 201, 205, 209, 219, 273]. This is certainly an area for future exploration.

Further, carefully obtained experimental data at early time points of healing (1, 3, and 6 weeks) as well as in the long-term (1, 2, and 3 years) will need to be collected in order to provide a more complete description of the ACL healing process. One exciting recent technology is a highly accurate biplanar fluoroscopy system to record in-vivo joint kinematics [92, 140, 240]. This system could allow for quantificantion of the changes in joint kinematics over time. After the animals are euthanized, the kinematics data could then be repeated using our robotic/UFS testing system such that the in-situ forces in the healing ACL during trotting or walking could be determined [258]. Other noninvasive ways to collect both the size and mechanical properties of the healing tissue could also be implemented in order to collect data at multiple time points within the same set of animals. Along these lines, ultrasound elastography has shown promise [229].

The data could also help to develop the mathematical model to describe ACL healing and test its predictive capabilities. Further, with an increasing amount of experimental data, it will be essential to revisit the assumptions of the model and make modifications as necessary. For example, as the cellular mechanisms for interpreting applied loads are elucidated, these could be incorporated into the stimulus functions to provide a more accurate description of the remodeling process. Finally, for tissue like the ACL, in which stresses and strains are difficult to measure experimentally due to its complex geometry, incorporation of the constitutive model into a finite element model could be used to calculate the stresses and strains in the healing ACL under physiological loading conditions.

APPENDIX A

IN-SITU FORCES IN SOFT TISSUE STRUCTURES OF THE GOAT STIFLE JOINT AT TIME-ZERO

The in-situ forces of the other tissues of the goat stifle joint at time-zero under a 67 N anterior tibial load and a 67 N anterior tibial load with 100 N axial compression are presented as reference data for future work.

A.1 IN-SITU FORCES IN RESPONSE TO 67 N ANTERIOR TIBIAL LOAD

The in-situ forces of the tissues of the goat stifle joint at time-zero under a 67 N anterior tibial load are detailed in Table 23. The in-situ force in the intact ACL was similar at 30° and 60° and slightly lower at 90° of joint flexion. These trends were similar for both the augmentation sutures and repair suturesThe in-situ force of the augmentation sutures was not significantly different from those for the intact ACL at all flexion angles ($p>0.05$). The in-situ force in the repair sutures was 19%, 17%, and 26% lower than the intact ACL; however, these differences was not statistically significant ($p>0.05$). Further, the values for the repair sutures were 21%,

19%, and 35% lower than the augmentation sutures at 30°, 60°, and 90°, respectively ($p<0.05$ at 30° and 90°).

For the intact joint, the MCL carried the largest forces, but they were minimal (<10 N) for all tissues at all flexion angles examined other than the ACL. This is largely due to the fact that the ACL carried the vast majority of the anterior load. After the ACL was transected and the load applied, the forces in both the MCL and medial meniscus increased dramatically at all flexion angles ($p<0.05$). The force in the MCL was relatively constant (17-18 N) throughout joint flexion. The force in the medial meniscus was highest at 60°, and slightly lower at both 30° and 90°. At 60°, the force of the medial meniscus was approximately half of the anterior load (33 N) and was about double the MCL. At 30° and 90°, the MCL and medial meniscus shared the anterior load more evenly (~20 N each). The force in the LCL increased slightly (6-10 N) at all flexion angles ($p<0.05$). The forces in the lateral meniscus and bony contact remained low at all flexion angles ($p>0.05$).

With suture repair or suture augmentation, the in-situ forces of the MCL could be restored near normal levels ($p>0.05$). The lone exception was at 90° for suture augmentation ($p>0.05$), but this difference was only 10 N. For the medial meniscus, both procedures could reduce the in-situ force compared to the ACL-deficient knee at all flexion angles, but statistical significance was achieved only at 60° ($p<0.05$). These forces were also within approximately 10N of the intact joint at both 30° and 60° ($p>0.05$, except for suture repair at 30°). At 90° the suture repair and suture augmentation groups were 16 N and 11 N higher than the intact joint, respectively ($p<0.05$). In the suture repair and suture augmentation groups, the values for the LCL, lateral meniscus, and bony contact were under 10 N and similar to the intact joint ($p>0.05$). The only exception was at 30° for lateral bony contact for the suture augmentation group which

was 10-13 N higher than all other groups ($p>0.05$). This difference was not found at 60° and 90° and was likely due to the initial tension applied to the augmentation sutures which dissipated with additional loading cycles.

Another way to express these in-situ force data is to determine the anterior component of the force in each tissue as a percentage of the applied 67 N anterior tibial load; in other words, to find the contribution of each structure in resisting the applied load. Figure 46 displays these data for each angle of joint flexion. For the intact joint, it is clear that the ACL resists almost all of the load (103 ± 11%, 102 ± 6%, and 88 ± 6% at 30°, 60°, and 90°, respectively). All other tissues contributed <5% to the total load and were on the order of the force repeatability of the robotic/UFS testing system. For the ACL-deficient joint at 30°, the capsular structures played the dominant role (38 ± 17%), followed by the medial meniscus (24 ± 14%) and MCL (20 ± 8%). At 60° and 90°, the medial meniscus was the most dominant (49 ± 15% and 37 ± 15%, respectively), followed by the MCL (25 ± 11% and 28 ± 14%, respectively) and capsular structures (13 ± 5% and 18 ± 9%, respectively).

With suture repair, the sutures resisted the majority of the load (75 ± 20%, 75 ± 18%, and 53 ± 22% at 30°, 60°, and 90°, respectively); although these values were lower than those for the intact ACL. As a result, the remaining tissues, most notably, the medial meniscus, MCL, and capsule, had an increased contribution; however, the values were much less than those for the ACL-deficient joint. With suture augmentation, the sutures bore similar values as those for the intact ACL (95 ± 9%, 96 ± 5%, and 83 ± 5% at 30°, 60°, and 90°, respectively), while the contribution of the other structures remained low.

Table 23. In-situ forces in the tissues surrounding the joint under a 67 N anterior tibial load (*p<0.05 compared to intact, +p<0.05 compared to ACL-deficient, #p<0.05 compared to suture repaired).

	Flexion Angle (degrees)											
	30				60				90			
			Suture Technique				Suture Technique				Suture Technique	
	Intact Knee	ACL-deficient	Repair	Augment-ation	Intact Knee	ACL-deficient	Repair	Augment-ation	Intact Knee	ACL-deficient	Repair	Augment-ation
ACL	62 ± 5	N/A	N/A	N/A	60 ± 6	N/A	N/A	N/A	48 ± 6	N/A	N/A	N/A
Sutures	N/A	N/A	50 ± 12	64 ± 9#	N/A	N/A	49 ± 12	61 ± 5	N/A	N/A	36 ± 14	55 ± 5#
MCL	8 ± 5	17 ± 6*	8 ± 4+	2 ± 2+	5 ± 2	17 ± 6*	9 ± 5	8 ± 4	9 ± 5	18 ± 8*	12 ± 7	20 ± 10*
LCL	1 ± 1	11 ± 7*	6 ± 10	5 ± 3	1 ± 1	7 ± 4*	5 ± 6	6 ± 6	1 ± 1	8 ± 4**	7 ± 6	3 ± 2++
Medial Meniscus	2 ± 2	19 ± 8*	11 ± 6*	8 ± 6	1 ± 1	33 ± 9*	11 ± 9+	11 ± 8+	1 ± 1	24 ± 9**	17 ± 10*	12 ± 6**
Lateral Meniscus	4 ± 3	7 ± 9	3 ± 2	4 ± 4	2 ± 2	1 ± 2	1 ± 1	2 ± 2	1 ± 1	1 ± 1	1 ± 1	1 ± 1
Bony Contact												
Total	5 ± 2	6 ± 2	6 ± 1	12 ± 6*	6 ± 3	6 ± 1	5 ± 1	7 ± 3	5 ± 2	5 ± 2	5 ± 1	5 ± 2
Medial	6 ± 1	6 ± 2	6 ± 1	6 ± 1	5 ± 1	5 ± 1	5 ± 1	6 ± 1	5 ± 2	5 ± 2	5 ± 1	6 ± 2
Lateral	4 ± 2	1 ± 1*	2 ± 1	14 ± 7*+#	3 ± 5	1 ± 1	1 ± 1	7 ± 5+	1 ± 1	1 ± 1	1 ± 1	2 ± 3

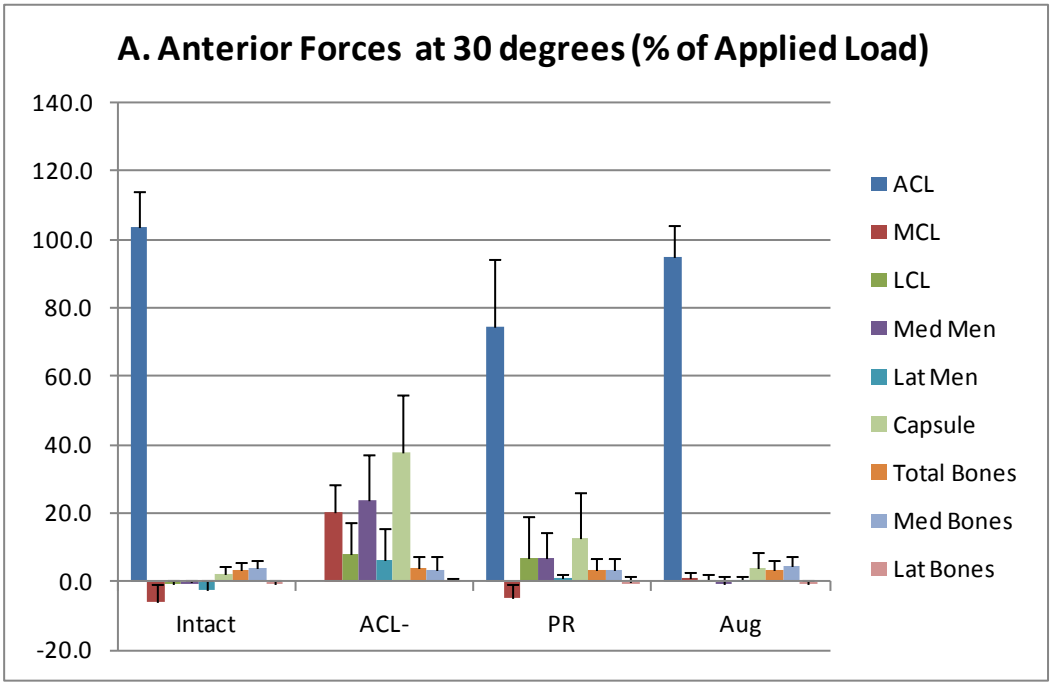
A. Anterior Forces at 30 degrees (% of Applied Load)
140.0
120.0
100.0
80.0
60.0
40.0
20.0
0.0
-20.0
Intact
ACL-
PR
Aug
ACL
MCL
LCL
Med Men
Lat Men
Capsule
Total Bones
Med Bones
Lat Bones

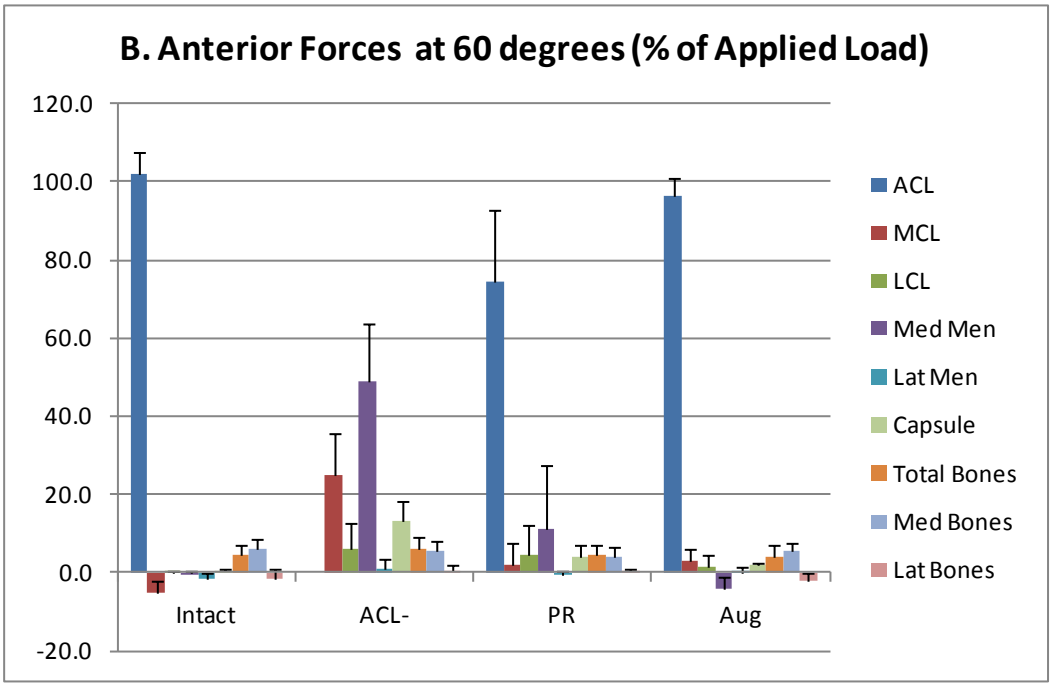
B. Anterior Forces at 60 degrees (% of Applied Load)
120.0
100.0
80.0
60.0
40.0
20.0
0.0
-20.0
Intact
ACL-
PR
Aug
ACL
MCL
LCL
Med Men
Lat Men
Capsule
Total Bones
Med Bones
Lat Bones

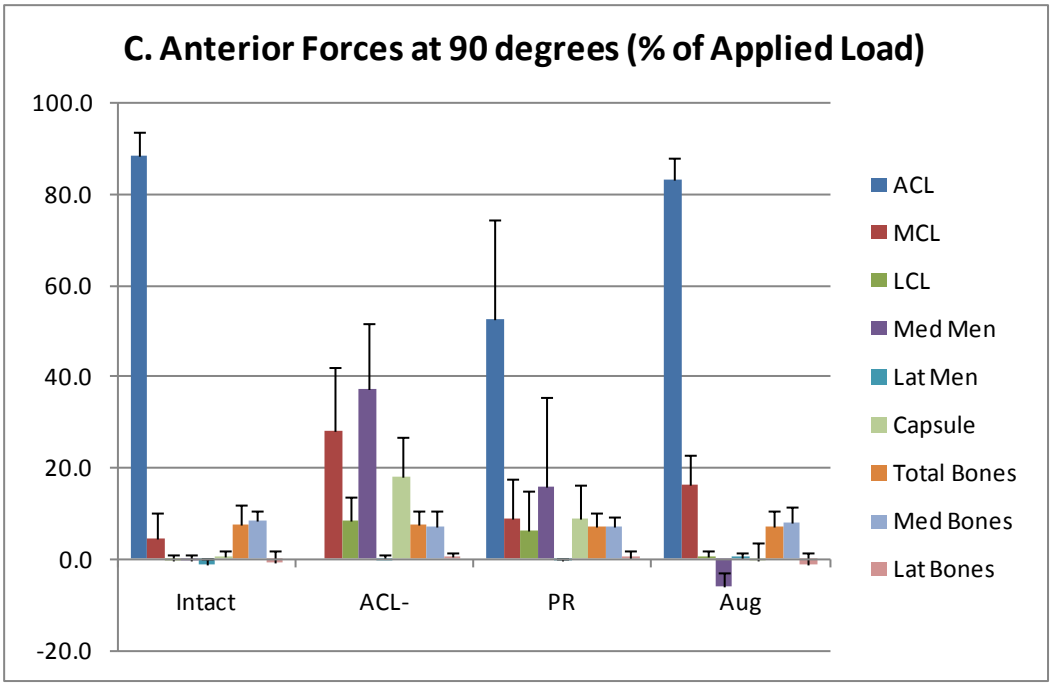

Figure 46. Relative contribution of soft tissue structures of the goat stifle joint under 67 N anterior tibial load at a) 30°, b) 60°, and c) 90° of joint flexion.

A.2 IN-SITU FORCES IN RESPONSE TO 67 N ANTERIOR TIBIAL LOAD WITH 100 N AXIAL COMPRESSION

The in-situ forces of the tissues of the goat stifle joint at time-zero under a 67 N anterior tibial load with 100 N axial compression are detailed in Table 24. With the added 100 N axial compression, the in-situ force in the intact ACL was 102 ± 16 N, 112 ± 10 N, and 95 ± 12 N at 30°, 60°, and 90° of knee flexion, respectively. Again, the ACL was largely responsible for carrying the anterior load. The in-situ force of the augmentation sutures were within 2-23 N of the intact ACL ($p>0.05$) and ranged from 78 N at 30° and 95 N at 60°. On the other hand, the in-

situ force in the primary repair sutures ranged between 34 N at 30° and 49 N at 90°. However, these values were only 33%, 33%, and 52% of the intact ACL ($p<0.05$) and 43%, 39%, and 53% of the augmentation sutures ($p<0.05$) at 30°, 60°, and 90°, respectively.

For the other tissues in the joint, the forces were largest for the bony contact in the intact joint, which transmitted the compressive load. In terms of bony contact, the force in the medial component was about double that of the lateral component at 30° and slightly higher at 60° and 90°. The other tissues carried relatively low forces at all flexion angles. At 60°, the MCL and lateral meniscus carried 14 and 17 N, respectively. At 90°, the MCL, medial meniscus, and lateral meniscus each had in-situ forces of 10-16 N. With ACL-deficiency, large changes were observed compared to the intact knee. The in-situ force due to bony contact was decreased dramatically at all flexion angles, with the largest differences at 60° ($p<0.05$). On the other hand, the force carried by the medial meniscus and lateral meniscus rose dramatically at all flexion angles ($p<0.05$) and were the primary stabilizers at 60° and 90°. For examples the force in the medial meniscus increased 13, 13, and 5 times that of the intact joint at 30°, 60°, and 90°, respectively. The in-situ force in the MCL also doubled at 60° and 90° with ACL-deficiency ($p<0.05$).

With suture repair, the in-situ forces due to bony contact were increased by 23%, 117%, and 50% compared to the ACL-deficient joint ($p<0.05$), but were still only 77%, 15%, and 33% of those for the intact joint ($p<0.05$). Meanwhile, the force in the medial meniscus was lowered by 13%, 14% and 18% compared to the ACL-deficient joint ($p<0.05$), but remained 11, 11, and 6 times higher than the intact joint. Similar findings were observed for the lateral meniscus. With suture augmentation, the forces due to bony contact were restored to similar levels as the intact knee ($p>0.05$). The forces of the medial and lateral menisci were reduced to 34%, 23%, and

26% of those in the ACL-deficient joint and 42%, 27%, and 31% of those in the suture repaired joint, in conjunction with similar changes to the lateral meniscus. Further, these values were within 10-20 N of the intact joint throughout flexion; however, the differences were still significant at 30° and 60° ($p<0.05$). Additionally, the in-situ forces of the MCL and LCL were similar to the intact joint at all flexion angles ($p>0.05$).

Another way to express these in-situ force data is in terms of the relative contribution of each tissue in resisting the applied load, as displayed in Figure 47. For the intact joint, the ACL resists large anterior forces in excess of the applied 67 N anterior tibial load (131 ± 22%, 150 ± 22%, and 141 ± 26% at 30°, 60°, and 90°, respectively). The ACL was opposed by the forces due to bony contact which were -34 ± 12%, -38 ± 17%, and -45 ± 16% at 30°, 60°, and 90°, respectively. All other tissues contributed <5% to the total load. For the ACL-deficient joint at 30°, the dominant structure was the medial meniscus, which carried 67 ± 36%, 110 ± 41%, and 98 ± 42% of the applied load at 30°, 60°, and 90°, respectively. At 30°, the lateral meniscus and capsular structures each carried approximately 40% of the anterior load, which was balanced by the posterior force due to bony contact. At 60° and 90°, the role of the MCL increased, as it carried about 25% of the applied load. Interestingly, at 60° and 90°, the lateral meniscus carried a posterior load approximately -50% and -25%, respectively. Meanwhile, at these flexion angles, there was little contribution due to bony contact, as most of the force in the bones was passed through the menisci.

With suture repair, the sutures resisted a significant portion of the load (44 ± 22%, 53 ± 48%, and 65 ± 43% at 30°, 60°, and 90°, respectively); although these values were much lower than those for the intact ACL. As a result, it was not the only contributor, as the medial meniscus also carried high loads (38 ± 37%, 80 ± 57%, and 58 ± 47% at 30°, 60°, and 90°,

respectively). Other significant contributors at 30° include the capsular tissues and bony contact. Similar to the ACL-deficient joint, lateral meniscus carried a posterior load of approximately -35-45%. With suture augmentation, the sutures bore similar values as those for the intact ACL (89 ± 7%, 88 ± 10%, and 71 ± 9% at 30°, 60°, and 90°, respectively). The relative contribution of the menisci decreased greatly compared to the ACL-deficient and suture repair groups and were minimal, similar to those for the intact joint. Meanwhile, the forces due to bony contact were increased and restored to the levels of the intact joint.

Table 24. In-situ forces in the tissues surrounding the joint under a 67 N anterior tibial load + 100 N joint compression (*p<0.05 compared to intact, +p<0.05 compared to ACL-deficient, #p<0.05 compared to suture repaired).

	Flexion Angle (degrees)											
	30				60				90			
			Suture Technique				Suture Technique				Suture Technique	
	Intact Joint	ACL-deficient	Repair	Augment-ation	Intact Joint	ACL-deficient	Repair	Augment-ation	Intact Joint	ACL-deficient	Repair	Augment-ation
ACL	102 ± 16	N/A	N/A	N/A	112 ± 10	N/A	N/A	N/A	95 ± 12	N/A	N/A	N/A
Sutures	N/A	N/A	34 ± 13*	78 ± 11*#	N/A	N/A	37 ± 28*	95 ± 9*#	N/A	N/A	49 ± 27*	93 ± 10#
MCL	11 ± 7	18 ± 6	11 ± 3*	4 ± 1+#	14 ± 4	29 ± 6*	11 ± 3+	4 ± 3*+#	16 ± 6	28 ± 16	14 ± 5	13 ± 9
LCL	2 ± 2	4 ± 2	6 ± 3	6 ± 2	1 ± 1	5 ± 4	7 ± 4*	4 ± 2	2 ± 1	9 ± 14	7 ± 3*	4 ± 2
Medial Meniscus	5 ± 2	64 ± 16*	53 ± 21*	22 ± 6*+#	8 ± 8	104 ± 11*	89 ± 17*	24 ± 17*+#	14 ± 16	94 ± 20*	77 ± 15*	24 ± 21+#
Lateral Meniscus	8 ± 5	35 ± 14*	17 ± 16+	9 ± 8	17 ± 9	71 ± 38*	60 ± 28*	24 ± 16#	10 ± 6	53 ± 37	64 ± 28*	22 ± 11#
Bony Contact												
Total	102 ± 6	64 ± 18*	79 ± 25	95 ± 16	85 ± 12	6 ± 3*	13 ± 13*	77 ± 20+#	82 ± 11	18 ± 15*	27 ± 29*	86 ± 23+#
Medial	76 ± 20	35 ± 14*	44 ± 26	46 ± 27	56 ± 17	6 ± 2*	5 ± 1*	27 ± 24*	48 ± 24	16 ± 16	19 ± 19	31 ± 23
Lateral	37 ± 17	25 ± 23	40 ± 35	59 ± 24*+	37 ± 19	1 ± 1*	9 ± 15*	57 ± 27*+#	38 ± 30	4 ± 7	11 ± 13	56 ± 35*+#

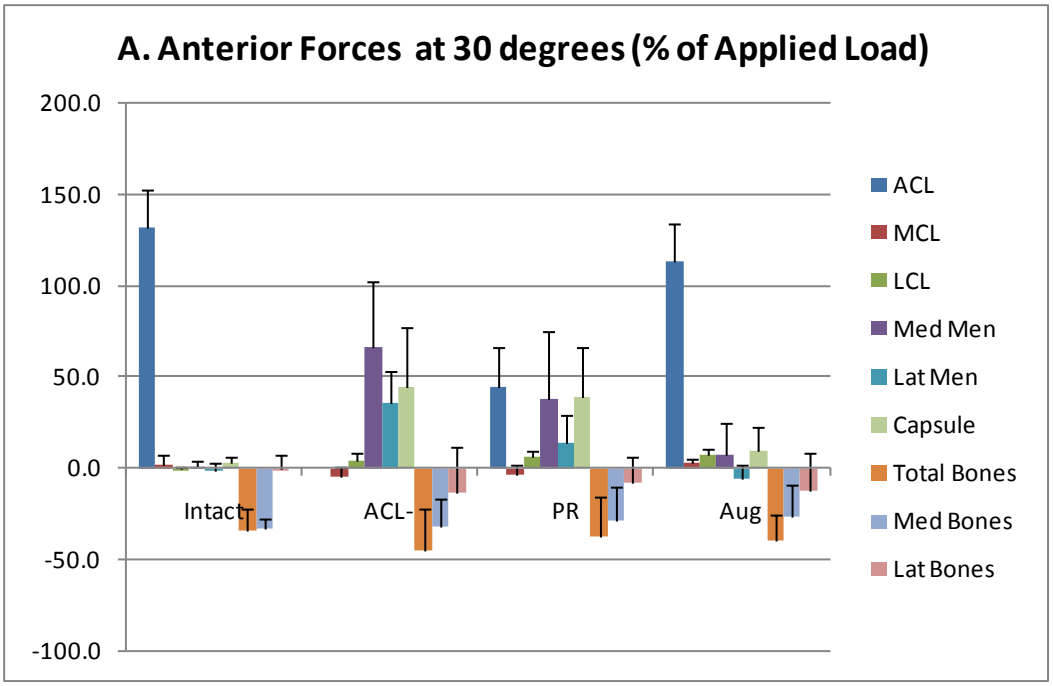
A. Anterior Forces at 30 degrees (% of Applied Load)
200.0
150.0
100.0
50.0
0.0
-50.0
-100.0
Intact
ACL-
PR
Aug
ACL
MCL
LCL
Med Men
Lat Men
Capsule
Total Bones
Med Bones
Lat Bones

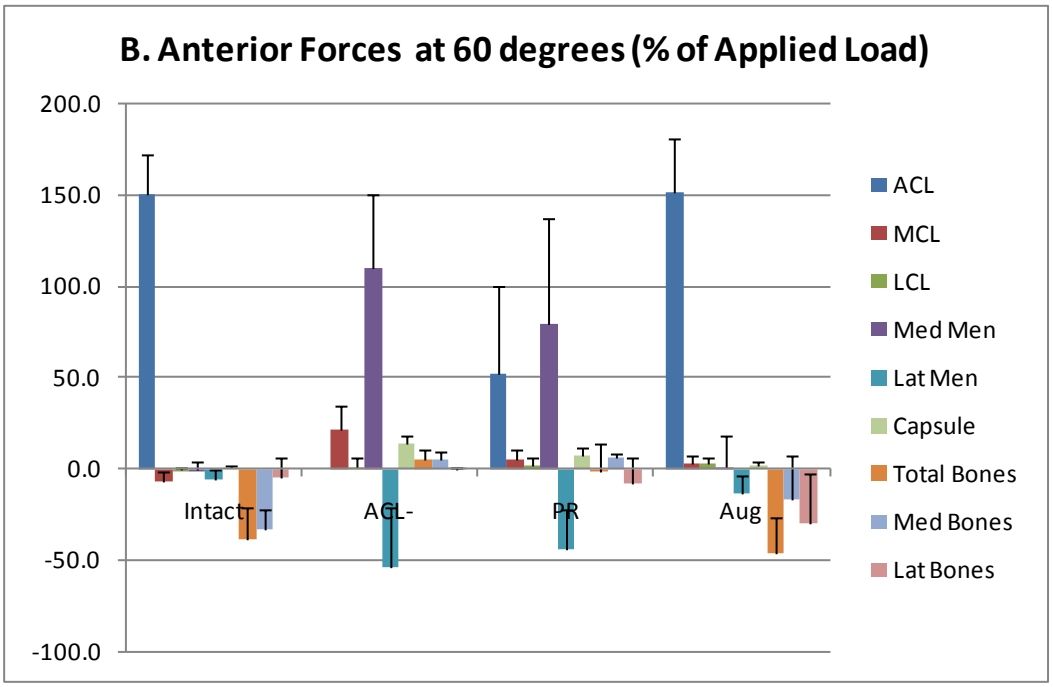
B. Anterior Forces at 60 degrees (% of Applied Load)
200.0
150.0
100.0
50.0
0.0
-50.0
-100.0
Intact
ACL-
PR
Aug
ACL
MCL
LCL
Med Men
Lat Men
Capsule
Total Bones
Med Bones
Lat Bones

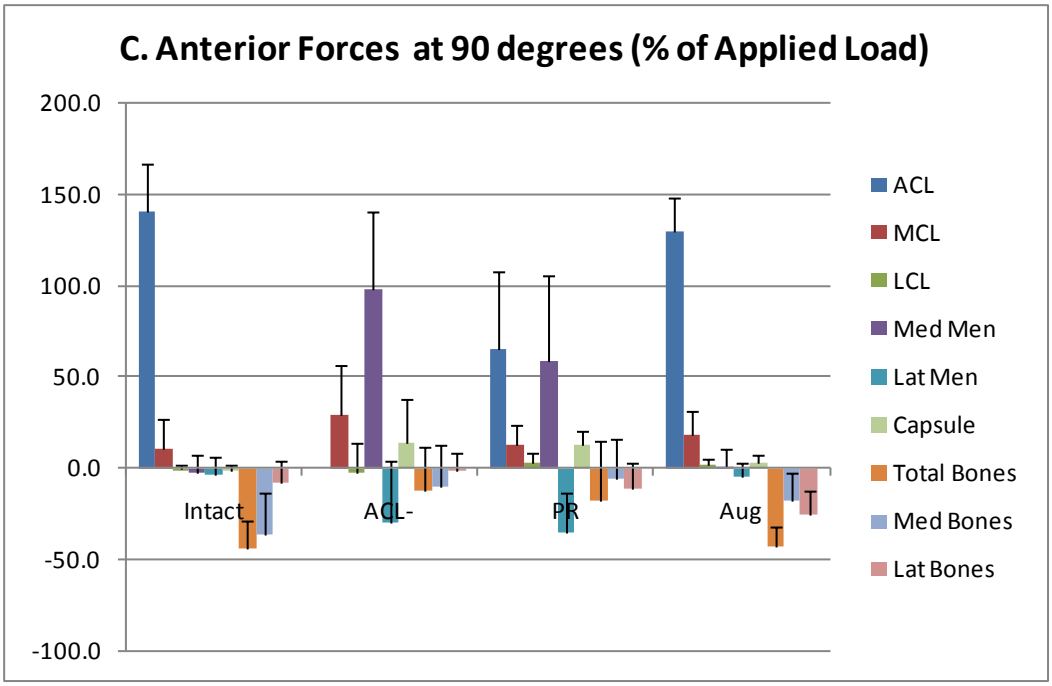

Figure 47. Relative contribution of soft tissue structures of the goat stifle joint under 67 N anterior tibial load + 100 N axial joint compression at a) 30°, b) 60°, and c) 90° of joint flexion.

A.3 COMPARISON OF IN-SITU FORCES IN RESPONSE TO 67 N ANTERIOR TIBIAL LOAD WITH 100 N AXIAL COMPRESSION

For the intact joint, the forces in the MCL were about 3 and 2 times higher with the added compressive load at 60° and 90°, respectively. Similar trends were observed for the ACL-deficient joint. With suture repair, the forces in the MCL remained similar under both loading conditions. This was also true to suture augmentation at 30° and 60°. Interestingly, at 90°, the

force with the compressive load decreased slightly from 20 N to 13 N on average. For the LCL, forces remained below 10 N for all groups under both loading conditions.

Not surprisingly, large differences were observed for both the medial and lateral meniscus when comparing the 67 N anterior tibial load alone versus with the added 100 N compressive load. For the intact joint, forces for both the medial and lateral meniscus remained low, although the values were slightly larger at 60° and 90° under the compressive load. The lateral meniscus reached a maximum of 17 N at 60°, while the medial meniscus reached 14 N at 90°. For the ACL-deficient joint, the force in the medial meniscus jumped by 3-4 times with the compressive load, while the force in the lateral meniscus spiked to from negligible forces under the anterior tibial load alone to 35 N, 71 N, and 53 N on average at 30°, 60°, and 90°, respectively. A similar pattern was observed for the suture repair group as relative increases of 5-11 times for the medial meniscus and forces of 17-60 N on average for the lateral meniscus. With suture augmentation, these large increases were reduced, although still present. For the medial meniscus, the increase in force was only 2-3 times that under the anterior tibial load alone. Likewise, for the lateral meniscus, the force values were only 9-24 N on average.

The in-situ force due to bony contact was also altered when comparing the 67 N anterior tibial load alone versus with the added 100 N compressive load. These forces were minimal for all experimental conditions under the 67 N anterior tibial load alone. For the large majority of the experimental conditions, the force due to bony contact increased with joint compression. It is not surprising that the added compressive load would engage the tissue structures which are designed to resist these types of loads. It is apparent that the force distribution among the tissue structures is much more complex when the compressive load is applied along with the anterior tibial load.

BIBLIOGRAPHY

1. Abramowitch S, Fu YC, Liang R, Woo SL-Y. 2006. *Functional Tissue Engineering of Patellar Tendon Healing: A Histological and Biomechanical Assessment*. Presented at ACSM, Denver, Colorado

2. Abramowitch S, Withrow J, Papageorgiou C, Woo SLY. 2000. *Effect of Initial Graft Tension on the Biomechanical Properties of ACL Reconstruction Grafts*. Presented at 46th Annual Meeting of the Orthop Res Soc, Orlando, FL

3. Abramowitch S, Woo SLY. 2005. *A phenomenological model to describe a dynamic viscoelastic behavior of the rabbit medial collateral ligament*. Presented at 2005 Summer Bioengineering Conference, Vail, CO

4. Abramowitch SD, Papageorgiou CD, Debski RE, Clineff TD, Woo SL. A biomechanical and histological evaluation of the structure and function of the healing medial collateral ligament in a goat model. Knee Surg Sports Traumatol Arthrosc. 11: 155-62, 2003.

5. Abramowitch SD, Papageorgiou CD, Withrow JD, Gilbert TW, Woo SL. The effect of initial graft tension on the biomechanical properties of a healing ACL replacement graft: a study in goats. J Orthop Res. 21: 708-15, 2003.

6. Abramowitch SD, Yagi M, Tsuda E, Woo SL. The healing medial collateral ligament following a combined anterior cruciate and medial collateral ligament injury--a biomechanical study in a goat model. J Orthop Res. 21: 1124-30, 2003.

7. Aglietti P, Buzzi R, D'Andria S, Zaccherotti G. Patellofemoral problems after intraarticular anterior cruciate ligament reconstruction. Clin Orthop Relat Res. 195-204, 1993.

8. Aglietti P, Buzzi R, Giron F, Simeone AJ, Zaccherotti G. Arthroscopic-assisted anterior cruciate ligament reconstruction with the central third patellar tendon. A 5-8-year follow-up. Knee Surg Sports Traumatol Arthrosc. 5: 138-44, 1997.

9. Aglietti P, Buzzi R, Zaccherotti G, De Biase P. Patellar tendon versus doubled semitendinosus and gracilis tendons for anterior cruciate ligament reconstruction. Am J Sports Med. 22: 211-7; discussion 7-8, 1994.

10. Agung M, Ochi M, Yanada S, Adachi N, Izuta Y, Yamasaki T, Toda K. Mobilization of bone marrow-derived mesenchymal stem cells into the injured tissues after intraarticular

injection and their contribution to tissue regeneration. Knee Surg Sports Traumatol Arthrosc. 14: 1307-14, 2006.

11. Ait Si Selmi T, Fithian D, Neyret P. The evolution of osteoarthritis in 103 patients with ACL reconstruction at 17 years follow-up. Knee. 13: 353-8, 2006.

12. Amiel D, Abel MF, Kleiner JB, Lieber RL, Akeson WH. Synovial fluid nutrient delivery in the diathrial joint: an analysis of rabbit knee ligaments. J Orthop Res. 4: 90-5, 1986.

13. Andersson C, Odensten M, Good L, Gillquist J. Surgical or non-surgical treatment of acute rupture of the anterior cruciate ligament. A randomized study with long-term follow-up. J Bone Joint Surg Am. 71: 965-74, 1989.

14. Ansaloni L, Catena F, Coccolini F, Gazzotti F, D'Alessandro L, Daniele Pinna A. Inguinal hernia repair with porcine small intestine submucosa: 3-year follow-up results of a randomized controlled trial of Lichtenstein's repair with polypropylene mesh versus Surgisis Inguinal Hernia Matrix. Am J Surg. 2009.

15. Arnoczky SP. Anatomy of the anterior cruciate ligament. Clin Orthop Relat Res. 19-25, 1983.

16. Arnoczky SP. Blood supply to the anterior cruciate ligament and supporting structures. Orthop Clin North Am. 16: 15-28, 1985.

17. Arnoczky SP, Lavagnino M, Egerbacher M, Caballero O, Gardner K, Shender MA. Loss of homeostatic strain alters mechanostat "set point" of tendon cells in vitro. Clin Orthop Relat Res. 466: 1583-91, 2008.

18. Arnoczky SP, Rubin RM, Marshall JL. Microvasculature of the cruciate ligaments and its response to injury. An experimental study in dogs. J Bone Joint Surg Am. 61: 1221-9, 1979.

19. Asano H, Muneta T, Ikeda H, Yagishita K, Kurihara Y, Sekiya I. Arthroscopic Evaluation of the Articular Cartilage after Anterior Cruciate Ligament Reconstruction: A Short-Term Prospective Study of 105 Patients. Arthroscopy - Journal of Arthroscopic and Related Surgery. 20: 474-81, 2004.

20. Badhe SP, Lawrence TM, Smith FD, Lunn PG. An assessment of porcine dermal xenograft as an augmentation graft in the treatment of extensive rotator cuff tears. J Shoulder Elbow Surg. 17: 35S-9S, 2008.

21. Badylak SF. The extracellular matrix as a biologic scaffold material. Biomaterials. 28: 3587-93, 2007.

22. Badylak SF, Park K, Peppas N, McCabe G, Yoder M. Marrow-derived cells populate scaffolds composed of xenogeneic extracellular matrix. Exp Hematol. 29: 1310-8, 2001.

23. Badylak SF, Record R, Lindberg K, Hodde J, Park K. Small intestinal submucosa: a substrate for in vitro cell growth. J Biomater Sci Polym Ed. 9: 863-78, 1998.

24. Banes AJ, Horesovsky G, Larson C, Tsuzaki M, Judex S, Archambault J, Zernicke R, Herzog W, Kelley S, Miller L. Mechanical load stimulates expression of novel genes in vivo and in vitro in avian flexor tendon cells. Osteoarthritis Cartilage. 7: 141-53, 1999.

25. Banes AJ, Weinhold P, Yang X, Tsuzaki M, Bynum D, Bottlang M, Brown T. Gap junctions regulate responses of tendon cells ex vivo to mechanical loading. Clin Orthop Relat Res. S356-70, 1999.

26. Barrack RL, Bruckner JD, Kneisl J, Inman WS, Alexander AH. The outcome of nonoperatively treated complete tears of the anterior cruciate ligament in active young adults. Clin Orthop Relat Res. 192-9, 1990.

27. Beaty J. "Knee and leg: soft tissue trauma". In OKU orthopaedic knowledge update, Edited by ed. Rosemont, IL: American Academy of Orthopaedic Surgeons, 1999, pp. xix, 442.

28. Bejjani GK, Zabramski J. Safety and efficacy of the porcine small intestinal submucosa dural substitute: results of a prospective multicenter study and literature review. J Neurosurg. 106: 1028-33, 2007.

29. Bellincampi LD, Closkey RF, Prasad R, Zawadsky JP, Dunn MG. Viability of fibroblast-seeded ligament analogs after autogenous implantation. J Orthop Res. 16: 414-20, 1998.

30. Beynnon BD, Johnson RJ, Fleming BC, Kannus P, Kaplan M, Samani J, Renstrom P. Anterior cruciate ligament replacement: comparison of bone-patellar tendon-bone grafts with two-strand hamstring grafts. A prospective, randomized study. J Bone Joint Surg Am. 84-A: 1503-13, 2002.

31. Birk DE. Type V collagen: heterotypic type I/V collagen interactions in the regulation of fibril assembly. Micron. 32: 223-37, 2001.

32. Birk DE, Hahn RA, Linsenmayer CY, Zycband EI. Characterization of collagen fibril segments from chicken embryo cornea, dermis and tendon. Matrix Biol. 15: 111-8, 1996.

33. Birk DE, Mayne R. Localization of collagen types I, III and V during tendon development. Changes in collagen types I and III are correlated with changes in fibril diameter. European Journal of Cell Biology. 72: 352-61, 1997.

34. Boorman RS, Shrive NG, Frank CB. Immobilization increases the vulnerability of rabbit medial collateral ligament autografts to creep. J Orthop Res. 16: 682-9, 1998.

35. Bray RC, Butterwick DJ, Doschak MR, Tyberg JV. Coloured microsphere assessment of blood flow to knee ligaments in adult rabbits: effects of injury. Journal of Orthopaedic Research. 14: 618-25, 1996.

36. Bray RC, Fisher AW, Frank CB. Fine vascular anatomy of adult rabbit knee ligaments. J Anat. 172: 69-79, 1990.

37. Breitfuss H, Frohlich R, Povacz P, Resch H, Wicker A. The tendon defect after anterior cruciate ligament reconstruction using the midthird patellar tendon--a problem for the patellofemoral joint? Knee Surg Sports Traumatol Arthrosc. 3: 194-8, 1996.

38. Brown B, Lindberg K, Reing J, Stolz DB, Badylak SF. The basement membrane component of biologic scaffolds derived from extracellular matrix. Tissue Eng. 12: 519-26, 2006.

39. Buss DD, Min R, Skyhar M, Galinat B, Warren RF, Wickiewicz TL. Nonoperative treatment of acute anterior cruciate ligament injuries in a selected group of patients. Am J Sports Med. 23: 160-5, 1995.

40. Cabaud HE, Rodkey WG, Feagin JA. Experimental studies of acute anterior cruciate ligament injury and repair. Am J Sports Med. 7: 18-22, 1979.

41. Catena F, Ansaloni L, Leone A, De Cataldis A, Gagliardi S, Gazzotti F, Peruzzi S, Agrusti S, D'Alessandro L, Taffurelli M. Lichtenstein repair of inguinal hernia with Surgisis inguinal hernia matrix soft-tissue graft in immunodepressed patients. Hernia. 9: 29-31, 2005.

42. Celotti F, Colciago A, Negri-Cesi P, Pravettoni A, Zaninetti R, Sacchi MC. Effect of platelet-rich plasma on migration and proliferation of SaOS-2 osteoblasts: role of platelet-derived growth factor and transforming growth factor-beta. Wound Repair Regen. 14: 195-202, 2006.

43. Chen CS, Mrksich M, Huang S, Whitesides GM, Ingber DE. Micropatterned surfaces for control of cell shape, position, and function. Biotechnol Prog. 14: 356-63, 1998.

44. Cole DW, Ginn TA, Chen GJ, Smith BP, Curl WW, Martin DF, Poehling GG. Cost comparison of anterior cruciate ligament reconstruction: Autograft versus allograft. Arthroscopy - Journal of Arthroscopic and Related Surgery. 21: 786-90, 2005.

45. Cowin SC. The mechanical and stress adaptive properties of bone. Ann Biomed Eng. 11: 263-95, 1983.

46. Cowin SC. Tissue growth and remodeling. Annu Rev Biomed Eng. 6: 77-107, 2004.

47. Cowin SC. The significance of bone microstructure in mechanotransduction. J Biomech. 40 Suppl 1: S105-9, 2007.

48. Cummings JF, Grood ES. The progression of anterior translation after anterior cruciate ligament reconstruction in a caprine model. J Orthop Res. 20: 1003-8, 2002.

49. Dahms SE, Piechota HJ, Nunes L, Dahiya R, Lue TF, Tanagho EA. Free ureteral replacement in rats: regeneration of ureteral wall components in the acellular matrix graft. Urology. 50: 818-25, 1997.

50. Dai Y, Vaught TD, Boone J, Chen SH, Phelps CJ, Ball S, Monahan JA, Jobst PM, McCreath KJ, Lamborn AE, Cowell-Lucero JL, Wells KD, Colman A, Polejaeva IA, Ayares DL.

Targeted disruption of the alpha1,3-galactosyltransferase gene in cloned pigs. Nat Biotechnol. 20: 251-5, 2002.

51. Daly KA, Stewart-Akers AM, Hara H, Ezzelarab M, Long C, Cordero K, Johnson SA, Ayares D, Cooper DK, Badylak SF. Effect of the alphaGal epitope on the response to small intestinal submucosa extracellular matrix in a nonhuman primate model. Tissue Eng Part A. 15: 3877-88, 2009.

52. Daniel DM, Stone ML, Dobson BE, Fithian DC, Rossman DJ, Kaufman KR. Fate of the ACL-injured patient. A prospective outcome study. American Journal of Sports Medicine. 22: 632-44, 1994.

53. Deie M, Ochi M, Ikuta Y. High intrinsic healing potential of human anterior cruciate ligament. Organ culture experiments. Acta Orthop Scand. 66: 28-32, 1995.

54. Drogset JO, Grontvedt T, Robak OR, Molster A, Viset AT, Engebretsen L. A sixteen-year follow-up of three operative techniques for the treatment of acute ruptures of the anterior cruciate ligament. J Bone Joint Surg Am. 88: 944-52, 2006.

55. Dunlap J, McCarthy JA, Joyce ME, Ogata K, Shively RA. Quantification of the perfusion of the anterior cruciate ligament and the effects of stress and injury to supporting structures. Am J Sports Med. 17: 808-10, 1989.

56. Edelman DS. Laparoscopic herniorrhaphy with porcine small intestinal submucosa: a preliminary study. Jsls. 6: 203-5, 2002.

57. Edwards JCW. "The Synovium". In Rheumatology, Edited by ed. Edinburgh: Elsevier, 2003, pp. 159-68.

58. Egerbacher M, Arnoczky SP, Caballero O, Lavagnino M, Gardner KL. Loss of homeostatic tension induces apoptosis in tendon cells: an in vitro study. Clin Orthop Relat Res. 466: 1562-8, 2008.

59. Elliott DM, Robinson PS, Gimbel JA, Sarver JJ, Abboud JA, Iozzo RV, Soslowsky LJ. Effect of altered matrix proteins on quasilinear viscoelastic properties in transgenic mouse tail tendons. Ann Biomed Eng. 31: 599-605, 2003.

60. Faul F, Erdfelder E, Lang AG, Buchner A. G*Power 3: a flexible statistical power analysis program for the social, behavioral, and biomedical sciences. Behav Res Methods. 39: 175-91, 2007.

61. Feagin JA, Jr., Curl WW. Isolated tear of the anterior cruciate ligament: 5-year follow-up study. Am J Sports Med. 4: 95-100, 1976.

62. Feller JA, Webster KE. A randomized comparison of patellar tendon and hamstring tendon anterior cruciate ligament reconstruction. Am J Sports Med. 31: 564-73, 2003.

63. Fetto JF, Marshall JL. The natural history and diagnosis of anterior cruciate ligament insufficiency. Clin Orthop Relat Res. 29-38, 1980.

64. Fink C, Hoser C, Benedetto KP. [Sports capacity after rupture of the anterior cruciate ligament--surgical versus non-surgical therapy]. Aktuelle Traumatol. 23: 371-5, 1993.

65. Fink C, Hoser C, Benedetto KP, Hackl W, Gabl M. [Long-term outcome of conservative or surgical therapy of anterior cruciate ligament rupture]. Unfallchirurg. 99: 964-9, 1996.

66. Fisher MB, Abramowitch, S.D., and Woo, S. L-Y. 2006. *The effects of assuming a negligible preload on the viscoelastic properties of the normal and healing rabbit patellar tendon*. Presented at ASME Summer Bioengineering Conference

67. Fisher MB, Jung H-J, Liang R, Kim KE, McMahon PJ, Woo SL-Y. 2010. *Use of Extracellular Matrix Bioscaffolds to Enhance ACL Healing: A Multidisciplinary Approach in a Goat Model*. Presented at ASME Summer Bioengineering Conference, Naples, FL

68. Fisher MB, Jung H-J, Woo SL-Y. 2010. *Suture Techniques for ACL Healing: Initial Knee Stability and Impact on the Medial Meniscus in the Goat*. Presented at 56th Annual Meeting of the Orthopaedic Research Society, New Orleans, LA

69. Fisher MB, Jung HJ, McMahon PJ, Woo SL-Y. Evaluation of bone tunnel placement for suture augmentation of an injured anterior cruciate ligament: effects on joint stability in a goat model. J Orthop Res. 28: 1373-9, 2010.

70. Fisher MB, Liang R, Jung H-J, McMahon PJ, Woo SL-Y. 2010. A Novel Extracellular Matrix Bioscaffold Can Enhance ACL Healing. In *International Symposium on Ligaments & Tendons, X*. Hong Kong, China

71. Fisher MB, Zamarra G, Cirillo A, Liang R, Almarza A, McMahon PJ, Woo SL-Y. 2009. *Improved Healing of the Anterior Cruciate Ligament Following Genetically-Engineered Bioscaffold Treatment in a Goat Model*. Presented at 55th Annual Meeting of the Orthopaedic Research Society, Las Vegas, NV

72. Fithian DC, Paxton EW, Stone ML, Luetzow WF, Csintalan RP, Phelan D, Daniel DM. Prospective trial of a treatment algorithm for the management of the anterior cruciate ligament-injured knee. American Journal of Sports Medicine. 33: 335-46, 2005.

73. Fleming BC, Carey JL, Spindler KP, Murray MM. Can suture repair of ACL transection restore normal anteroposterior laxity of the knee? An ex vivo study. J Orthop Res. 26: 1500-5, 2008.

74. Frank C, Amiel D, Akeson WH. Healing of the medial collateral ligament of the knee. A morphological and biochemical assessment in rabbits. Acta Orthop Scand. 54: 917-23, 1983.

75. Frank C, McDonald D, Shrive N. Collagen fibril diameters in the rabbit medial collateral ligament scar: a longer term assessment. Connective Tissue Research. 36: 261-9, 1997.

76. Frank C, Schachar N, Dittrich D. Natural history of healing in the repaired medial collateral ligament. J Orthop Res. 1: 179-88, 1983.

77. Frank C, Woo SL, Amiel D, Harwood F, Gomez M, Akeson W. Medial collateral ligament healing. A multidisciplinary assessment in rabbits. Am J Sports Med. 11: 379-89, 1983.

78. Frank CB, Hart DA, Shrive NG. Molecular biology and biomechanics of normal and healing ligaments--a review. Osteoarthritis & Cartilage. 7: 130-40, 1999.

79. Franklin ME, Jr., Gonzalez JJ, Jr., Glass JL. Use of porcine small intestinal submucosa as a prosthetic device for laparoscopic repair of hernias in contaminated fields: 2-year follow-up. Hernia. 8: 186-9, 2004.

80. Franklin ME, Jr., Trevino JM, Portillo G, Vela I, Glass JL, Gonzalez JJ. The use of porcine small intestinal submucosa as a prosthetic material for laparoscopic hernia repair in infected and potentially contaminated fields: long-term follow-up. Surg Endosc. 22: 1941-6, 2008.

81. Freedman KB, D'Amato MJ, Nedeff DD, Kaz A, Bach BR, Jr. Arthroscopic anterior cruciate ligament reconstruction: a metaanalysis comparing patellar tendon and hamstring tendon autografts. Am J Sports Med. 31: 2-11, 2003.

82. Freytes DO, Martin J, Velankar SS, Lee AS, Badylak SF. Preparation and rheological characterization of a gel form of the porcine urinary bladder matrix. Biomaterials. 29: 1630-7, 2008.

83. Fujie H, Livesay GA, Woo SL, Kashiwaguchi S, Blomstrom G. The use of a universal force-moment sensor to determine in-situ forces in ligaments: a new methodology. J Biomech Eng. 117: 1-7, 1995.

84. Fukui N, Katsuragawa Y, Kawakami A, Sakai H, Oda H, Nakamura K. Metabolic activity in disrupted human anterior cruciate ligament. Evaluation of procollagen mRNA expression in 29 patients. Joint Bone Spine. 68: 318-26, 2001.

85. Fung YC. Biomechanics: Mechanical Properties of Living Tissues. New York: Springer, 1993,

86. Fung YC. Stress, strain, growth, and remodeling of living organisms. ZAMP. 46: S469-82, 1995.

87. Gabriel MT, Wong EK, Woo SL, Yagi M, Debski RE. Distribution of in situ forces in the anterior cruciate ligament in response to rotatory loads. J Orthop Res. 22: 85-9, 2004.

88. Galili U. Evolution and pathophysiology of the human natural anti-alpha-galactosyl IgG (anti-Gal) antibody. Springer Semin Immunopathol. 15: 155-71, 1993.

89. Gardner K, Arnoczky SP, Caballero O, Lavagnino M. The effect of stress-deprivation and cyclic loading on the TIMP/MMP ratio in tendon cells: an in vitro experimental study. Disabil Rehabil. 30: 1523-9, 2008.

90. Gilbert TW, Stolz DB, Biancaniello F, Simmons-Byrd A, Badylak SF. Production and characterization of ECM powder: implications for tissue engineering applications. Biomaterials. 26: 1431-5, 2005.

91. Gillquist J, Liljedahl SO, Lindvall H. Reconstruction for old rupture of the anterior cruciate ligament. A follow-up study. Injury. 2: 271-8, 1971.

92. Giphart JE, Shelburne KB, Anstett K, Brunkhorst JP, Pault JD, Woo SL-Y, Steadman JR, Torry MR. 2008. *Measurement of 3D In Vivo Knee Motion Using Biplane Fluoroscopy: Investigation of Non-contact ACL Injuries*. Presented at XVIth International Conference on Mechanics in Medicine and Biology, Pittsburgh, PA

93. Gleason RL, Humphrey JD. A mixture model of arterial growth and remodeling in hypertension: altered muscle tone and tissue turnover. J Vasc Res. 41: 352-63, 2004.

94. Gobbi A. 2008. The use of bone marrow and growth factors for the treatment of primary ACL lesions In *5th Meeting of the European Federation of National Associations of Orthopaedic Sports Traumatology*. Antalya, Turkey

95. Gobbi A, Bathan L, Boldrini L. Primary repair combined with bone marrow stimulation in acute anterior cruciate ligament lesions: results in a group of athletes. Am J Sports Med. 37: 571-8, 2009.

96. Hansen L, Wan W, Gleason RL. Microstructurally motivated constitutive modeling of mouse arteries cultured under altered axial stretch. J Biomech Eng. 131: 101015, 2009.

97. Haus J, Refior HJ. A study of the synovial and ligamentous structure of the anterior cruciate ligament. Int Orthop. 11: 117-24, 1987.

98. Hefti FL, Kress A, Fasel J, Morscher EW. Healing of the transected anterior cruciate ligament in the rabbit. J Bone Joint Surg Am. 73: 373-83, 1991.

99. Hefzy MS, Grood ES. Sensitivity of insertion locations on length patterns of anterior cruciate ligament fibers. J Biomech Eng. 108: 73-82, 1986.

100. Hodde J. Naturally occurring scaffolds for soft tissue repair and regeneration. Tissue Eng. 8: 295-308, 2002.

101. Hodde J, Record R, Tullius R, Badylak S. Fibronectin peptides mediate HMEC adhesion to porcine-derived extracellular matrix. Biomaterials. 23: 1841-8, 2002.

102. Hoel PG. Introduction to mathematical statistics. New York,: Wiley, 1971, x, 409 pp.

103. Holden JP, Grood ES, Korvick DL, Cummings JF, Butler DL, Bylski-Austrow DI. In vivo forces in the anterior cruciate ligament: direct measurements during walking and trotting in a quadruped. J Biomech. 27: 517-26, 1994.

104. Holzapfel GA, Gasser TC, Ogden RW. Comparison of a multi-layer structural model for arterial walls with a fung-type model, and issues of material stability. J Biomech Eng. 126: 264-75, 2004.

105. Howell SM, Gittins ME, Gottlieb JE, Traina SM, Zoellner TM. The relationship between the angle of the tibial tunnel in the coronal plane and loss of flexion and anterior laxity after anterior cruciate ligament reconstruction. Am J Sports Med. 29: 567-74, 2001.

106. Humphrey JD. Remodeling of a collagenous tissue at fixed lengths. J Biomech Eng. 121: 591-7, 1999.

107. Humphrey JD, Strumpf RK, Yin FC. Determination of a constitutive relation for passive myocardium: I. A new functional form. J Biomech Eng. 112: 333-9, 1990.

108. Hurschler C, Loitz-Ramage B, Vanderby R, Jr. A structurally based stress-stretch relationship for tendon and ligament. J Biomech Eng. 119: 392-9, 1997.

109. Iannotti JP, Codsi MJ, Kwon YW, Derwin K, Ciccone J, Brems JJ. Porcine small intestine submucosa augmentation of surgical repair of chronic two-tendon rotator cuff tears. A randomized, controlled trial. J Bone Joint Surg Am. 88: 1238-44, 2006.

110. Indelicato P. Isolated medial collateral ligament injuries in the knee. J Am Acad Orthop Surg. 3: 9-14, 1995.

111. Inoue M, McGurk-Burleson E, Hollis JM, Woo SL. Treatment of the medial collateral ligament injury. I: The importance of anterior cruciate ligament on the varus-valgus knee laxity. Am J Sports Med. 15: 15-21, 1987.

112. Inoue M, Woo SL, Gomez MA, Amiel D, Ohland KJ, Kitabayashi LR. Effects of surgical treatment and immobilization on the healing of the medial collateral ligament: a long-term multidisciplinary study. Connect Tissue Res. 25: 13-26, 1990.

113. Jackson DW, Schreck P, Jacobson S, Simon TM. Reduced anterior tibial translation associated with adaptive changes in the anterior cruciate ligament-deficient joint: goat model. J Orthop Res. 17: 810-6, 1999.

114. Jackson DW, Simon TM, Lowery W, Gendler E. Biologic remodeling after anterior cruciate ligament reconstruction using a collagen matrix derived from demineralized bone. An experimental study in the goat model. Am J Sports Med. 24: 405-14, 1996.

115. Jarvela T, Paakkala T, Kannus P, Jarvinen M. The incidence of patellofemoral osteoarthritis and associated findings 7 years after anterior cruciate ligament reconstruction with a bone-patellar tendon-bone autograft. American Journal of Sports Medicine. 29: 18-24, 2001.

116. Jomha NM, Pinczewski LA, Clingeleffer A, Otto DD. Arthroscopic reconstruction of the anterior cruciate ligament with patellar-tendon autograft and interference screw fixation. The results at seven years. Journal of Bone and Joint Surgery - Series B. 81: 775-9, 1999.

117. Jones KG. Reconstruction of the anterior cruciate ligament using the central one-third of the patellar ligament. J Bone Joint Surg Am. 52: 838-9, 1970.

118. Joshi SM, Mastrangelo AN, Magarian EM, Fleming BC, Murray MM. Collagen-platelet composite enhances biomechanical and histologic healing of the porcine anterior cruciate ligament. Am J Sports Med. 37: 2401-10, 2009.

119. Kannus P, Jarvinen M. Conservatively treated tears of the anterior cruciate ligament. Long-term results. J Bone Joint Surg Am. 69: 1007-12, 1987.

120. Kaplan N, Wickiewicz TL, Warren RF. Primary surgical treatment of anterior cruciate ligament ruptures. A long-term follow-up study. Am J Sports Med. 18: 354-8, 1990.

121. Karaoglu S, Fisher MB, Woo SL-Y, Fu YC, Liang R, Abramowitch SD. Use of a Bioscaffold to Improve Healing of a Patellar Tendon Defect After Graft Harvest for ACL Reconstruction: A Study in Rabbits. J Orthop Res. 26: 255-63, 2008.

122. Kartus J, Magnusson L, Stener S, Brandsson S, Eriksson BI, Karlsson J. Complications following arthroscopic anterior cruciate ligament reconstruction. A 2-5-year follow-up of 604 patients with special emphasis on anterior knee pain. Knee Surg Sports Traumatol Arthrosc. 7: 2-8, 1999.

123. Kelly DW, Carter VS, Jobe FW, Kerlan RK. Patellar and quadriceps tendon ruptures--jumper's knee. Am J Sports Med. 12: 375-80, 1984.

124. Khalfayan EE, Sharkey PF, Alexander AH, Bruckner JD, Bynum EB. The relationship between tunnel placement and clinical results after anterior cruciate ligament reconstruction. Am J Sports Med. 24: 335-41, 1996.

125. Klisch SM, Asanbaeva A, Oungoulian SR, Masuda K, Thonar EJ, Davol A, Sah RL. A cartilage growth mixture model with collagen remodeling: validation protocols. J Biomech Eng. 130: 031006, 2008.

126. Knoll LD. Use of porcine small intestinal submucosal graft in the surgical management of tunical deficiencies with penile prosthetic surgery. Urology. 59: 758-61, 2002.

127. Kobayashi D, Kurosaka M, Yoshiya S, Mizuno K. Effect of basic fibroblast growth factor on the healing of defects in the canine anterior cruciate ligament. Knee Surg Sports Traumatol Arthrosc. 5: 189-94, 1997.

128. Kobayashi K, Healey RM, Sah RL, Clark JJ, Tu BP, Goomer RS, Akeson WH, Moriya H, Amiel D. Novel method for the quantitative assessment of cell migration: a study on the motility of rabbit anterior cruciate (ACL) and medial collateral ligament (MCL) cells. Tissue Eng. 6: 29-38, 2000.

129. Kobayashi S, Baba H, Uchida K, Negoro K, Sato M, Miyazaki T, Nomura E, Murakami K, Shimizubata M, Meir A. Microvascular system of anterior cruciate ligament in dogs. J Orthop Res. 24: 1509-20, 2006.

130. Kurosaka M, Yoshiya S, Andrish JT. A biomechanical comparison of different surgical techniques of graft fixation in anterior cruciate ligament reconstruction. Am J Sports Med. 15: 225-9, 1987.

131. Lanir Y. Constitutive equations for fibrous connective tissues. J Biomech. 16: 1-12, 1983.

132. Lanir Y, Fung YC. Two-dimensional mechanical properties of rabbit skin. II. Experimental results. J Biomech. 7: 171-82, 1974.

133. Laros GS, Tipton CM, Cooper RR. Influence of physical activity on ligament insertions in the knees of dogs. J Bone Joint Surg Am. 53: 275-86, 1971.

134. Lavagnino M, Arnoczky SP. In vitro alterations in cytoskeletal tensional homeostasis control gene expression in tendon cells. J Orthop Res. 23: 1211-8, 2005.

135. Lavagnino M, Arnoczky SP, Kepich E, Caballero O, Haut RC. A finite element model predicts the mechanotransduction response of tendon cells to cyclic tensile loading. Biomech Model Mechanobiol. 7: 405-16, 2008.

136. Lavagnino M, Arnoczky SP, Tian T, Vaupel Z. Effect of amplitude and frequency of cyclic tensile strain on the inhibition of MMP-1 mRNA expression in tendon cells: an in vitro study. Connect Tissue Res. 44: 181-7, 2003.

137. Lee J, Harwood FL, Akeson WH, Amiel D. Growth factor expression in healing rabbit medial collateral and anterior cruciate ligaments. Iowa Orthop J. 18: 19-25, 1998.

138. Lee TQ, Woo SL. A new method for determining cross-sectional shape and area of soft tissues. J Biomech Eng. 110: 110-4, 1988.

139. Li F, Li W, Johnson S, Ingram D, Yoder M, Badylak S. Low-molecular-weight peptides derived from extracellular matrix as chemoattractants for primary endothelial cells. Endothelium. 11: 199-206, 2004.

140. Li G, Van de Velde SK, Bingham JT. Validation of a non-invasive fluoroscopic imaging technique for the measurement of dynamic knee joint motion. J Biomech. 41: 1616-22, 2008.

141. Liang R, Woo SL-Y, Takakura Y, Moon DK, Jia F, Abramowitch SD. Long-term effects of porcine small intestine submucosa on the healing of medial collateral ligament: a functional tissue engineering study. J Orthop Res. 24: 811-9, 2006.

142. Liang R, Woo SL, Nguyen TD, Liu PC, Almarza A. Effects of a bioscaffold on collagen fibrillogenesis in healing medial collateral ligament in rabbits. J Orthop Res. 26: 1098-104, 2008.

143. Liang R, Woo SL, Takakura Y, Moon DK, Jia F, Abramowitch SD. Long-term effects of porcine small intestine submucosa on the healing of medial collateral ligament: a functional tissue engineering study. J Orthop Res. 24: 811-9, 2006.

144. Lin VS, Lee MC, O'Neal S, McKean J, Sung KL. Ligament tissue engineering using synthetic biodegradable fiber scaffolds. Tissue Eng. 5: 443-52, 1999.

145. Linsenmayer TF, Gibney E, Igoe F, Gordon MK, Fitch JM, Fessler LI, Birk DE. Type V collagen: molecular structure and fibrillar organization of the chicken alpha 1(V) NH2-terminal domain, a putative regulator of corneal fibrillogenesis. J Cell Biol. 121: 1181-9, 1993.

146. Liu SH, Yang RS, al-Shaikh R, Lane JM. Collagen in tendon, ligament, and bone healing. A current review. Clin Orthop Relat Res. 265-78, 1995.

147. Livesay GA, Rudy TW, Woo SL, Runco TJ, Sakane M, Li G, Fu FH. Evaluation of the effect of joint constraints on the in situ force distribution in the anterior cruciate ligament. J Orthop Res. 15: 278-84, 1997.

148. Liyanage SH, Purohit GS, Frye JN, Giordano P. Anterior abdominal wall reconstruction with a Permacol implant. J Plast Reconstr Aesthet Surg. 59: 553-5, 2006.

149. Lobenhoffer P, Tscherne H. [Rupture of the anterior cruciate ligament. Current status of treatment]. Unfallchirurg. 96: 150-68, 1993.

150. Loh JC, Fukuda Y, Tsuda E, Steadman RJ, Fu FH, Woo SL. Knee stability and graft function following anterior cruciate ligament reconstruction: Comparison between 11 o'clock and 10 o'clock femoral tunnel placement. 2002 Richard O'Connor Award paper. Arthroscopy. 19: 297-304, 2003.

151. Loitz-Ramage BJ, Frank CB, Shrive NG. Injury size affects long-term strength of the rabbit medial collateral ligament. Clinical Orthopaedics & Related Research. 272-80, 1997.

152. Ma CB, Papageogiou CD, Debski RE, Woo SL. Interaction between the ACL graft and MCL in a combined ACL+MCL knee injury using a goat model. Acta Orthop Scand. 71: 387-93, 2000.

153. Macher BA, Galili U. The Galalpha1,3Galbeta1,4GlcNAc-R (alpha-Gal) epitope: a carbohydrate of unique evolution and clinical relevance. Biochim Biophys Acta. 1780: 75-88, 2008.

154. Malcarney HL, Bonar F, Murrell GA. Early inflammatory reaction after rotator cuff repair with a porcine small intestine submucosal implant: a report of 4 cases. Am J Sports Med. 33: 907-11, 2005.

155. Maletius W, Messner K. Eighteen- to twenty-four-year follow-up after complete rupture of the anterior cruciate ligament. American Journal of Sports Medicine. 27: 711-7, 1999.

156. Marshall JL, Warren RF, Wickiewicz TL. Primary surgical treatment of anterior cruciate ligament lesions. Am J Sports Med. 10: 103-7, 1982.

157. Mayr HO, Troger M, Hein W. Patellofemoral arthritis following arthrofibrosis. Causes and therapy. Arthroskopie. 18: 308-12, 2005.

158. Mayr HO, Weig TG, Plitz W. Arthrofibrosis following ACL reconstruction - Reasons and outcome. Archives of Orthopaedic and Trauma Surgery. 124: 518-22, 2004.

159. McPherson TB, Liang H, Record RD, Badylak SF. Galalpha(1,3)Gal epitope in porcine small intestinal submucosa. Tissue Eng. 6: 233-9, 2000.

160. Mostow EN, Haraway GD, Dalsing M, Hodde JP, King D. Effectiveness of an extracellular matrix graft (OASIS Wound Matrix) in the treatment of chronic leg ulcers: a randomized clinical trial. J Vasc Surg. 41: 837-43, 2005.

161. Murakami Y, Ochi M, Ikuta Y, Higashi Y. Permeation from the synovial fluid as nutritional pathway for the anterior cruciate ligament in rabbits. Acta Physiol Scand. 158: 181-7, 1996.

162. Murray MM. Current status and potential of primary ACL repair. Clin Sports Med. 28: 51-61, 2009.

163. Murray MM, Fleming BC, Abreu E, Magarian E, Mastrangelo A, Palmer M, Spindler KP. 2008. *Collagen-Platelet Rich Plasma Hydrogel Enhances Primary Repair of the Porcine Anterior Cruciate Ligament*. Presented at International Symposium on Ligaments and Tendons VIII, Stanford, CA

164. Murray MM, Martin SD, Martin TL, Spector M. Histological changes in the human anterior cruciate ligament after rupture. J Bone Joint Surg Am. 82-A: 1387-97, 2000.

165. Murray MM, Palmer M, Abreu E, Spindler KP, Zurakowski D, Fleming BC. Platelet-rich plasma alone is not sufficient to enhance suture repair of the ACL in skeletally immature animals: an in vivo study. J Orthop Res. 27: 639-45, 2009.

166. Murray MM, Spector M. The migration of cells from the ruptured human anterior cruciate ligament into collagen-glycosaminoglycan regeneration templates in vitro. Biomaterials. 22: 2393-402, 2001.

167. Murray MM, Spindler KP, Abreu E, Muller JA, Nedder A, Kelly M, Frino J, Zurakowski D, Valenza M, Snyder BD, Connolly SA. Collagen-platelet rich plasma hydrogel enhances primary repair of the porcine anterior cruciate ligament. J Orthop Res. 25: 81-91, 2007.

168. Murray MM, Spindler KP, Devin C, Snyder BS, Muller J, Takahashi M, Ballard P, Nanney LB, Zurakowski D. Use of a collagen-platelet rich plasma scaffold to stimulate healing of a central defect in the canine ACL. J Orthop Res. 24: 820-30, 2006.

169. Murray MMaS, K. P. . Anterior Cruciate Ligament Healing and Repair. Sports Med Arthrosc Rev. 13: 151-5, 2005.

170. Musahl V, Abramowitch SD, Gabriel MT, Debski RE, Hertel P, Fu FH, Woo SL. Tensile properties of an anterior cruciate ligament graft after bone-patellar tendon-bone press-fit fixation. Knee Surg Sports Traumatol Arthrosc. 11: 68-74, 2003.

171. Musahl V, Abramowitch SD, Gilbert TW, Tsuda E, Wang JH, Badylak SF, Woo SL. The use of porcine small intestinal submucosa to enhance the healing of the medial collateral ligament--a functional tissue engineering study in rabbits. J Orthop Res. 22: 214-20, 2004.

172. Nagineni CN, Amiel D, Green MH, Berchuck M, Akeson WH. Characterization of the intrinsic properties of the anterior cruciate and medial collateral ligament cells: an in vitro cell culture study. J Orthop Res. 10: 465-75, 1992.

173. Newton PO, Woo SL, MacKenna DA, Akeson WH. Immobilization of the knee joint alters the mechanical and ultrastructural properties of the rabbit anterior cruciate ligament. J Orthop Res. 13: 191-200, 1995.

174. Ng GY, Oakes BW, Deacon OW, McLean ID, Eyre DR. Long-term study of the biochemistry and biomechanics of anterior cruciate ligament-patellar tendon autografts in goats. J Orthop Res. 14: 851-6, 1996.

175. Ng GY, Oakes BW, Deacon OW, McLean ID, Lampard D. Biomechanics of patellar tendon autograft for reconstruction of the anterior cruciate ligament in the goat: three-year study. J Orthop Res. 13: 602-8, 1995.

176. Nguyen TD, Liang R, Woo SL, Burton SD, Wu C, Almarza A, Sacks MS, Abramowitch S. Effects of cell seeding and cyclic stretch on the fiber remodeling in an extracellular matrix-derived bioscaffold. Tissue Eng Part A. 15: 957-63, 2009.

177. Niyibizi C, Kavalkovich K, Yamaji T, Woo SL. Type V collagen is increased during rabbit medial collateral ligament healing. Knee Surg Sports Traumatol Arthrosc. 8: 281-5, 2000.

178. Niyibizi C, Visconti CS, Kavalkovich K, Woo SL. Collagens in an adult bovine medial collateral ligament: immunofluorescence localization by confocal microscopy reveals that type XIV collagen predominates at the ligament-bone junction. Matrix Biol. 14: 743-51, 1995.

179. Noyes FR. Functional properties of knee ligaments and alterations induced by immobilization: a correlative biomechanical and histological study in primates. Clin Orthop Relat Res. 210-42, 1977.

180. Noyes FR, Mooar PA, Matthews DS, Butler DL. The symptomatic anterior cruciate-deficient knee. Part I: the long-term functional disability in athletically active individuals. J Bone Joint Surg Am. 65: 154-62, 1983.

181. O'Connor R C, Harding JN, 3rd, Steinberg GD. Novel modification of partial nephrectomy technique using porcine small intestine submucosa. Urology. 60: 906-9, 2002.

182. O'Donoghue DH. An analysis of end results of surgical treatment of major injuries to the ligaments of the knee. J Bone Joint Surg Am. 37-A: 1-13; passim, 1955.

183. O'Donoghue DH, Frank GR, Jeter GL, Johnson W, Zeiders JW, Kenyon R. Repair and reconstruction of the anterior cruciate ligament in dogs. Factors influencing long-term results. J Bone Joint Surg Am. 53: 710-8, 1971.

184. O'Donoghue DH, Rockwood CA, Jr., Frank GR, Jack SC, Kenyon R. Repair of the anterior cruciate ligament in dogs. J Bone Joint Surg Am. 48: 503-19, 1966.

185. Odensten M, Lysholm J, Gillquist J. Suture of fresh ruptures of the anterior cruciate ligament. A 5-year follow-up. Acta Orthop Scand. 55: 270-2, 1984.

186. Ohland KJ, Woo SL-Y, Weiss JA, Takai S, Shelley FJ. 1991. *Healing of Combined Injuries of the Rabbit Medial Collateral Ligament and Its Insertions: A Long Term Study on the Effects of Conservative vs. Surgical Treatment*. Presented at The Winter Annual Meeting of the American Society of Mechanical Engineers, Atlanta, GA

187. Ohno K, Pomaybo AS, Schmidt CC, Levine RE, Ohland KJ, Woo SL. Healing of the medial collateral ligament after a combined medial collateral and anterior cruciate ligament injury and reconstruction of the anterior cruciate ligament: comparison of repair and nonrepair of medial collateral ligament tears in rabbits. J Orthop Res. 13: 442-9, 1995.

188. Okuda K, Kawase T, Momose M, Murata M, Saito Y, Suzuki H, Wolff LF, Yoshie H. Platelet-rich plasma contains high levels of platelet-derived growth factor and transforming growth factor-beta and modulates the proliferation of periodontally related cells in vitro. J Periodontol. 74: 849-57, 2003.

189. Papageorgiou CD, Gil JE, Kanamori A, Fenwick JA, Woo SL, Fu FH. The biomechanical interdependence between the anterior cruciate ligament replacement graft and the medial meniscus. Am J Sports Med. 29: 226-31, 2001.

190. Papageorgiou CD, Ma CB, Abramowitch SD, Clineff TD, Woo SL. A multidisciplinary study of the healing of an intraarticular anterior cruciate ligament graft in a goat model. Am J Sports Med. 29: 620-6, 2001.

191. Paulos LE, Rosenberg TD, Drawbert J, Manning J, Abbott P. Infrapatellar contracture syndrome. An unrecognized cause of knee stiffness with patella entrapment and patella infera. Am J Sports Med. 15: 331-41, 1987.

192. Phelps CJ, Koike C, Vaught TD, Boone J, Wells KD, Chen SH, Ball S, Specht SM, Polejaeva IA, Monahan JA, Jobst PM, Sharma SB, Lamborn AE, Garst AS, Moore M, Demetris AJ, Rudert WA, Bottino R, Bertera S, Trucco M, Starzl TE, Dai Y, Ayares DL. Production of alpha 1,3-galactosyltransferase-deficient pigs. Science. 299: 411-4, 2003.

193. Piechota HJ, Gleason CA, Dahms SE, Dahiya R, Nunes LS, Lue TF, Tanagho EA. Bladder acellular matrix graft: in vivo functional properties of the regenerated rat bladder. Urol Res. 27: 206-13, 1999.

194. Plaas AH, Wong-Palms S, Koob T, Hernandez D, Marchuk L, Frank CB. Proteoglycan metabolism during repair of the ruptured medial collateral ligament in skeletally mature rabbits. Archives of Biochemistry & Biophysics. 374: 35-41, 2000.

195. Quapp KM, Weiss JA. Material characterization of human medial collateral ligament. J Biomech Eng. 120: 757-63, 1998.

196. Raghavan D, Kropp BP, Lin HK, Zhang Y, Cowan R, Madihally SV. Physical characteristics of small intestinal submucosa scaffolds are location-dependent. J Biomed Mater Res A. 73: 90-6, 2005.

197. Raykin J, Rachev AI, Gleason RL, Jr. A phenomenological model for mechanically mediated growth, remodeling, damage, and plasticity of gel-derived tissue engineered blood vessels. J Biomech Eng. 131: 101016, 2009.

198. Record RD, Hillegonds D, Simmons C, Tullius R, Rickey FA, Elmore D, Badylak SF. In vivo degradation of 14C-labeled small intestinal submucosa (SIS) when used for urinary bladder repair. Biomaterials. 22: 2653-9, 2001.

199. Reider B, Sathy MR, Talkington J, Blyznak N, Kollias S. Treatment of isolated medial collateral ligament injuries in athletes with early functional rehabilitation. A five-year follow-up study. Am J Sports Med. 22: 470-7, 1994.

200. Rodriguez EK, Hoger A, McCulloch AD. Stress-dependent finite growth in soft elastic tissues. J Biomech. 27: 455-67, 1994.

201. Roe J, Pinczewski LA, Russell VJ, Salmon LJ, Kawamata T, Chew M. A 7-year follow-up of patellar tendon and hamstring tendon grafts for arthroscopic anterior cruciate ligament reconstruction: Differences and similarities. American Journal of Sports Medicine. 33: 1337-45, 2005.

202. Roesler H. The history of some fundamental concepts in bone biomechanics. J Biomech. 20: 1025-34, 1987.

203. Rudy TW, Livesay GA, Woo SL, Fu FH. A combined robotic/universal force sensor approach to determine in situ forces of knee ligaments. J Biomech. 29: 1357-60, 1996.

204. Ruiz AL, Kelly M, Nutton RW. Arthroscopic ACL reconstruction: A 5-9 year follow-up. Knee. 9: 197-200, 2002.

205. Sachs RA, Daniel DM, Stone ML, Garfein RF. Patellofemoral problems after anterior cruciate ligament reconstruction. Am J Sports Med. 17: 760-5, 1989.

206. Sacks MS. Incorporation of experimentally-derived fiber orientation into a structural constitutive model for planar collagenous tissues. J Biomech Eng. 125: 280-7, 2003.

207. Sacks MS, Gloeckner DC. Quantification of the fiber architecture and biaxial mechanical behavior of porcine intestinal submucosa. J Biomed Mater Res. 46: 1-10, 1999.

208. Sakane M, Livesay GA, Fox RJ, Rudy TW, Runco TJ, Woo SL. Relative contribution of the ACL, MCL, and bony contact to the anterior stability of the knee. Knee Surg Sports Traumatol Arthrosc. 7: 93-7, 1999.

209. Salmon LJ, Russell VJ, Refshauge K, Kader D, Connolly C, Linklater J, Pinczewski LA. Long-term outcome of endoscopic anterior cruciate ligament reconstruction with patellar tendon autograft: minimum 13-year review. Am J Sports Med. 34: 721-32, 2006.

210. Sanchez AR, Sheridan PJ, Kupp LI. Is platelet-rich plasma the perfect enhancement factor? A current review. Int J Oral Maxillofac Implants. 18: 93-103, 2003.

211. Scapinelli R. Vascular anatomy of the human cruciate ligaments and surrounding structures. Clin Anat. 10: 151-62, 1997.

212. Scavenius M, Bak K, Hansen S, Norring K, Jensen KH, Jorgensen U. Isolated total ruptures of the anterior cruciate ligament--a clinical study with long-term follow-up of 7 years. Scand J Med Sci Sports. 9: 114-9, 1999.

213. Scheffler SU, Clineff TD, Papageorgiou CD, Debski RE, Benjamin C, Woo SL. Structure and function of the healing medial collateral ligament in a goat model. Ann Biomed Eng. 29: 173-80, 2001.

214. Schreck PJ, Kitabayashi LR, Amiel D, Akeson WH, Woods VL, Jr. Integrin display increases in the wounded rabbit medial collateral ligament but not the wounded anterior cruciate ligament. J Orthop Res. 13: 174-83, 1995.

215. Schultz DJ, Brasel KJ, Spinelli KS, Rasmussen J, Weigelt JA. Porcine small intestine submucosa as a treatment for enterocutaneous fistulas. J Am Coll Surg. 194: 541-3, 2002.

216. Schutte MJ, Dabezies EJ, Zimny ML, Happel LT. Neural anatomy of the human anterior cruciate ligament. J Bone Joint Surg Am. 69: 243-7, 1987.

217. Sclamberg SG, Tibone JE, Itamura JM, Kasraeian S. Six-month magnetic resonance imaging follow-up of large and massive rotator cuff repairs reinforced with porcine small intestinal submucosa. J Shoulder Elbow Surg. 13: 538-41, 2004.

218. Seitz H, Menth-Chiari WA, Lang S, Nau T. Histological evaluation of the healing potential of the anterior cruciate ligament by means of augmented and non-augmented repair: an in vivo animal study. Knee Surg Sports Traumatol Arthrosc. 16: 1087-93, 2008.

219. Shelbourne KD, Klotz C. What I have learned about the ACL: Utilizing a progressive rehabilitation scheme to achieve total knee symmetry after anterior cruciate ligament reconstruction. Journal of Orthopaedic Science. 11: 318-25, 2006.

220. Sherman MF, Lieber L, Bonamo JR, Podesta L, Reiter I. The long-term followup of primary anterior cruciate ligament repair. Defining a rationale for augmentation. Am J Sports Med. 19: 243-55, 1991.

221. Shrive N, Chimich D, Marchuk L, Wilson J, Brant R, Frank C. Soft-tissue "flaws" are associated with the material properties of the healing rabbit medial collateral ligament. Journal of Orthopaedic Research. 13: 923-9, 1995.

222. Skalak R, Dasgupta G, Moss M, Otten E, Dullumeijer P, Vilmann H. Analytical description of growth. J Theor Biol. 94: 555-77, 1982.

223. Skalak R, Zargaryan S, Jain RK, Netti PA, Hoger A. Compatibility and the genesis of residual stress by volumetric growth. J Math Biol. 34: 889-914, 1996.

224. Slowman-Kovacs SD, Braunstein EM, Brandt KD. Rapidly progressive Charcot arthropathy following minor joint trauma in patients with diabetic neuropathy. Arthritis Rheum. 33: 412-7, 1990.

225. Smith JP, 3rd, Barrett GR. Medial and lateral meniscal tear patterns in anterior cruciate ligament-deficient knees. A prospective analysis of 575 tears. Am J Sports Med. 29: 415-9, 2001.

226. Sommer C, Friederich NF, Muller W. Improperly placed anterior cruciate ligament grafts: correlation between radiological parameters and clinical results. Knee Surg Sports Traumatol Arthrosc. 8: 207-13, 2000.

227. Sommerlath K, Lysholm J, Gillquist J. The long-term course after treatment of acute anterior cruciate ligament ruptures. A 9 to 16 year followup. American Journal of Sports Medicine. 19: 156-62, 1991.

228. Song Y, Debski RE, Musahl V, Thomas M, Woo SL. A three-dimensional finite element model of the human anterior cruciate ligament: a computational analysis with experimental validation. J Biomech. 37: 383-90, 2004.

229. Spalazzi JP, Gallina J, Fung-Kee-Fung SD, Konofagou EE, Lu HH. Elastographic imaging of strain distribution in the anterior cruciate ligament and at the ligament-bone insertions. J Orthop Res. 24: 2001-10, 2006.

230. Spindler KP, Kuhn JE, Freedman KB, Matthews CE, Dittus RS, Harrell FE, Jr. Anterior cruciate ligament reconstruction autograft choice: bone-tendon-bone versus hamstring: does it really matter? A systematic review. Am J Sports Med. 32: 1986-95, 2004.

231. Spindler KP, Murray MM, Detwiler KB, Tarter JT, Dawson JM, Nanney LB, Davidson JM. The biomechanical response to doses of TGF-beta 2 in the healing rabbit medial collateral ligament. J Orthop Res. 21: 245-9, 2003.

232. Stankus JJ, Freytes DO, Badylak SF, Wagner WR. Hybrid nanofibrous scaffolds from electrospinning of a synthetic biodegradable elastomer and urinary bladder matrix. J Biomater Sci Polym Ed. 19: 635-52, 2008.

233. Stankus JJ, Guan J, Fujimoto K, Wagner WR. Microintegrating smooth muscle cells into a biodegradable, elastomeric fiber matrix. Biomaterials. 27: 735-44, 2006.

234. Steadman JR, Cameron-Donaldson ML, Briggs KK, Rodkey WG. A minimally invasive technique ("healing response") to treat proximal ACL injuries in skeletally immature athletes. J Knee Surg. 19: 8-13, 2006.

235. Steadman JR, Cameron ML, Briggs KK, Rodkey WG. Healing-response treatment for ACL injuries. Orthopedic Technology Review. 32002.

236. Steadman JR, Rodkey WG. Role of primary anterior cruciate ligament repair with or without augmentation. Clin Sports Med. 12: 685-95, 1993.

237. Strand T, Molster A, Hordvik M, Krukhaug Y. Long-term follow-up after primary repair of the anterior cruciate ligament: clinical and radiological evaluation 15-23 years postoperatively. Arch Orthop Trauma Surg. 125: 217-21, 2005.

238. Streich NA, Friedrich K, Gotterbarm T, Schmitt H. Reconstruction of the ACL with a semitendinosus tendon graft: a prospective randomized single blinded comparison of double-bundle versus single-bundle technique in male athletes. Knee Surg Sports Traumatol Arthrosc. 16: 232-8, 2008.

239. Taber LA. Towards a unified theory for morphomechanics. Philos Transact A Math Phys Eng Sci. 367: 3555-83, 2009.

240. Tashman S, Kolowich P, Collon D, Anderson K, Anderst W. Dynamic function of the ACL-reconstructed knee during running. Clin Orthop Relat Res. 454: 66-73, 2007.

241. Taylor DC, Posner M, Curl WW, Feagin JA. Isolated tears of the anterior cruciate ligament: over 30-year follow-up of patients treated with arthrotomy and primary repair. Am J Sports Med. 37: 65-71, 2009.

242. Tonino AJ, Davidson CL, Klopper PJ, Linclau LA. Protection from stress in bone and its effects. Experiments with stainless steel and plastic plates in dogs. J Bone Joint Surg Br. 58: 107-13, 1976.

243. Valentin A, Humphrey JD. Modeling effects of axial extension on arterial growth and remodeling. Med Biol Eng Comput. 47: 979-87, 2009.

244. Valentin A, Humphrey JD. Parameter sensitivity study of a constrained mixture model of arterial growth and remodeling. J Biomech Eng. 131: 101006, 2009.

245. von Porat A, Roos EM, Roos H. High prevalence of osteoarthritis 14 years after an anterior cruciate ligament tear in male soccer players: a study of radiographic and patient relevant outcomes. Ann Rheum Dis. 63: 269-73, 2004.

246. Von Porat A. REM, Roos H. High prevalence of osteoarthritis 14 years after an anterior cruciate ligament tear in male soccer players: a study of radiographic and patient relevant outcomes. Br J Sports Med. 38: 263, 2004.

247. Voytik-Harbin SL, Brightman AO, Kraine MR, Waisner B, Badylak SF. Identification of extractable growth factors from small intestinal submucosa. J Cell Biochem. 67: 478-91, 1997.

248. Warren RF. Primary repair of the anterior cruciate ligament. Clin Orthop Relat Res. 65-70, 1983.

249. Weiler A, Peine R, Pashmineh-Azar A, Abel C, Sudkamp NP, Hoffmann RF. Tendon healing in a bone tunnel. Part I: Biomechanical results after biodegradable interference fit fixation in a model of anterior cruciate ligament reconstruction in sheep. Arthroscopy. 18: 113-23, 2002.

250. Weiss JA, Woo SL, Ohland KJ, Horibe S, Newton PO. Evaluation of a new injury model to study medial collateral ligament healing: primary repair versus nonoperative treatment. Journal of Orthopaedic Research. 9: 516-28, 1991.

251. Wiig ME, Amiel D, Ivarsson M, Nagineni CN, Wallace CD, Arfors KE. Type I procollagen gene expression in normal and early healing of the medial collateral and anterior cruciate ligaments in rabbits: an in situ hybridization study. J Orthop Res. 9: 374-82, 1991.

252. Wiig ME, Amiel D, VandeBerg J, Kitabayashi L, Harwood FL, Arfors KE. The early effect of high molecular weight hyaluronan (hyaluronic acid) on anterior cruciate ligament healing: an experimental study in rabbits. J Orthop Res. 8: 425-34, 1990.

253. Wittenberg RH, Oxfort HU, Plafki C. A comparison of conservative and delayed surgical treatment of anterior cruciate ligament ruptures. A matched pair analysis. Int Orthop. 22: 145-8, 1998.

254. Wognum S, Schmidt DE, Sacks MS. On the mechanical role of de novo synthesized elastin in the urinary bladder wall. J Biomech Eng. 131: 101018, 2009.

255. Woo S, An K-N, Frank C, Livesay G, Ma C, Zeminski J. "Anatomy, Biology and Biomechanics of Tendon and Ligaments". In Orthopaedic basic science : biology and biomechanics of the musculoskeletal system, Edited by ed. Rosemont, Ill.: American Academy of Orthopaedic Surgeons, 2000, pp. 581-616.

256. Woo SL-Y, Kuei SC, Gomez MA, Winters JM, Amiel D, Akeson WH. Effects of immobilization and exercise on the strength characteristics of bone-medial collateral ligament-bone comples. ASME Biomechanical Symposium. 32: 67-70, 1979.

257. Woo SL-Y, Takakura Y, Liang R. Treatment with bioscaffold enhances the collagen composition and fibril morphology of the healing medial collateral ligament in rabbits. Tissue Eng. 12: 159-66, 2006.

258. Woo SL, Abramowitch SD, Kilger R, Liang R. Biomechanics of knee ligaments: injury, healing, and repair. J Biomech. 39: 1-20, 2006.

259. Woo SL, Debski RE, Wong EK, Yagi M, Tarinelli D. Use of robotic technology for diathrodial joint research. J Sci Med Sport. 2: 283-97, 1999.

260. Woo SL, Gelberman RH, Cobb NG, Amiel D, Lothringer K, Akeson WH. The importance of controlled passive mobilization on flexor tendon healing. A biomechanical study. Acta Orthop Scand. 52: 615-22, 1981.

261. Woo SL, Gomez MA, Amiel D, Ritter MA, Gelberman RH, Akeson WH. The effects of exercise on the biomechanical and biochemical properties of swine digital flexor tendons. J Biomech Eng. 103: 51-6, 1981.

262. Woo SL, Gomez MA, Sites TJ, Newton PO, Orlando CA, Akeson WH. The biomechanical and morphological changes in the medial collateral ligament of the rabbit after immobilization and remobilization. J Bone Joint Surg Am. 69: 1200-11, 1987.

263. Woo SL, Gomez MA, Woo YK, Akeson WH. Mechanical properties of tendons and ligaments. II. The relationships of immobilization and exercise on tissue remodeling. Biorheology. 19: 397-408, 1982.

264. Woo SL, Inoue M, McGurk-Burleson E, Gomez MA. Treatment of the medial collateral ligament injury. II: Structure and function of canine knees in response to differing treatment regimens. Am J Sports Med. 15: 22-9, 1987.

265. Woo SL, Orlando CA, Camp JF, Akeson WH. Effects of postmortem storage by freezing on ligament tensile behavior. J Biomech. 19: 399-404, 1986.

266. Woo SL, Peterson RH, Ohland KJ, Sites TJ, Danto MI. The effects of strain rate on the properties of the medial collateral ligament in skeletally immature and mature rabbits: a biomechanical and histological study. J Orthop Res. 8: 712-21, 1990.

267. Woo SL, Takakura Y, Liang R, Jia F, Moon DK. Treatment with bioscaffold enhances the the fibril morphology and the collagen composition of healing medial collateral ligament in rabbits. Tissue Eng. 12: 159-66, 2006.

268. Wren TA, Beaupre GS, Carter DR. A model for loading-dependent growth, development, and adaptation of tendons and ligaments. J Biomech. 31: 107-14, 1998.

269. Wren TA, Beaupre GS, Carter DR. Tendon and ligament adaptation to exercise, immobilization, and remobilization. J Rehabil Res Dev. 37: 217-24, 2000.

270. Xerogeanes JW, Fox RJ, Takeda Y, Kim HS, Ishibashi Y, Carlin GJ, Woo SL. A functional comparison of animal anterior cruciate ligament models to the human anterior cruciate ligament. Ann Biomed Eng. 26: 345-52, 1998.

271. Yagi M, Wong EK, Kanamori A, Debski RE, Fu FH, Woo SL. Biomechanical analysis of an anatomic anterior cruciate ligament reconstruction. Am J Sports Med. 30: 660-6, 2002.

272. Yamamoto Y, Hsu WH, Woo SL, Van Scyoc AH, Takakura Y, Debski RE. Knee stability and graft function after anterior cruciate ligament reconstruction: a comparison of a lateral and an anatomical femoral tunnel placement. Am J Sports Med. 32: 1825-32, 2004.

273. Yasuda K, Tsujino J, Ohkoshi Y, Tanabe Y, Kaneda K. Graft site morbidity with autogenous semitendinosus and gracilis tendons. Am J Sports Med. 23: 706-14, 1995.

274. Yoshiya S, Andrish JT, Manley MT, Bauer TW. Graft tension in anterior cruciate ligament reconstruction. An in vivo study in dogs. Am J Sports Med. 15: 464-70, 1987.

275. Young RG, Butler DL, Weber W, Caplan AI, Gordon SL, Fink DJ. Use of mesenchymal stem cells in a collagen matrix for Achilles tendon repair. J Orthop Res. 16: 406-13, 1998.

276. Yunes M, Richmond JC, Engels EA, Pinczewski LA. Patellar versus hamstring tendons in anterior cruciate ligament reconstruction: A meta-analysis. Arthroscopy. 17: 248-57, 2001.

277. Zantop T, Gilbert TW, Yoder MC, Badylak SF. Extracellular matrix scaffolds are repopulated by bone marrow-derived cells in a mouse model of achilles tendon reconstruction. J Orthop Res. 24: 1299-309, 2006.

278. Zhang X, Wu C, Jiang G, Woo SL-Y. 2008. *The Effects of Geometry and Fiber Bundle Orientation on the Finite Element Modeling of the Anterior Cruciate Ligament*. Presented at 30th Annual International IEEE EMBS Conference, Vancouver, Canada

279. Zhou D, Lee HS, Villarreal F, Teng A, Lu E, Reynolds S, Qin C, Smith J, Sung KL. Differential MMP-2 activity of ligament cells under mechanical stretch injury: an in vitro study on human ACL and MCL fibroblasts. J Orthop Res. 23: 949-57, 2005.

280. Zulliger MA, Fridez P, Hayashi K, Stergiopulos N. A strain energy function for arteries accounting for wall composition and structure. J Biomech. 37: 989-1000, 2004.

281. Zysk SP, Refior HJ. Operative or conservative treatment of the acutely torn anterior cruciate ligament in middle-aged patients. A follow-up study of 133 patients between the ages of 40 and 59 years. Arch Orthop Trauma Surg. 120: 59-64, 2000.